

SSC-399

**STRENGTH AND STABILITY
TESTING OF STIFFENED PLATE
COMPONENTS**



This document has been approved
For public release and sale; its
Distribution is unlimited

SHIP STRUCTURE COMMITTEE
1997

SHIP STRUCTURE COMMITTEE

The SHIP STRUCTURE COMMITTEE is constituted to prosecute a research program to improve the hull structures of ships and other marine structures by an extension of knowledge pertaining to design, materials, and methods of construction.

RADM J. C. Card, USCG (Chairman)
Chief, Office of Marine Safety, Security
and Environmental Protection
U. S. Coast Guard

Mr. John Grinstead
Director, Policy and Legislation
Marine Regulatory Directorate
Transport Canada

Mr. Edwin B. Schimler
Associate Administrator for Ship-
building and Technology Development
Maritime Administration

Dr. Donald Liu
Senior Vice President
American Bureau of Shipping

Mr. Robert McCarthy
Director, Survivability and Structural
Integrity Group (SEA O3P)
Naval Sea Systems Command

Mr. Thomas Connors
Acting Director of Engineering (N7)
Military Sealift Command

Dr. Ross Graham
Head, Hydronautics Section
Defence Research Establishment-Atlantic

EXECUTIVE DIRECTOR

CDR Stephen E. Sharpe, USCG
LT Tom Miller, USCG

CONTRACTING OFFICER TECHNICAL REPRESENTATIVE

Mr. William J. Siekierka
Naval Sea Systems Command

SHIP STRUCTURE SUBCOMMITTEE

The SHIP STRUCTURE SUBCOMMITTEE acts for the Ship Structure Committee on technical matters by providing technical coordination for determining the goals and objectives of the program and by evaluating and interpreting the results in terms of structural design, construction, and operation.

MILITARY SEALIFT COMMAND

Mr. Robert E. Van Jones (Chairman)
Mr. Rickard A. Andanson
Mr. Michael W. Touma
Mr. Jeffrey E. Beach

MARITIME ADMINISTRATION

Mr. Frederick Seibold
Mr. Richard P. Voelker
Mr. Chao H. Lin
Dr. Walter M. Maclean

U. S. COAST GUARD

CAPT George Wright
Mr. Walter Lincoln
Mr. Rubin Sheinbarg

AMERICAN BUREAU OF SHIPPING

Mr. Glenn Ashe
Mr. John F. Conlon
Mr. Phillip G. Rynn
Mr. William Hanzalek

NAVAL SEA SYSTEMS COMMAND

Mr. W. Thomas Packard
Mr. Charles L. Null
Mr. Edward Kadala
Mr. Allen H. Engle

TRANSPORT CANADA

Mr. Peter Timonin
Mr. Felix Connolly
Mr. Francois Lamanque

DEFENCE RESEARCH ESTABLISHMENT ATLANTIC

Dr. Neil Pegg
LCDR Stephen Gibson
Dr. Roger Hollingshead
Mr. John Porter

SHIP STRUCTURE SUBCOMMITTEE LIAISON MEMBERS

SOCIETY OF NAVAL ARCHITECTS AND MARINE ENGINEERS

Dr. William Sandberg

NATIONAL ACADEMY OF SCIENCES - MARINE BOARD

Dr. Robert Sielski

CANADA CENTRE FOR MINERALS AND ENERGY TECHNOLOGIES

Dr. William R. Tyson

NATIONAL ACADEMY OF SCIENCES - COMMITTEE ON MARINE STRUCTURES

Dr. John Landes

U. S. NAVAL ACADEMY

Dr. Ramswar Bhattacharyya

WELDING RESEARCH COUNCIL

Dr. Martin Prager

U. S. MERCHANT MARINE ACADEMY

Dr. C. B. Kim

AMERICAN IRON AND STEEL INSTITUTE

Mr. Alexander D. Wilson

U. S. COAST GUARD ACADEMY

CDR Bruce R. Mustain

OFFICE OF NAVAL RESEARCH

Dr. Yapa D. S. Rajapaske

U. S. TECHNICAL ADVISORY GROUP TO THE INTERNATIONAL STANDARDS ORGANIZATION

CAPT Charles Piersall

MASSACHUSETTS INSTITUTE OF TECHNOLOGY

CAPT Alan J. Brown

AMERICAN WELDING SOCIETY

Mr. Richard French

STUDENT MEMBER

Mr. Jason Miller
Massachusetts Institute of Technology

Member Agencies:

*American Bureau of Shipping
Defence Research Establishment
Atlantic
Maritime Administration
Military Sealift Command
Naval Sea Systems Command
Transport Canada
United States Coast Guard*



**Ship
Structure
Committee**

Address Correspondence to:

Executive Director
Ship Structure Committee
U.S. Coast Guard (G-MSE/SSC)
2100 Second Street, S.W.
Washington, D.C. 20593-0001
Ph: (202) 267-0003
Fax: (202) 267-4816

An Interagency Advisory Committee

SSC-399
SR1378

April 23, 1997

STRENGTH AND STABILITY TESTING OF STIFFENED PLATE PANELS

The Interagency Ship Structure Committee (SSC) and the Canadian Forces, joint sponsors of this work, have several recent initiatives [SSC-375, SSC-381, SSC-382] which require improved methods of assessing hull structural integrity for both design and in-service conditions. One failure limit state considered is the ultimate hull girder strength, for which advanced methods of analysis including elasto-plastic buckling instability are being developed.

An increasingly popular approximate method for assessing ship hull girder ultimate strength is to combine the individual elasto-plastic load carrying characteristics of each single stiffened plate unit comprising the ship hull cross section. To evaluate methods for developing these load carrying characteristics, a full-scale testing system was designed and constructed to provide data for stiffened steel plate units under combined axial and lateral loads. The system included an assembly of discrete plate edge restraints developed to represent symmetric boundary conditions within a grillage system. Twelve full scale panels, including "as-built", "deformed" and "damaged" specimens, were tested in this set-up. This initial limited test program was to provide some results and determine the appropriate methods for further tests.

The specimens failed by combined plate and flexural buckling, stiffener tripping or local collapse, depending on the magnitude of lateral loads and local damage. Load-shortening curves associated with different failure modes were found to be distinctly different and it was found that a small lateral load could change the failure mode from flexural buckling to tripping. Current design criteria should directly consider effects of the lateral loads on the failure modes and the collapse loads of stiffened plates. The nonlinear finite element analyses of the panel collapse showed very good agreement with the experimental results indicating the suitability of this method for performing these types of calculations.

J.C. CARD
Rear Admiral, U. S. Coast Guard
Chairman, Ship Structure Committee

Technical Report Documentation Page

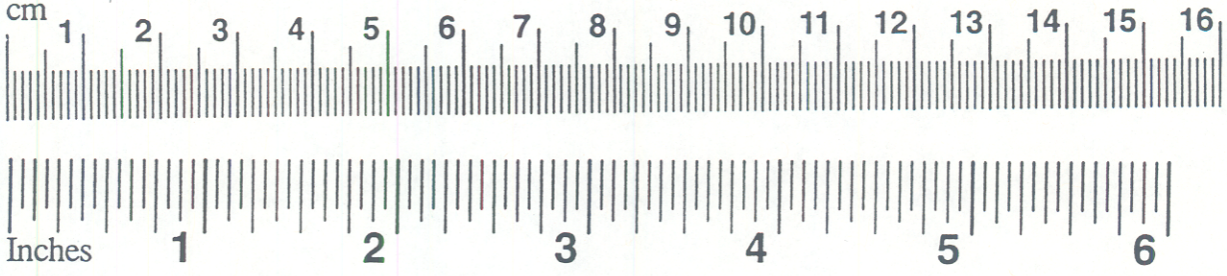
1. Report No.		2. Government Accession No.		3. Recipient's Catalog No.	
4. Title and Subtitle Strength and Stability Testing of Stiffened Plate Components				5. Report Date September 1996	
				6. Performing Organization Code 95026	
7. Author(s) Q. Chen, T.J.E. Zimmerman, D.D. DeGeer, B.W. Kennedy				8. Performing Organization Report No. SR-1378	
9. Performing Agency Name and Address Centre For Engineering Research Inc. 200 Karl Clark Road Edmonton, Alberta T6N 1H2 Canada				10. Work Unit No. (TRAIS)	
				11. Contract or Grant No.	
				13. Type of Report and Period Covered Final Report	
12. Sponsoring Agency Name and Address Ship Structure Committee c/o U.S. Coast Guard (G-MMS/SSC) 2100 Second St. SW Washington, DC 20593-0001				14. Sponsoring Agency Code G-M	
15. Supplementary Notes Sponsored by the Ship Structure Committee. Jointly funded by its member agencies.					
16. Abstract A full-scale testing system was designed and constructed to test stiffened steel plate specimens under combined axial and lateral loads. The system included an assembly of plate edge restraints that was developed to represent the appropriate boundary conditions for a stiffened plate grillage system. A total of twelve specimens, including "as-built" specimens, "deformed" specimens and "damaged" specimens, were tested in this set-up. Test variables included magnitude and direction of lateral loads, plate edge restraints, and local damage. The specimens failed by plate buckling, stiffener tripping or local collapse, as governed by the particular specimen and loading details. Load and displacement responses were determined for all specimens. To simulate the physical tests by numerical methods, a finite element model was constructed using ABAQUS. Five representative tests were analyzed to verify the numerical model. Comparison with the test results showed that the finite element analyses predict the failure mode and the ultimate strength with satisfactory accuracy.					
17. Key Words Stiffened Plate, Axial Compression, Testing, Ultimate Strength, Buckling				18. Distribution Statement Distribution Unlimited, Available From: National Technical Information Service U.S. Department of Commerce Springfield, VA 22151 Ph.(703) 487-4650	
19. Security Classif. (of this report) Unclassified		20. SECURITY CLASSIF. (of this page) Unclassified		21. No. of Pages	22. Price

METRIC CONVERSION CARD

Approximate Conversions to Metric Measures

Symbol	When You Know	Multiply by	To Find	Symbol
LENGTH				
in	inches	2.5	centimeters	cm
ft	feet	30	centimeters	cm
yd	yards	0.9	meters	m
mi	miles	1.6	kilometers	km
AREA				
in ²	square inches	6.5	square centimeters	cm ²
ft ²	square feet	0.09	square meters	m ²
yd ²	square yards	0.8	square meters	m ²
mi ²	square miles	2.6	square kilometers	km ²
	acres	0.4	hectares	ha
MASS (weight)				
oz	ounces	28	grams	g
lb	pounds	0.45	kilograms	kg
	short tons (2000 lb)	0.9	metric ton	t
VOLUME				
tsp	teaspoons	5	milliliters	mL
Tbsp	tablespoons	15	milliliters	mL
in ³	cubic inches	16	milliliters	mL
fl oz	fluid ounces	30	milliliters	mL
c	cups	0.24	liters	L
pt	pints	0.47	liters	L
qt	quarts	0.95	liters	L
gal	gallons	3.8	liters	L
ft ³	cubic feet	0.03	cubic meters	m ³
yd ³	cubic yards	0.76	cubic meters	m ³

TEMPERATURE (exact)	
°F	degrees Fahrenheit
	subtract 32,
	multiply by 5/9
	degrees Celsius



Approximate Conversions from Metric Measures

Symbol	When You Know	Multiply by	To Find	Symbol
LENGTH				
mm	millimeters	0.04	inches	in
cm	centimeters	0.4	inches	in
m	meters	3.3	feet	ft
m	meters	1.1	yards	yd
km	kilometers	0.6	miles	mi
AREA				
cm ²	square centimeters	0.16	square inches	in ²
m ²	square meters	1.2	square yards	yd ²
km ²	square kilometers	0.4	square miles	mi ²
ha	hectares (10,000 m ²)	2.5	acres	
MASS (weight)				
g	grams	0.035	ounces	oz
kg	kilograms	2.2	pounds	lb
t	metric ton (1,000 kg)	1.1	short tons	
VOLUME				
mL	milliliters	0.03	fluid ounces	fl oz
mL	milliliters	0.06	cubic inches	in ³
L	liters	2.1	pints	pt
L	liters	1.06	quarts	qt
L	liters	0.26	gallons	gal
m ³	cubic meters	35	cubic feet	ft ³
m ³	cubic meters	1.3	cubic yards	yd ³

TEMPERATURE (exact)	
°C	degrees Celsius
	multiply by 9/5,
	add 32
	degrees Fahrenheit

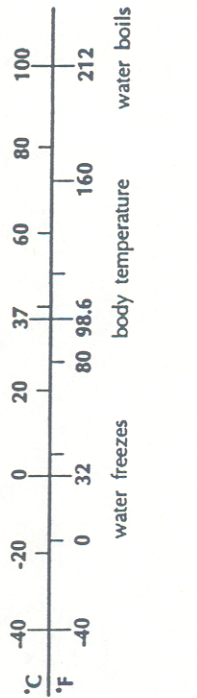


TABLE OF CONTENTS

1.0 INTRODUCTION.....	1
1.1 Background.....	1
1.2 Objectives	2
1.3 Scope of Work	2
2.0 TESTING SYSTEM.....	4
2.1 Test Set-Up	4
2.1.1 TTS Testing System.....	4
2.1.2 End Supports.....	5
2.2 Plate Edge Restraints	5
2.2.1 Requirements	5
2.2.2 Design	7
2.3 Instrumentation and Data Acquisition	7
2.4 Test Procedure	8
3.0 TEST SPECIMENS.....	19
3.1 Design and Fabrication	19
3.2 Initial Imperfections.....	20
3.3 Residual Stresses.....	21
3.4 Material Properties.....	21
4.0 TEST RESULTS	29
4.1 Buckling Modes.....	29
4.2 Load-Displacement Response.....	30
4.2.1 “As-Built” Specimens Failing by Plate Buckling.....	30
4.2.2 “As-Built” Specimens Failing by Stiffener Tripping	31
4.2.3 “Deformed” Specimens	31
4.2.4 “Damaged” Specimens	31
4.3 Discussion	32
5.0 FINITE ELEMENT ANALYSIS	60
5.1 Numerical Model	60
5.2 Comparison with Test Results	61
5.3 Summary	62
6.0 CONCLUSIONS AND RECOMMENDATIONS	69
6.1 Conclusions.....	69
6.2 Recommendations for Future Research.....	69

7.0 ACKNOWLEDGMENTS 71

APPENDICES

Appendix A Finite Element Analysis

Appendix B Residual Stresses and Material Properties

1.0 INTRODUCTION

The purpose of this study was to design and build an experimental testing system for conducting buckling tests of stiffened steel plate components representative of those used in ship structures, and conduct a series of full-scale tests to demonstrate the use of the system. The project was jointly funded by the Ship Structure Committee (SSC, Project No. SR-1378) and the Defense Research Establishment Atlantic of Canada (DREA, Contract No. W7707-4-3116/01-HAL).

This report summarizes the work completed and the experimental results obtained. Section 2 describes the concept and design of the experimental system, including the test set-up, instrumentation, and loading procedures. Section 3 presents test specimen measurement data, including initial imperfections, residual stresses, and material properties. Test results are summarized and discussed in Section 4. Section 5 describes a finite element model which was developed to simulate the physical tests, and compares the numerical results with the test results. Background information, which provides perspective for this work, is given in the remainder of this section.

Professors J. J. Cheng, A. E. Elwi, G. Y. Grondin and G. L. Kulak, of the University of Alberta, acted as sub-contractors for the project. Their work, which included finite element analyses, residual stress measurements, and material property tests, is presented in Appendices A and B.

Metric units are used throughout the report. Conversions to imperial units can be found in the table preceding the Table of Contents.

1.1 Background

In ship structures, stiffened plate panels are usually subjected to a combination of lateral and in-plane loads. The lateral loads cause bending in the panel (positive or negative), while the in-plane loads cause axial tension or compression. When the applied load is dominated by axial compression, the strength of a stiffened panel is affected by three basic failure modes: compression failure of the stiffener, compression failure of the plating and combined failure of the stiffener and plating.

Plate failure, usually by buckling, occurs when a small or moderate lateral load, combined with in-plane compression, puts the plate in axial compression. The result of plate buckling between stiffeners can be the redistribution of load into the stiffeners and subsequent overall flexural failure. For the combination of axial load and bending which puts the stiffener in compression, failure of the stiffener can occur, either by compressive yielding or by buckling (tripping). There can also be a rather complex interaction among these basic failure modes,

which is one of the reasons for this investigation. A complete discussion concerning the ultimate strength of stiffened plate panels can be found in Hughes (1983¹).

Factors which influencing the failure mode and the associated load carrying capacity include loading combination and direction, geometry, boundary restraint, initial imperfections and residual stresses, and location and pattern of damage (if any). All of these factors were considered in this work,

1.2 Objectives

The primary objective of this research was to design and build a large-scale experimental testing system that could be used to study the multiple buckling modes of the stiffened steel plate components used in the construction of ship structures. System requirements included the capability to test stiffened steel plate specimens under combined in-plane and out-of-plane loads, while maintaining an accurate representation of the boundary conditions applicable to a unidirectional stiffened plate within a grillage system.

A second objective was to conduct a series of twelve full-scale tests in order to verify the functionality of the testing system and to demonstrate the type of research results obtainable. Variables selected for these demonstration tests included: magnitude and direction of lateral loads, type of plate edge restraint, and the existence of large initial deformations or local damage. Three types of specimens were tested:

- “as-built” specimens that were fabricated using representative shipyard procedures;
- “deformed” specimens that contained deliberately induced initial deformations; and
- “damaged” specimens that used locally reduced stiffener areas to approximate the effect of metal loss corrosion.

A third objective was to determine the accuracy with which specimen buckling behaviour could be predicted using state-of-the-art finite element analytical procedures.

These objectives were met through the research described in this report.

1.3 Scope of Work

The work consisted of the following major tasks:

- design and construction of the testing system;

¹ Hughes, O. 1983. Ship Structural Design: A Rationally-Based, Computer-Aided, Optimization Approach. John Wiley & Sons, Inc.

- design and fabrication of the test specimens;
- measurement of initial imperfections and residual stresses;
- material property tests;
- tests of “as-built” specimens;
- tests of “deformed” specimens;
- tests of “damaged” specimens;
- finite element analyses;
- data reduction and results comparison; and
- preparation of a final report.

The entire scope of work is discussed in the following sections.

2.0 TESTING SYSTEM

2.1 Test Set-Up

Figure 2-1 shows an isometric view of the type of test specimen for which the testing system was to be designed. Typical specimens consisted of a 2000 x 500 mm plate with a T-stiffener welded along the centerline of the plate. Both ends of each specimen were welded to a 25 mm thick end plate. This configuration represents a single plate panel in a ship hull or deck element. Its longitudinal edges match the centerlines between stiffeners; both ends of the panel are bounded by grillage girders. The X-Y-Z coordinate system shown in the figure, in which the X-Y plane coincides with the mid-surface of an idealized, perfectly flat plate, was used for test set-up design, specimen alignment, and finite element modelling, and is referenced throughout this report.

The testing system was designed and constructed using several pieces of existing equipment, along with several new fixtures designed and built specifically for this project. The total system is illustrated in Figures 2-2 to 2-4. Major components of the system include:

- the existing servo-hydraulic “TTS” testing machine to apply axial load;
- two existing hydraulic jacks to apply lateral load;
- new end fixtures to provide simple support at both ends; and
- a new system of linear bearings and restraining devices to provide the specimen plate edge restraint required to simulate the actual plate-edge boundary conditions.

2.1.1 TTS Testing System

The existing TTS (Tubular Testing System) at C-FER’s laboratory is a high capacity testing system that has both axial and lateral load capabilities (Figures 2-3 and 2-4). The computer controlled servo-hydraulic loading system, which was manufactured by MTS Systems Corporation (Minneapolis), is integrated into a prestressed concrete strong wall which provides lateral support to the steel rails which connect the upper and lower crossheads, and also serves as a lateral loading reaction frame. The TTS is capable of axial static loading to 15,000 kN, axial fatigue loading to 5,000 kN, and static or fatigue lateral loading to 5,000 kN. The machine configuration permits both axial tensile and compressive loads to be applied to specimens.

As shown in Figure 2-2, the test specimens for this work were vertically positioned in the TTS. Axial compressive loads were applied by the load actuator located in the lower crosshead beneath the specimen. Lateral loads were applied at third points along the 2 m long span of a specimen, using two hydraulic actuators fastened to the strong wall (Figures 2-2 and 2-4). The loading direction of the hydraulic actuators was reversible so that

either the plate or the stiffener could be subjected to flexural compression. A servo-hydraulic control system connected to the lateral loading actuators enabled a constant pressure to be maintained throughout each test.

2.1.2 End Supports

The end supports were designed to provide “pinned” connections. The design is similar to that previously used at Lehigh University for testing steel beam-columns (SSRC 1988²). As shown in Figure 2-5, each support consisted of a half-cylinder bearing attached to the test specimen, and a thick base plate bolted to the TTS. Cement grout placed between the specimen and the bearing distributed contact stresses uniformly. As a specimen deformed, the cylindrical bearing rotated on the base plate, with the axial load always passing through the centre of rotation (point O in Figure 2-5).

The design thus provided simple support boundary conditions to the test specimen, as both ends were free to rotate. Horizontal reactions were transferred through friction between the cylindrical bearing and the base plate.

2.2 Plate Edge Restraints

Achieving proper boundary conditions along specimen plate edges was considered an important aspect of the system design, due to the perceived importance of boundary conditions to buckling behaviour. Design and fabrication of the plate edge restraint system was therefore given considerable attention.

2.2.1 Requirements

Plate edge displacements can be described by the six degrees of freedom shown in Figure 2-6. The three translational displacements (u_x , u_y and u_z) are defined in the global X-Y-Z coordinate system; the three rotational displacements (θ_ξ , θ_η and θ_ζ) defined in the local ξ - η - ζ coordinate system.

Since for this work the longitudinal edges of a test specimen were intended to coincide with the centerline between stiffeners in an actual structure, it was desirable to restrain these edges as symmetric boundaries. Such symmetry requires that three degrees of freedom (lateral in-plane displacement u_y , tangential rotation along the edge θ_ξ , and in-plane rotation θ_ζ) be restrained, while the other three (longitudinal displacement u_x , lateral out-of-plane displacement u_z , and out-of-plane flexural rotation θ_η) remain free. Preliminary analysis by

² SSRC 1988. Guide to Stability Design Criteria for Metal Structures. Structural Stability Research Council, ed. By T.V. Galambos, 4th ed., Wiley, New York.

DREA indicated that, of the three degrees of freedom to be restrained, tangential rotation (θ_x) is the most important in terms of its effect on buckling strength. The test setup was therefore designed to provide such restraint.

Although the above degrees of freedom are restrained continuously in an actual structure, for practical reasons the experimental set-up for a single panel specimen had to approximate the continuous boundary by a group of discrete restraints. In order to determine the appropriate number of discrete restraints required to adequately approximate continuous restraint, a series of finite element analyses were carried out for the following boundary conditions:

- continuously supported edges;
- discretely support edges; and
- free edges without any restraints.

Details of the analyses are given in Appendix A; a brief summary is given below.

Two types of lateral loads were considered (plate on compression side or stiffener on compression side) so that the evaluation could be applied to both plate buckling and stiffener tripping. The analyses incorporated imperfections, residual stresses and material properties representative of test specimen measured values.

For failures induced by plate buckling (plate in flexural compression), differences were shown to exist in the buckling modes for different boundary conditions. Models with continuous and five point discrete supports predicted similar multiple buckling waves, while the free edge model buckled in a single wave along the longitudinal edge (Figure 2-7); however, all three models demonstrated similar load-displacement responses (Figure A-6). For discrete supports at less than four locations, an earlier analysis showed a noticeable decrease in ultimate load capacity.

When subjected to relatively large lateral loads (30 kN) that put the stiffener on the compression side, discrete supports resulted in failure modes and load capacities similar to those with continuous supports, independent of the number of supports (Figure A-7b). At relatively small lateral loads (10 kN), a stiffened plate with continuous support was expected to fail by stiffener tripping. This failure mode was also observed in the physical test of SP1.6, a further indication that five discrete supports was an adequate approximation for continuous support. (The preliminary finite element analysis shown in Figure A-7a was not able to predict stiffener tripping for discretely supported plates because the simulation for boundary conditions was very approximate.)

In summary, the finite element results suggested that:

- a minimum of four discrete supports was required; and
- an increase to more than four discrete supports would not significantly change either the failure mode or the ultimate load.

In order to provide support at the midspan where the tangential rotation was likely to reach the maximum if the edges were not restrained, the final design used five discrete supports along each longitudinal edge.

2.2.2 Design

The plate edge rotational restraining system designed is shown in Figures 2-8 and 2-9. Each discrete support consisted of a compact and rigid carriage employing ball bearings to minimize friction. These bearings include:

- linear ball bearings that allowed free displacements of u_x and u_z ; and
- angular spherical bearings that permitted free θ_η rotation, while restraining rotation θ_ξ and displacement u_y .

Each carriage consists of three major components (Figure 2-8):

- Carriage A travels on shafts along the X direction (in the page) as the plate shortens under axial load. The shafts are approximately two meters long, extending the full length of the specimen. As shown in Figure 2-9, there were five such units on each side.
- Carriage B travels on shafts along the Z direction as the plate deflects laterally. These shafts are fixed on Carriage A.
- Grip Fixture C held a 100 x 30 mm area of the plate edge to prevent the edge from rotating about the tangent. Rotation about the η axis was free, since C was inserted into a pair of angular spherical bearings located at the center of Carriage B.

Figure 2-9 shows the assembly of the plate edge restraint system: ten carriages (five on each side) travelled on the main rails which were attached to the support frame. Together the system allowed free displacements in the X-Z plane and free rotation about the η axis, and restrained tangential rotation (θ_ξ), lateral in-plane displacement (u_y), and in-plane rotation (θ_ζ).

2.3 Instrumentation and Data Acquisition

The instrumentation is shown in Figure 2-10. It consisted of the following elements:

- nine displacement transducers for measuring end shortening, lateral deflection, and torsional displacement of the stiffener;
- two rotation meters (clinometers) for measuring rotations at the simply supported ends;
- two load cells for measuring lateral loads (axial load is measured by the TTS piston pressure); and
- seven strain gauges for measuring axial strains at midspan.

All of the above instruments were calibrated prior to testing. Test data was acquired via a computer-controlled system using LabVIEW[®], a commercially available data acquisition software package.

The instrumentation focused on measuring:

- axial and lateral load;
- specimen end shortening;
- lateral out-of-plane deflection at the plate to stiffener junction; and
- horizontal displacement of the stiffener flange as an indication of stiffener tripping.

Strain gauge readings served the purpose of monitoring stress distribution along the cross-section, and identifying the initiation of plate buckling.

2.4 Test Procedure

Test specimen preparation involved pre-test initial imperfection measurements (Section 3.2), strain gauging (Figure 2-11), alignment in the TTS, and remaining instrumentation. To align specimens in the TTS, a geometrical method (SSRC 1988³) was used whereby reference coordinates were selected based on the three-dimensional configuration of the specimen determined from pre-test measurements. This alignment method enabled the axial load to be applied through the centroid of the end cross-sections and parallel to the X-Y plane, which was defined by the geometry survey as the mid-surface of the idealized perfect plate. Plate edge restraints and instruments were mounted on the specimen after it was positioned in the TTS (Figure 2-12).

For testing, axial compression was applied using displacement control, which permitted the post-ultimate strength response range to be captured. For tests in which lateral loading was required, a small axial load sufficient to generate friction resistance at the end supports was applied at the beginning of the test. Lateral loads were then applied and maintained at a constant level during testing. At each load step beyond the elastic range, loads were held constant for two minutes prior to taking a data read. This allowed the static response to be determined.

After passing the ultimate load point, the test continued until axial shortening reached approximately 10 mm. This was deemed sufficient to adequately characterize the post-peak buckling response. Figure 2-13 shows a buckled specimen after completion of the test.

³ SSRC 1988. Guide to Stability Design Criteria for Metal Structures. Structural Stability Research Council, ed. By T.V. Galambos, 4th ed., Wiley, New York.



Figure 2-3 TTS Testing Machine at C-FER

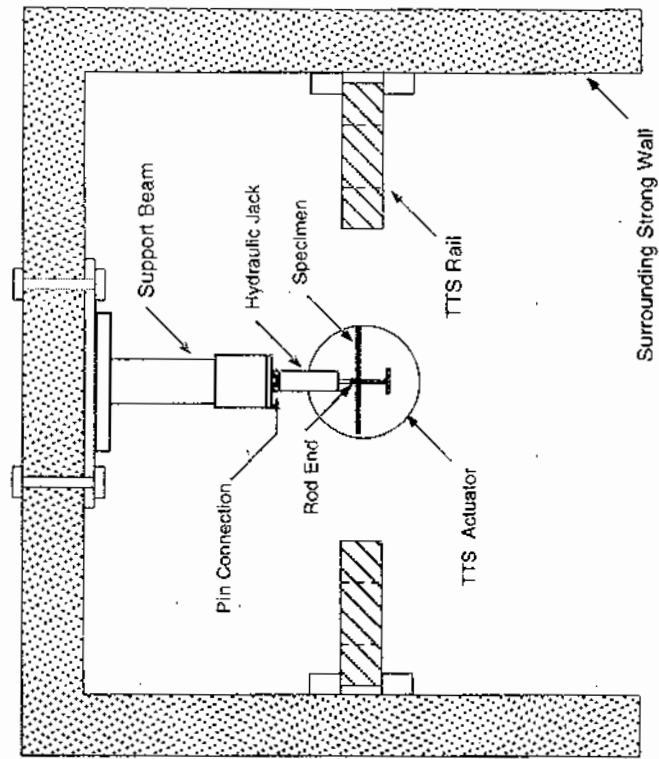
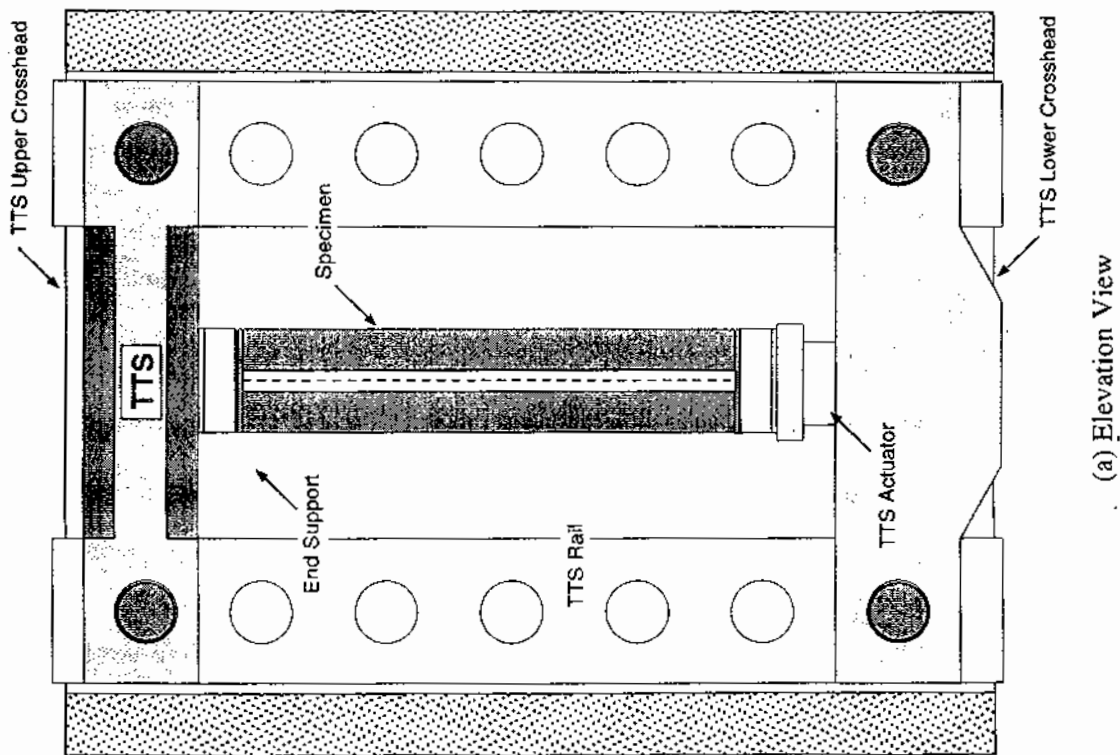


Figure 2-4 Schematic of TTS Testing System
(without plate edge restraint system)

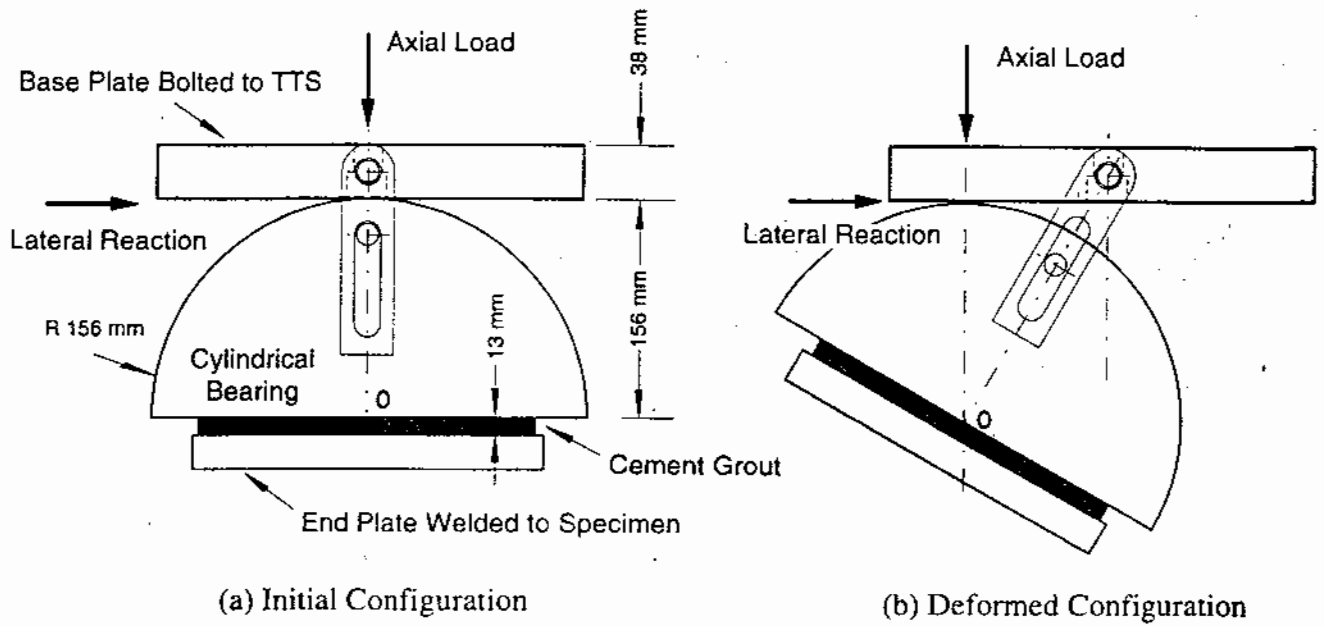
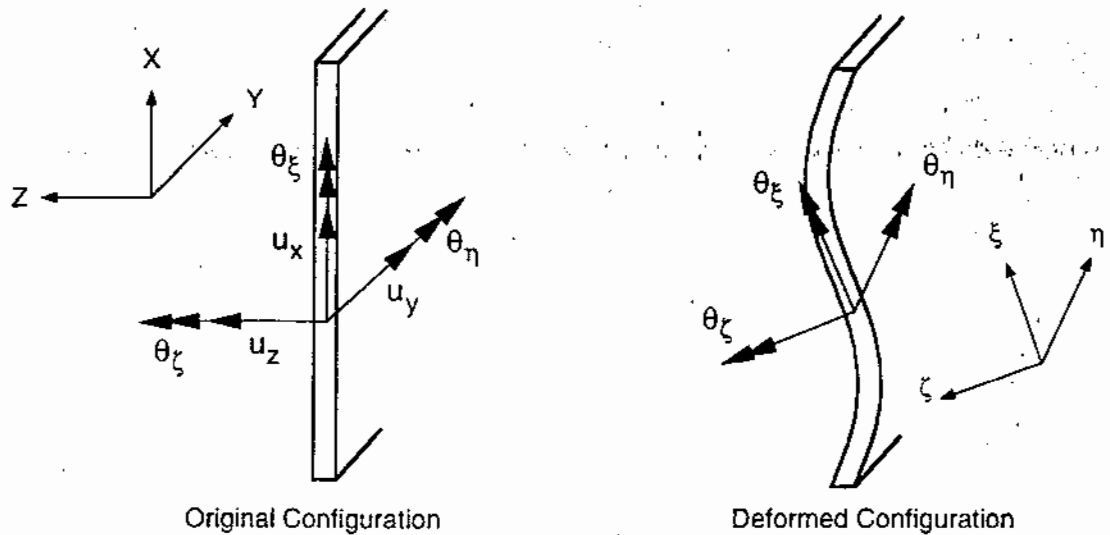


Figure 2-5 End Support Set-Up



(a) Degrees of Freedom for Plate-Shell Structures

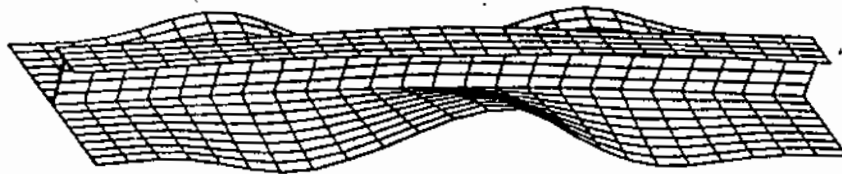
u_x	u_y	u_z	θ_ξ	θ_η	θ_ζ
Free	Fixed	Free	Fixed	Free	Fixed

(b) Restraints for Symmetric Boundaries

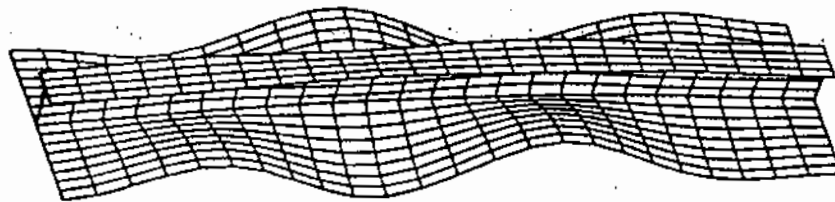
Figure 2-6 Displacements for Symmetric Boundary Conditions



(a) Free edge without any restraints

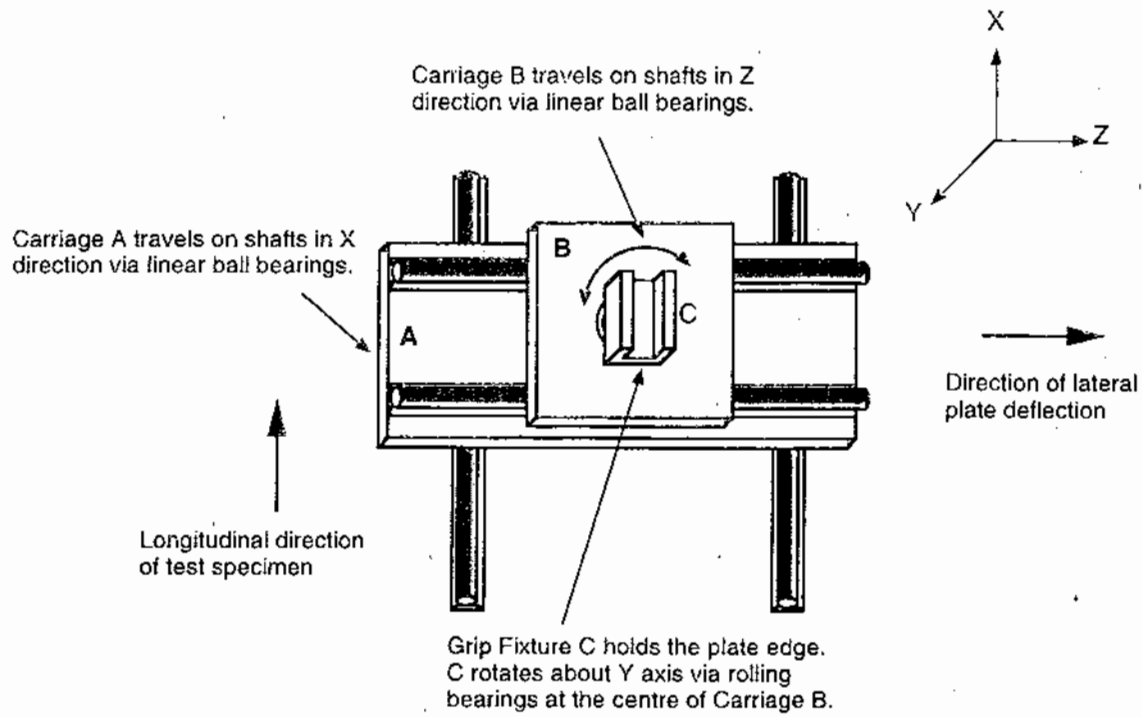


(b) Five discrete supports

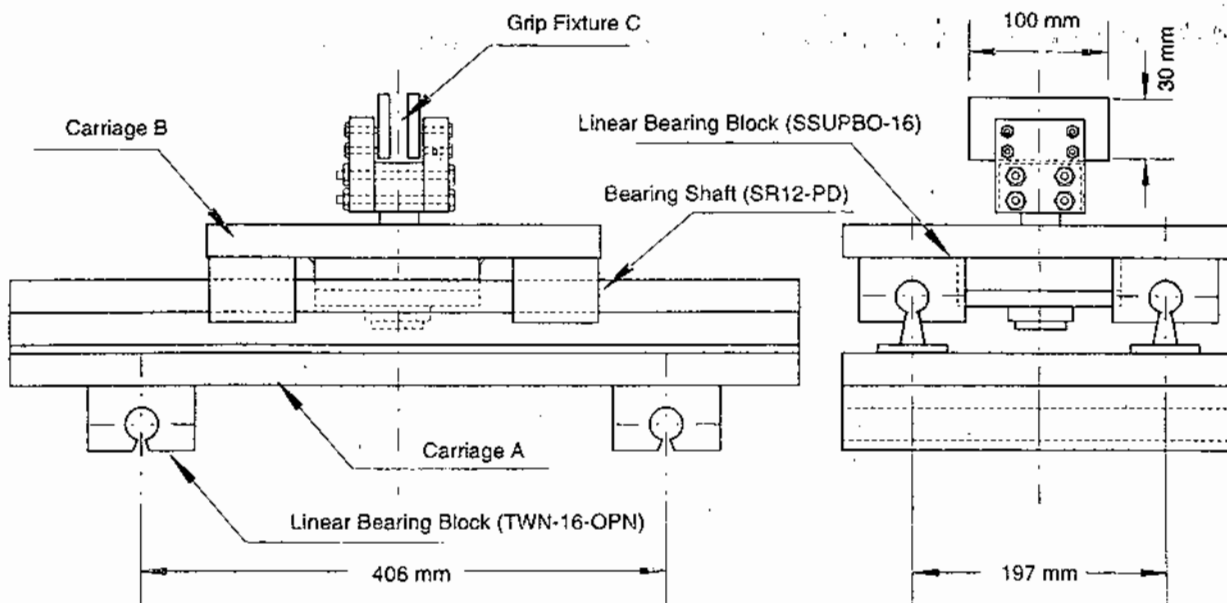


(c) Continuous support

Figure 2-7 Buckling Modes for Different Plate Edge Support



(a) Illustration of Design Concept



(b) Detail of Carriage Design

Figure 2-8 Plate Edge Restraint Carriage

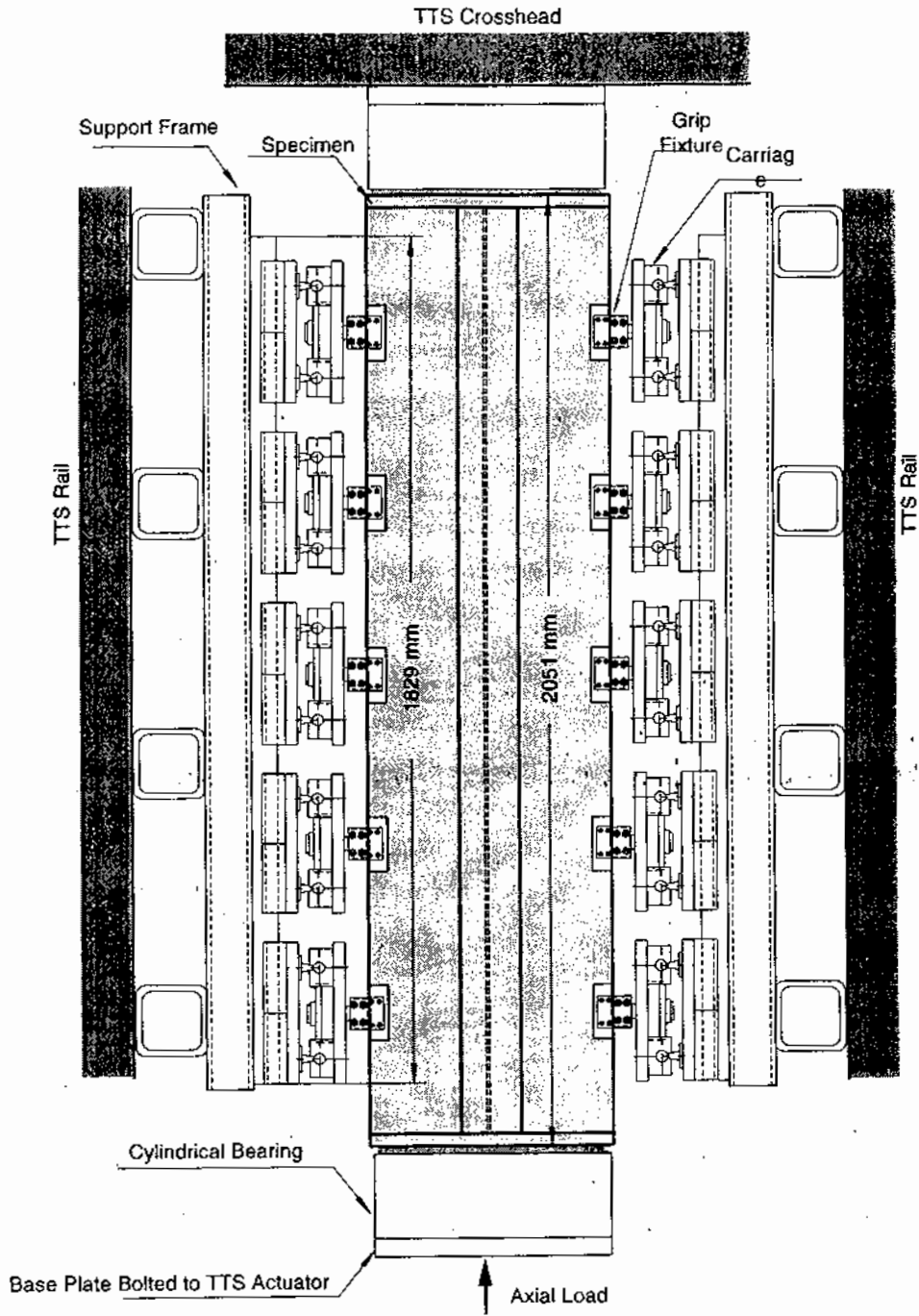
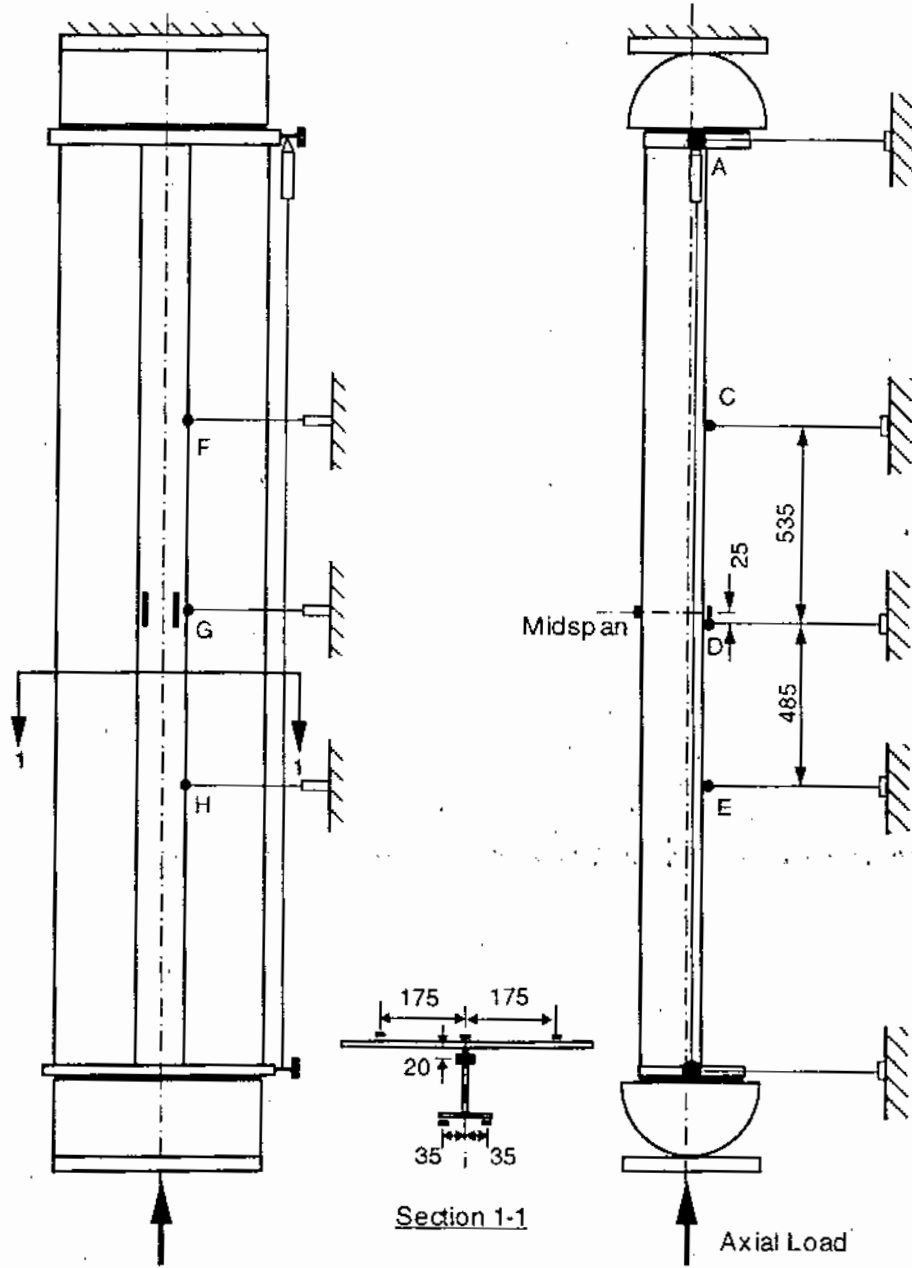


Figure 2-9 Assembly of Plate Edge Restraint System



Measurement	
• Lateral displacements of A, B, C, D, E	• Vertical TTS load & displacement
• Lateral displacements of F, G, H	• Lateral loads
• Vertical displacement of B relative to A	• Axial strains as shown in Section 1-1
• Rotations of A, B	(All dimensions are in mm)

Figure 2-10 Design of Instrumentation

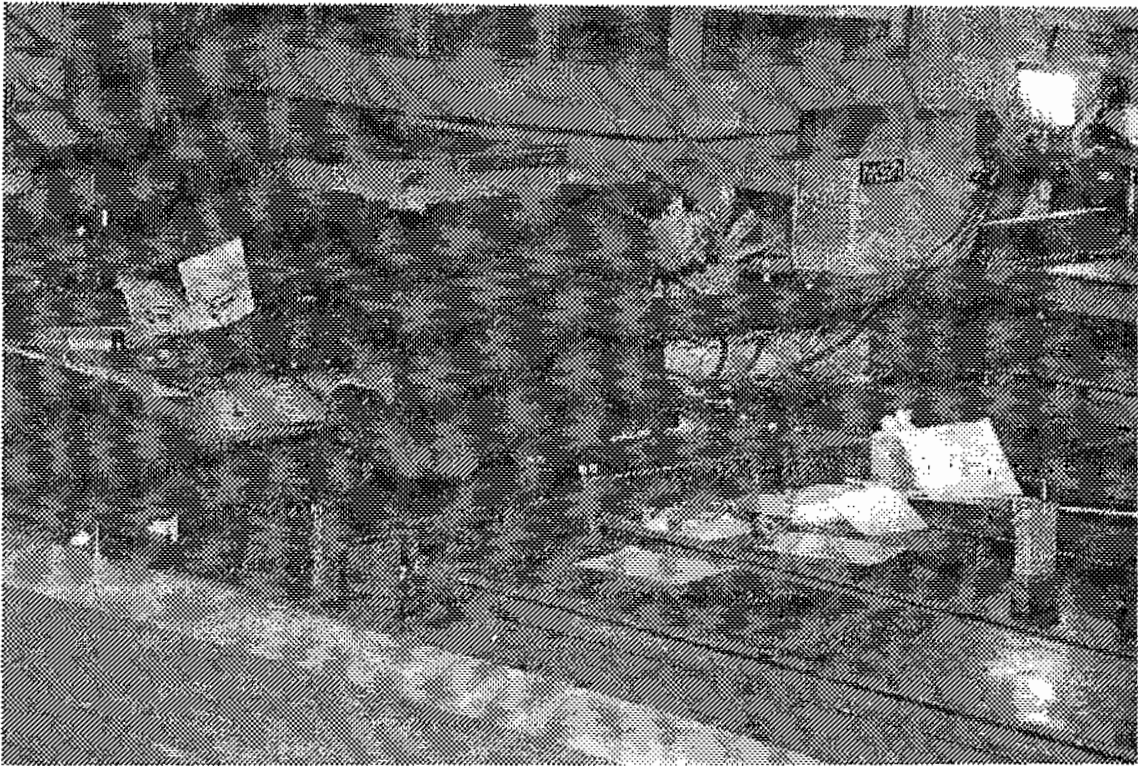


Figure 2-11 Preparation of Test Specimens

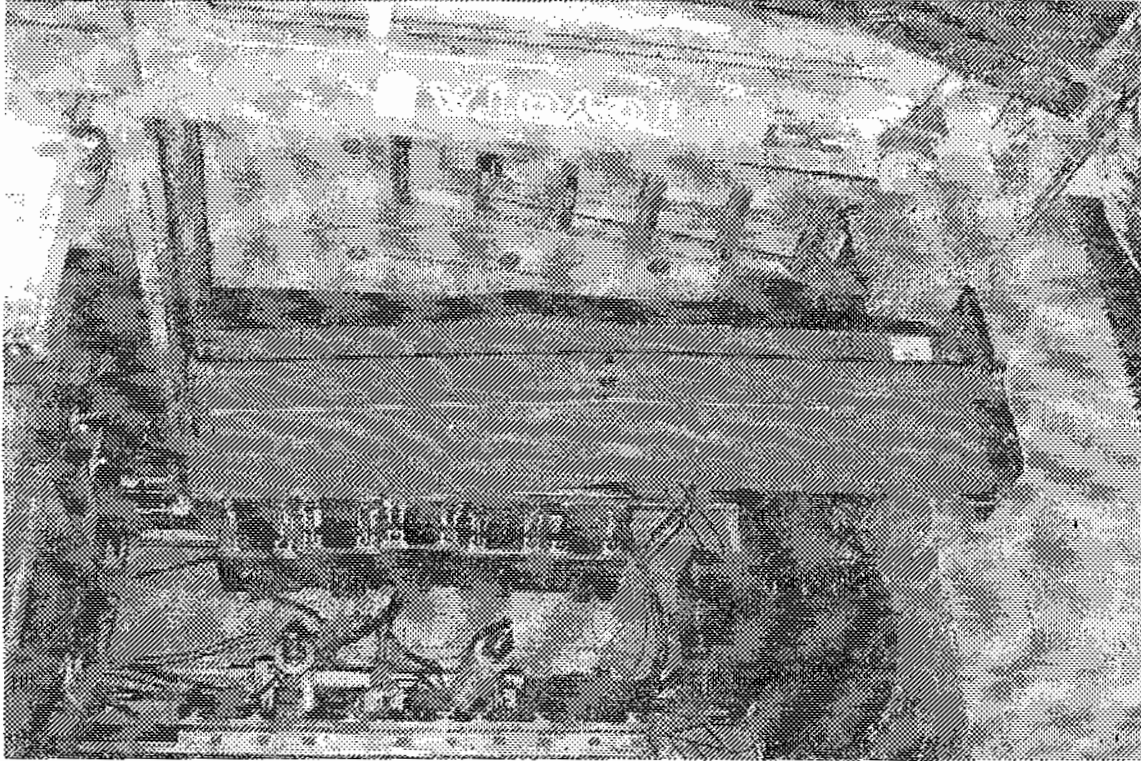


Figure 2-13 Removing Specimen after Test

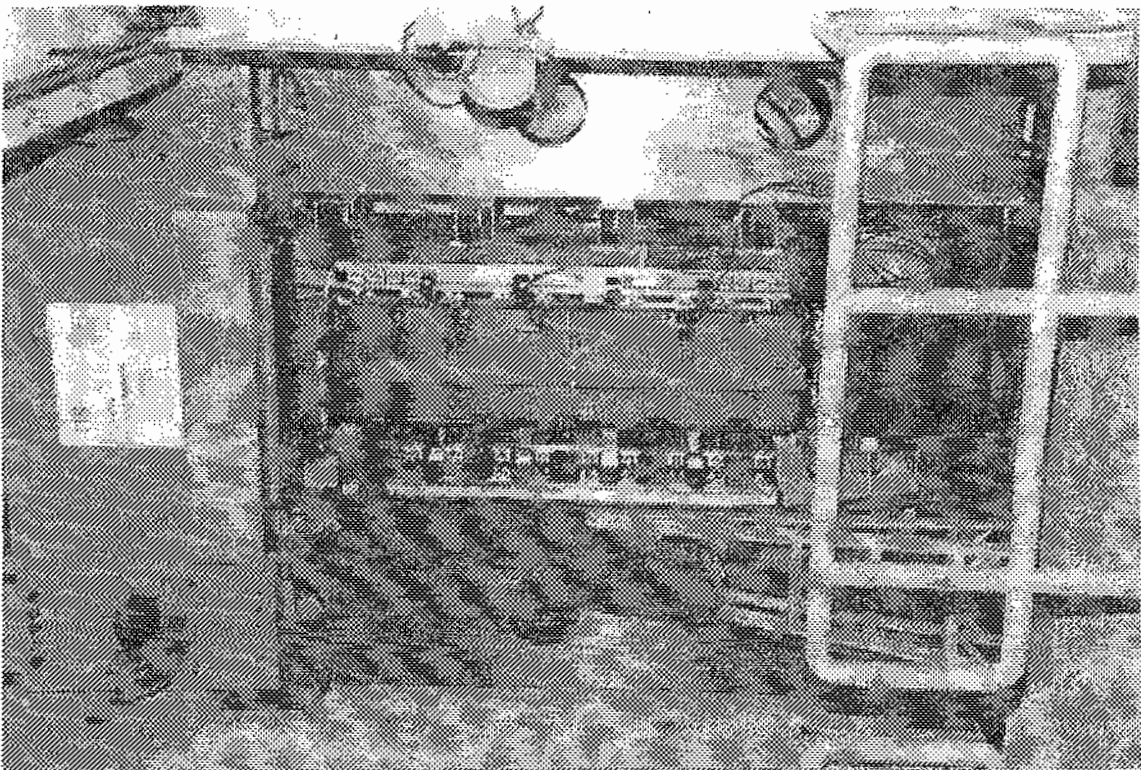


Figure 2-12 Mounting Instrumentations

3.0 TEST SPECIMENS

The twelve test specimens were divided into three categories:

- seven “as-built” specimens (SP1.x) that were fabricated following typical industrial procedures;
- two “deformed” specimens (SP2.x) that were deliberately plastically deformed before testing; and
- three “damaged” specimens (SP3.x) that had some web or flange material removed from the stiffener at midspan.

The test variables for all twelve specimens are summarized in Table 3-1.

3.1 Design and Fabrication

All twelve specimens had identical nominal dimensions. The basic geometry was selected by DREA to represent a typical deck plate for the mid-section of a frigate. Hot-rolled, 350 WT steel was used for specimen fabrication, which was the same as that used by Saint John Shipbuilding Ltd. (SJS�), New Brunswick, for recent frigate fabrication. Each specimen consisted of a 127 x 102 mm T-stiffener (actually obtained from SJS�) fillet welded to a 10 mm steel plate. Each specimen had a 50 mm end plate welded to each end.

The welding procedures used to fabricate the specimens were of particular concern since they have a significant influence on residual stresses and the associated residual deformations (initial imperfections). In order to fabricate test specimens with residual stress patterns similar to those of existing ship structures, fabrication procedures were selected representative of those used at SJS� for frigate construction. The fabrication procedures used were as follows:

- hydraulic jets were used to cut the plate so that the affected zone of local plastic deformation was minimized;
- a twin-head SAW (sub-arc weld) procedure was used to weld the stiffener to the plate simultaneously on both sides. The 6 mm fillet weld, and the heat input of 1.0 to 1.2 kJ/mm, were consistent with those used by SJS�; and
- rigid tolerances were specified for fabrication imperfections; limits for out-of-plane stiffener deflection, and for plate deflection at any given cross-section, were specified as 1/1000 of the span. This tolerance was met after an improved jiggling method was suggested to the fabricator.

One further procedure was required for fabricating the “damaged” test specimens. In order to simulate corrosion on the stiffener, portions of the flange or web were removed by milling out sections according to specifications provided by DREA. Figure 3-2 shows the sections removed from these specimens.

All specimens were measured to determine relevant dimensions prior to testing. These dimensions included element thickness, plate and flange width, and overall specimen depth. To determine “average” dimensions, a total of 36 readings were taken for each individual dimension (three readings per specimen). The means and standard deviations of these measurements are summarized in Table 3-2. All measurements were found to be consistent: the maximum deviation from the mean was ± 1.3 mm for width and depth, and ± 0.24 mm for thickness.

3.2 Initial Imperfections

In order to accurately model the imperfect geometry of the test specimens in the finite element analyses, and to align the test specimen properly using the geometrical method, it was necessary to define the three dimensional configuration of the specimen within a global three-dimensional reference frame.

The measurement procedure employed a Nardini-SZ25120T lathe machine to provide a three-dimensional reference system (Figure 3-3). Displacement gauges were mounted on the carriage of the lathe and travelled along gridlines on the specimen's surface to obtain a geometric profile. The measurement grid included nine longitudinal gridlines (five on the plate, two on the web, and two on the flange) intersected by nine cross sections. The grid size was selected based on practical considerations, while still being fine enough to capture imperfections with dimensions of sufficient size to influence plate buckling or stiffener tripping.

The test specimens were comprehensively surveyed to determine the extent of fabrication induced imperfections with emphasis being placed on following measurements:

- out-of-flatness of the plate which would promote local plate buckling;
- out-of-plane deviations of the T-stiffener which would promote overall out-of-plane flexure; and
- torsional deformation and in-plane deviations of the T-stiffener which would promote stiffener tripping.

The data was later converted to the X-Y-Z coordinates of the mid-surface of the three plate components. These coordinates were then used for both the finite element analyses as well as specimen alignment in the TTS.

Imperfection profiles of the first three specimens are shown graphically in Figure 3-4. Measured results are summarized in Table 3-3. The following can be noted:

- maximum deflection of the stiffener (u_1) was 1.9 mm;
- maximum deflection of the plate from a perfect plane (u_2) was less than 3.7 mm;
- maximum off-center distance of the web to flange junction (u_3) was 5.8 mm; and

- maximum off-center distance of the web to plate junction (u_4) was 2.2 mm.

The “deformed” specimens were not surveyed because the initial imperfections were insignificant compared to the large plastic deformations imposed prior to testing.

3.3 Residual Stresses

Axial residual stress measurements were made by the University of Alberta using a sectioning method with mechanical strain gauges 100 mm in length. The procedure is based on the assumption that axial residual stresses are uniformly distributed through the thickness and along the length (except in the vicinity of the ends).

The measurements were made on 300 mm long segments obtained at four separate cross-sections, as shown in Figure B-2. A total of 75 strips were cut from the first cross-section (Figure 3-5) to evaluate residual stresses throughout the cross-section. The remaining three cross-sections used only ten strips to quantify residual stresses in the immediate vicinity of the weld. Measured axial strains were converted into axial stresses according to the measured material properties and the assumed uniaxial stress condition. The results show that tensile residual stresses at the plate-to-stiffener junction were close to the yield stress, and the average compressive residual stress that spreads over most of the rest of the plate was approximately 50 MPa (Figure 3-5). The magnitude and distribution of the residual stresses measured are considered normal for this type of welded structure.

3.4 Material Properties

Both the plate and the stiffener were hot-rolled structural steels (Grade G40.21M 350WT). A total of fifteen tension coupons (six from the web and six from the flange of a section of T-stiffener, and three from the parent plate) were prepared and tested in accordance with ASTM Standard A370 to determine the material properties. Since all specimens were fabricated from the same batch of material, it was assumed that the average properties are representative for each individual specimens. Table 3-4 summarizes the average material properties obtained from the coupon tests. All stress-strain curves show a well defined yield plateau typical of hot-rolled steels. Representative stress-strain curves are shown in Figure 3-6.

Details of the material property tests are given in Appendix B.

TABLE 3-1 SUMMARY OF TEST VARIABLES

Specimen	Local Damage	Initial Deformation	Lateral Load, kN	Bending Direction	Plate Edge Restraint
SP 1.1	No	No	10	Plate on compression side	Yes
SP 1.2	No	No	0	N/A	Yes
SP 1.3	No	No	25	Plate on compression side	Yes
SP 1.4	No	No	25	Plate on tension side	Yes
SP 1.5	No	No	25	Plate on tension side	No
SP 1.6	No	No	10	Plate on tension side	Yes
SP 1.7	No	No	25	Plate on compression side	No
SP 2.1	No	20 mm at midspan (plate on compression side)	0	N/A	Yes
SP 2.2	No	35 mm at midspan (plate on compression side)	0	N/A	Yes
SP 3.1	On web	No	0	N/A	Yes
SP 3.2	On flange (on both sides)	No	0	N/A	Yes
SP 3.3	On flange (one side only)	No	0	N/A	Yes

TABLE 3-2 DIMENSIONS OF TEST SPECIMEN

	Plate		Web		Flange	
	b	t	d	t _w	b _f	t _f
Mean, mm	500.4	9.67	136.8	6.22	103.9	8.06
Standard Deviation, mm	0.46	0.027	0.56	0.047	0.52	0.11

The diagram illustrates the geometry of the test specimen. It shows a cross-section of a beam with a central web and two side flanges. The total width of the top plate is labeled 'b'. The thickness of the top plate is 't'. The depth of the web is 'd'. The thickness of the web is 't_w'. The width of the flange is 'b_f', and the thickness of the flange is 't_f'. Arrows indicate the direction of measurement for each dimension.

TABLE 3-3 SUMMARY OF INITIAL IMPERFECTIONS

Specimen	u_1 , mm	u_2 , mm	u_3 , mm	u_4 , mm
SP1.1	0 to 1.9	-1.9 to 3.4	-3.6 to -0.5	-1.2 to 0.5
SP1.2	0 to 1.1	-2.4 to 3.0	-5.8 to -4.3	-2.0 to -1.0
SP1.3	-0.1 to 0.4	-2.2 to 3.3	-3.4 to -0.2	-2.2 to -0.5
SP1.4	0 to 0.6	-0.7 to 1.9	-4.9 to -3.3	-0.8 to -0.2
SP1.5	-0.5 to 0	-3.1 to 2.7	1.2 to 3.9	-0.4 to 0.3
SP1.6	0 to 0.4	-2.3 to 3.0	-2.6 to -1.2	-1.3 to 0.1
SP1.7	0 to 0.5	-1.9 to 1.0	-1.5 to -0.4	-1.7 to -0.2
SP3.1	0 to 0.3	-1.7 to 3.4	-3.4 to -1.4	-1.0 to -0.3
SP3.2	0 to 1.1	-2.6 to 3.7	0.4 to 2.2	-1.7 to -0.9
SP3.3	0 to 1.7	-1.2 to 3.1	-2.8 to -0.7	0.1 to 1.7

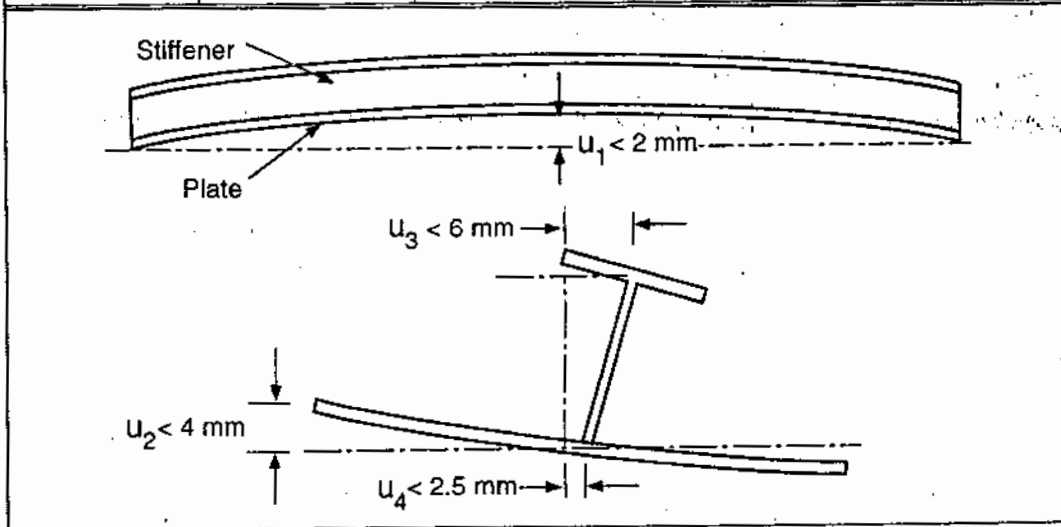


TABLE 3-4 AVERAGE MATERIAL PROPERTIES

Components	Static Yield, MPa	Static Ultimate, MPa	Rupture Strain	Area Reduction, %
Plate	425	509	0.371	68.8
Web	411	532	0.291	68.0
Flange	395	529	0.318	68.8

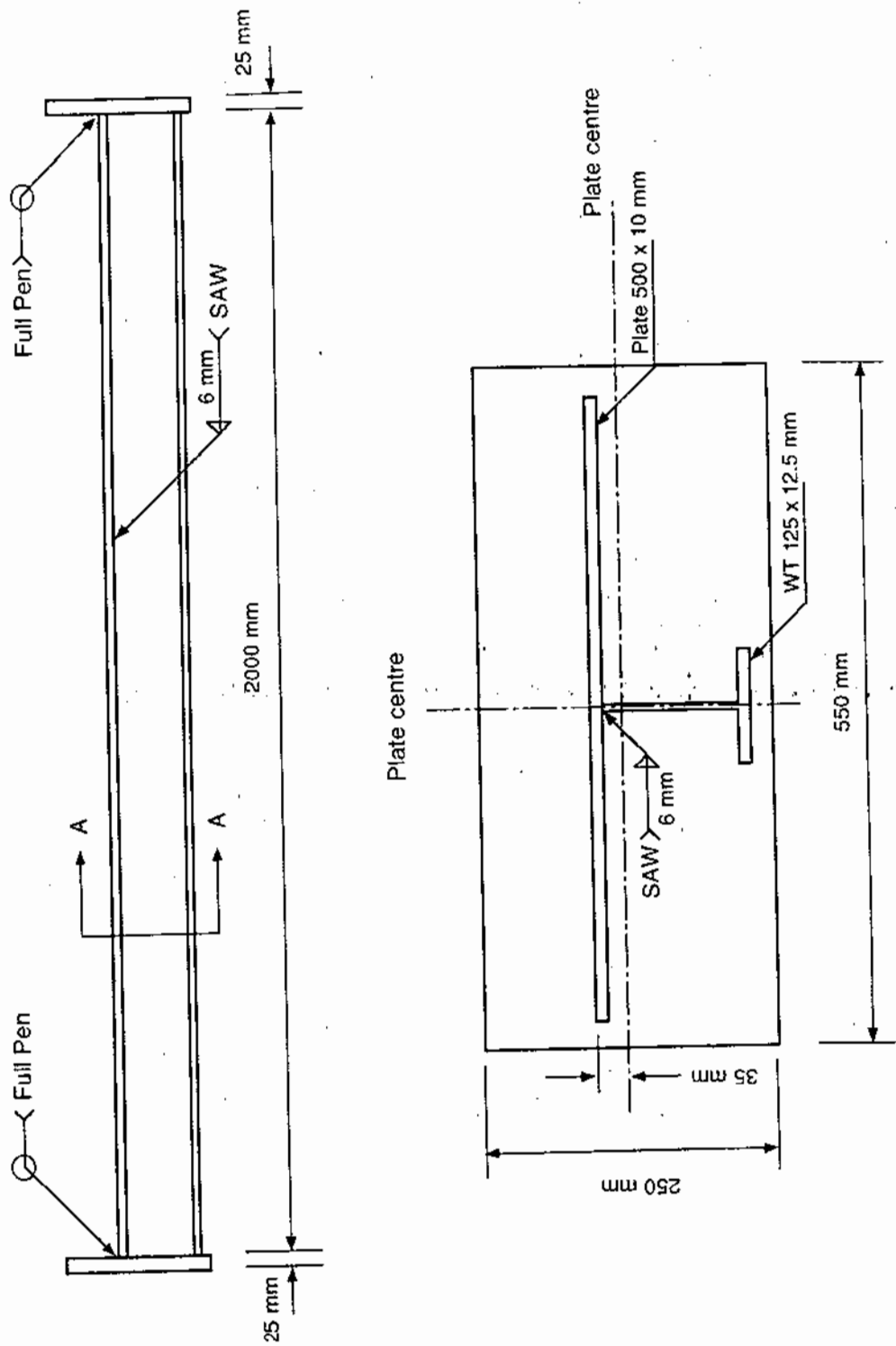


Figure 3-1 Design of Test Specimen

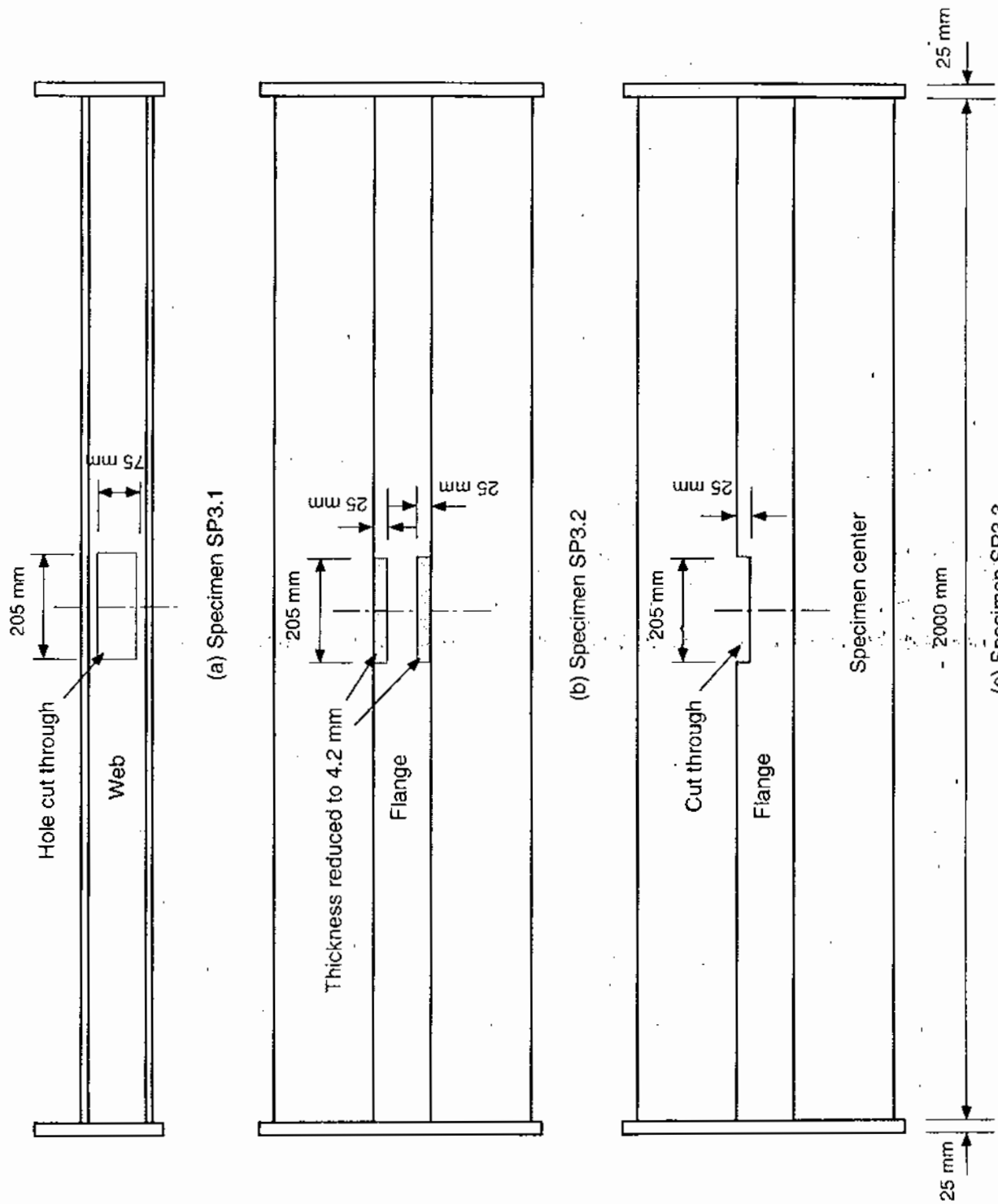


Figure 3-2 Specimens with Local Damage

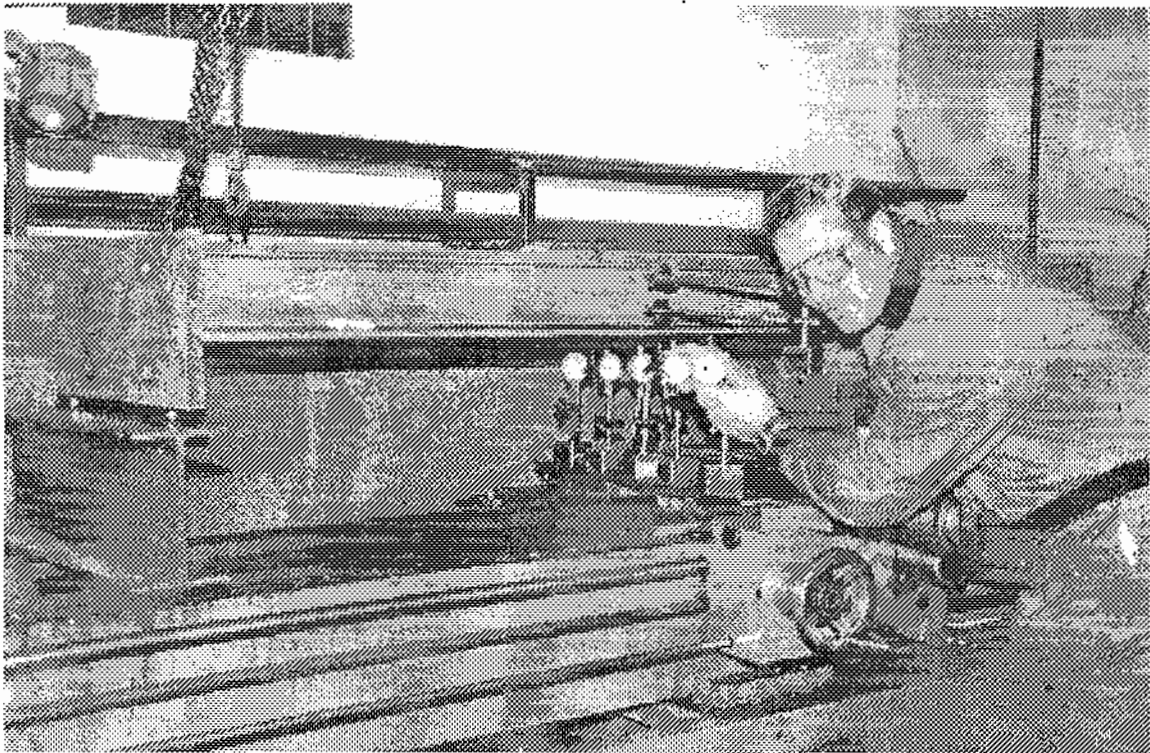
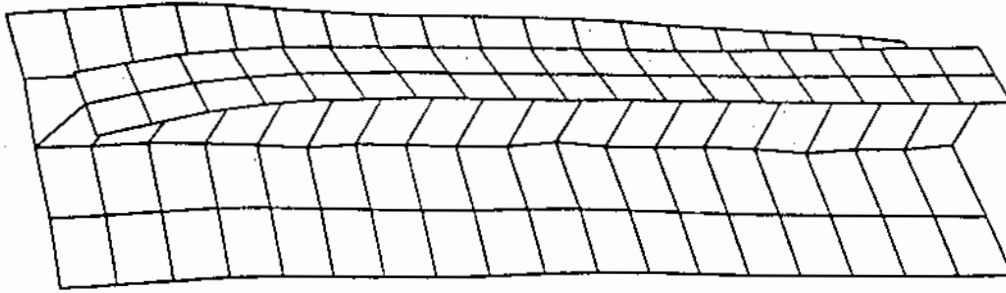
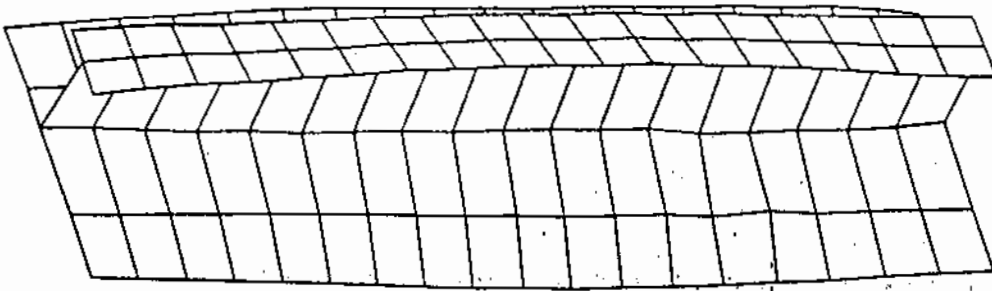


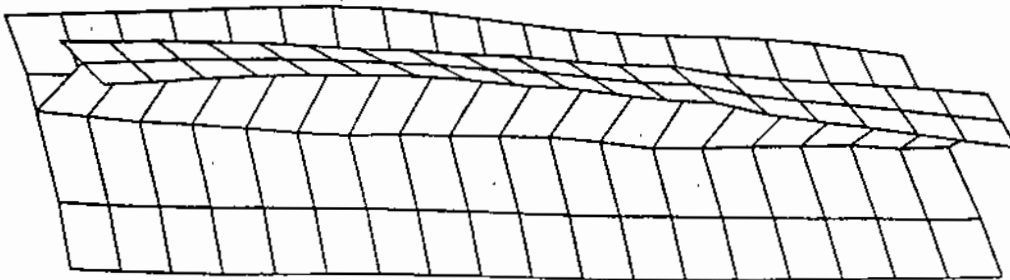
Figure 3-3 Measuring Imperfections



(a) Specimen SP1.1



(b) Specimen SP1.2



(c) Specimen SP1.3

Figure 3-4 Initial Imperfections
(magnified by 20)

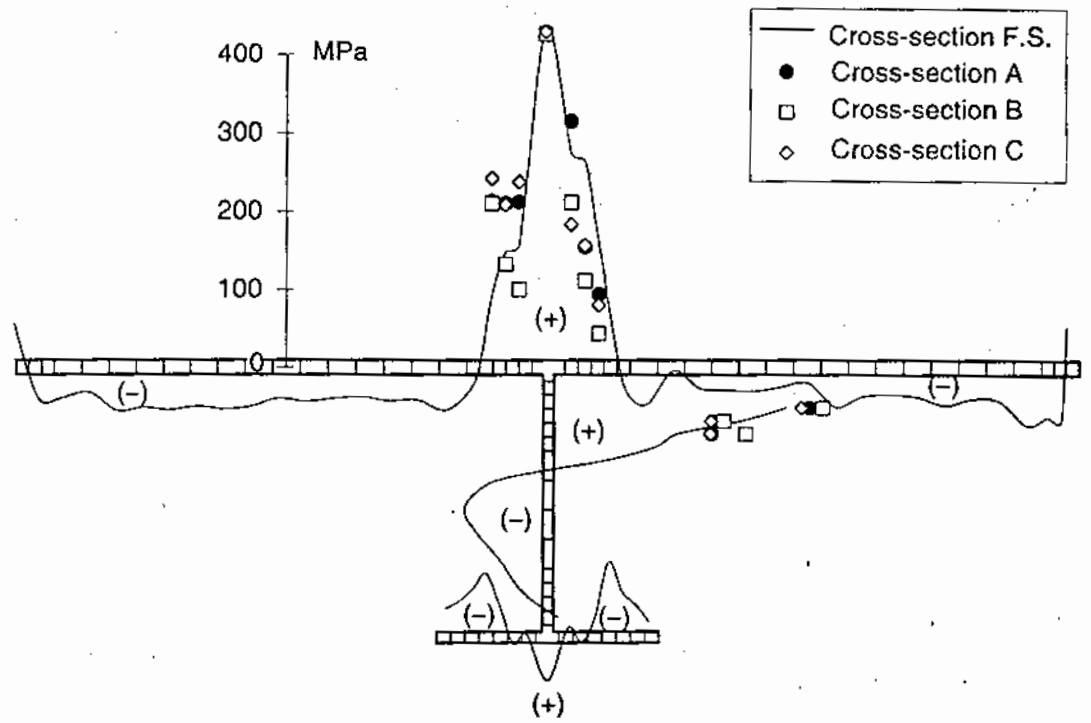


Figure 3-5 Measured Residual Stresses and Sectioning Pattern

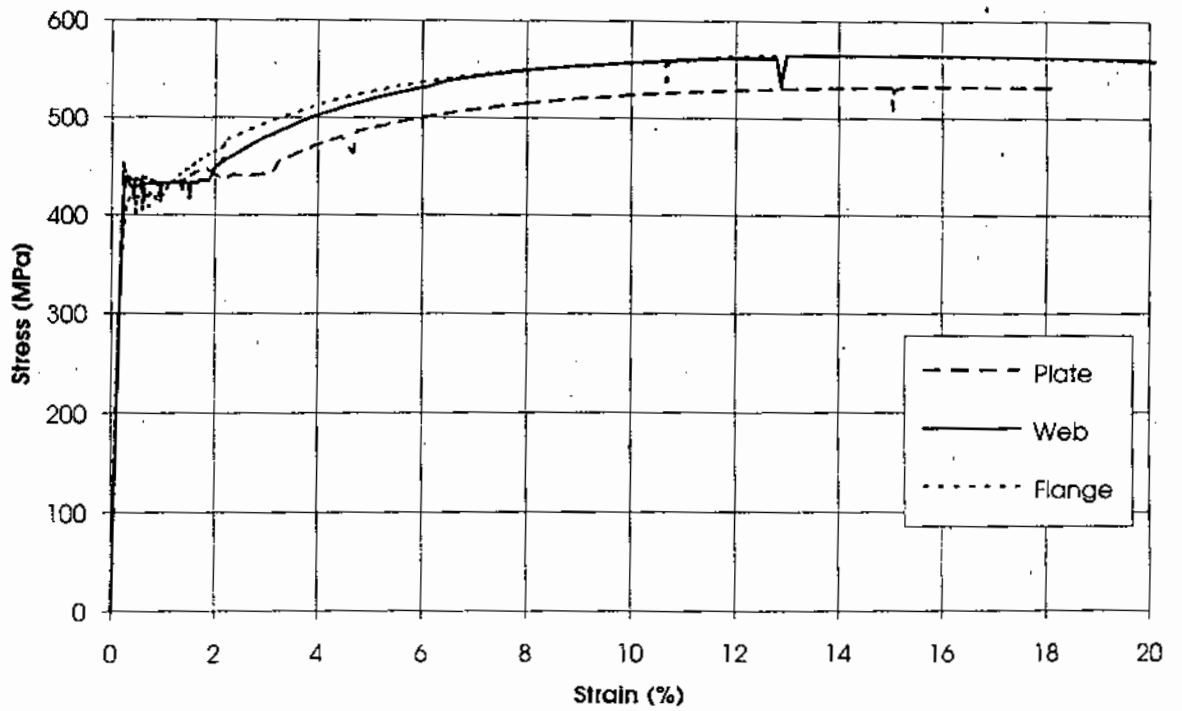


Figure 3-6 Axial Load versus End Rotation Response for Plate Buckling

4.0 TEST RESULTS

Table 4-1 gives the failure mode and ultimate axial load of all twelve specimens, along with a description of individual test parameters. Specimens SP1.1 and SP1.3 to SP1.7 were subjected to combined axial and lateral load, some with, and some without, plate edge restraint. Specimens SP1.2 and SP2.1 to SP3.3 were subjected only to axial compression. All of these specimens were tested with restrained plate edges.

4.1 Buckling Modes

All specimens, with the exception of SP3.1, exhibited one of two basic buckling failure modes (Figure 4-1); either plate buckling or stiffener tripping. This was not unexpected, given the geometry of the test specimens and the dominant axial load. Deformations associated with overall out-of-plane flexural buckling became significant immediately following buckling of the plate or stiffener. These overall flexural deformations were caused by a reduction in flexural stiffness due to component buckling. The direction of overall bending was always towards the unbuckled portion of the specimen (*i.e.*, towards the stiffener when the plate buckled or towards the plate when the stiffener buckled) because of the neutral axis shift and the accompanying P- Δ effect. Since individual components were more vulnerable to buckling than the member as a whole, failures were always initiated by plate buckling or stiffener tripping.

Significant differences were noted in the behavior of the two component buckling modes mentioned above. Stiffener tripping was abrupt and was usually associated with a significant load decrease. Plate buckling, on the other hand, developed gradually with no dramatic changes in the post-ultimate range. This is consistent with the general understanding that stiffener tripping can lead to sudden collapse, while plate buckling simply reduces the effective plate width.

Since all specimens had similar geometry, buckling modes were primarily dependent on the direction of lateral force (*i.e.*, the plate or the stiffener was subject to flexural compression). When lateral loads were not present (SP1.2) the specimens failed by plate buckling (the slender plate was relatively weak compared to the stiffener).

These trends were not generally exhibited by the specimens with local damage. Removal of part of the flange on one side of specimen SP3.3 lead to stiffener tripping rather than the plate buckling exhibited by companion specimens SP1.2 (the “as-built” specimen subjected to axial compression) and SP3.2 (symmetrical reduction on the flange thickness). A rectangular opening in the web of specimen SP3.1 resulted in a dramatic failure, as the upper half of the specimen snapped away from the lower half (see Figure 4-15). Buckling waves which had initiated in the plate dispersed during this sudden failure.

“Deformed” specimens SP2.1 and SP2.2 were plastically deformed prior to testing by applying lateral and axial loads large enough to achieve the desired initial deformations.

Using this method, residual midspan deflections of 20 mm and 35 mm were obtained for specimens SP2.1 and SP2.2, respectively. As expected, both specimens failed due to combined flexural and plate buckling.

Figures 4-2 to 4-4 illustrate the behavior of specimen SP1.1. The “as-built” specimen was subjected to 10 kN lateral loads that put the plate in flexural compression. Multiple longitudinal plate buckling waves were observed as the axial load approached the ultimate capacity (Figure 4-3). As the capacity decreased beyond the peak, buckling waves near the midspan continued to amplify until the end of the test (Figure 4-4). The final deformed shape consisted of longitudinal half-waves at midspan, in opposite directions on either side of the stiffener (Figures 4-5 and 4-6). This local plastic mechanism was typical for specimens that failed by plate buckling. Deformed shapes of other test specimens are shown in Figures 4-5 to 4-17.

4.2 Load-Displacement Response

Tables 4-2 to 4-13 present test results for each individual test. The information includes:

- a description of the specimen and load combination;
- the failure mode and ultimate axial load;
- observations concerning pre-ultimate, ultimate and post ultimate behavior; and
- a plot showing axial load versus axial shortening response.

The load-displacement response of the various groups of specimens is discussed below.

4.2.1 “As-Built” Specimens Failing by Plate Buckling

Four “as-built” specimens failed in this particular mode. Their load versus displacement responses are shown in Figures 4-18 to 4-20. In each case, the response can be divided in the three regions of behaviour: 1) a linear elastic region; 2) a nonlinear region resulting from the initiation of plate buckling; and 3) a stable post peak buckling region. End rotations and lateral deflections were generally small at the ultimate load point, but became significant in the post-buckling range.

From these plots, it can be seen that increasing the lateral load reduced the ultimate load capacity and increased both end rotations and lateral deflection (as expected). A lack of plate edge rotational restraint (SP1.7) caused a further reduction in ultimate load.

4.2.2 “As-Built” Specimens Failing by Stiffener Tripping

Figures 4-21 to 4-23 show the load versus displacement curves for specimens failing by stiffener tripping. The most obvious difference between these and the plate buckling specimens, was the sudden loss of axial load capacity which occurred at the onset of stiffener tripping. Again, increased lateral loads reduced the ultimate load capacity, as did the lack of plate edge restraint (SP1.5).

4.2.3 “Deformed” Specimens

Before testing, specimens SP2.1 and SP2.2 underwent a “deformation” cycle, where lateral loads, accompanied by a 600 kN axial load, were applied to plastically deform the specimens in bending (with the plate on the compression side). The deformation cycle load-displacement responses are shown in Figure 4-24. Both lateral and axial load were removed at the end of the “deformation” cycle. Residual midspan deflections of 20 and 35 mm were achieved for SP2.1 and SP2.2, respectively.

The load-shortening responses in the buckling tests of these specimens is shown in Figure 4-25. It appears that the initial plastic deformations reduced the ultimate load of these by 23% and 36%, respectively. For comparison, the response of specimen SP1.2 (the companion specimen with no initial plastic deformations) is also shown.

4.2.4 “Damaged” Specimens

Responses of the “damaged” specimens are shown in Figure 4-26, where they are compared with undamaged specimen SP1.2 (“as-built” specimen with same loading and boundary conditions). The results can be summarized as follows:

- The rectangular 205 x 75 mm web opening caused a sudden collapse when the upper portion of the specimen snapped away from the lower portion (SP3.1). The axial load immediately decreased from the ultimate to a low residual strength of about 500 kN.
- Reducing the flange thickness symmetrically in an area 205 x 25 mm made no difference in terms of failure mode and load capacity (SP3.2). Similar to SP1.2, the specimen failed by plate buckling.
- Removal of a 205 x 25 mm section on one side of the flange forced the stiffener to trip (SP3.3).

It is apparent that the failure mode and post-buckling behavior of the stiffened plates under study were sensitive to certain types of local damage in the stiffener, even though the differences in ultimate loads were within 8%.

4.3 Discussion

The twelve tests conducted verified the ability of the testing system to study stiffened plate buckling behaviour with single stiffener component tests and demonstrated the type of results obtainable from such tests. They further demonstrated the importance of accurately representing plate edge boundary conditions.

In addition, test data, which is useful in its own right, was obtained for a number of different loading conditions and specimen damage configurations.

TABLE 4-1 SUMMARY OF TEST RESULTS

Specimen	Test Variables			Lateral Load		Test Results	
	Local Damage	Initial Distortion	Plate Edge Restraint	Magnitude, kN	Direction	Max. Axial Load, kN	Buckling Mode
SP 1.1	No	No	Yes	10	Plate on compression side	1572	Plate buckling
SP 1.2	No	No	Yes	0	N/A	1736	Plate buckling
SP 1.3	No	No	Yes	25	Plate on compression side	1453	Plate buckling
SP 1.4	No	No	Yes	25	Plate on tension side	1275	Stiffener tripping
SP 1.5	No	No	No	25	Plate on tension side	1134	Stiffener tripping
SP 1.6	No	No	Yes	10	Plate on tension side	1673	Stiffener tripping
SP 1.7	No	No	No	25	Plate on compression side	1361	Plate buckling
SP 2.1	No	20 mm	Yes	-0	N/A	1331	Plate buckling
SP 2.2	No	35 mm	Yes	0	N/A	1116	Plate buckling
SP 3.1	On web	No	Yes	0	N/A	1636	Local failure
SP 3.2	On flange	No	Yes	0	N/A	1773	Plate buckling
SP 3.3	On flange	No	Yes	0	N/A	1683	Stiffener tripping

TABLE 4-2 TEST RESULTS OF SP1.1

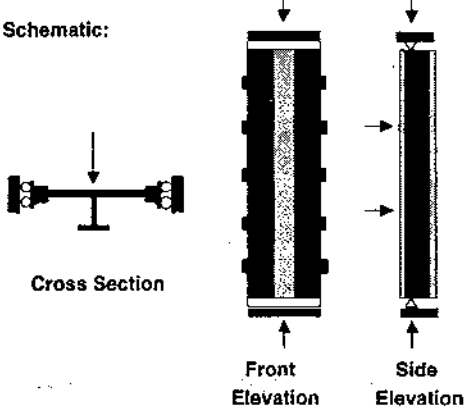
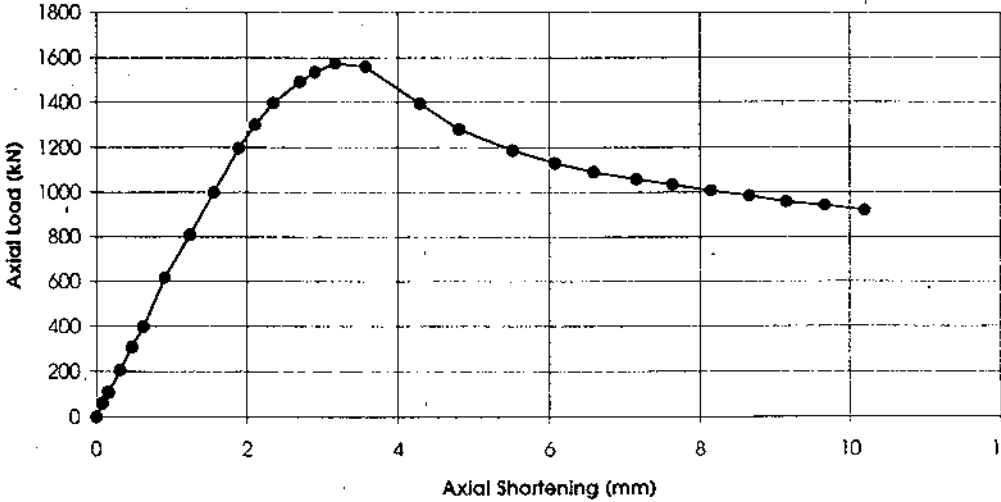
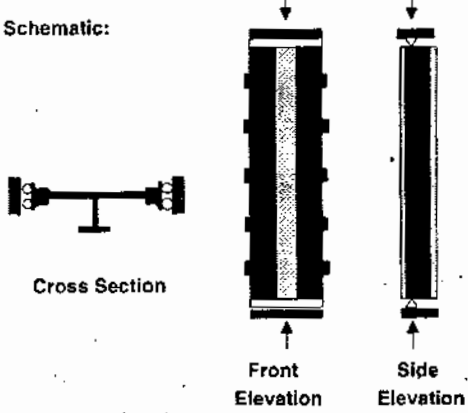
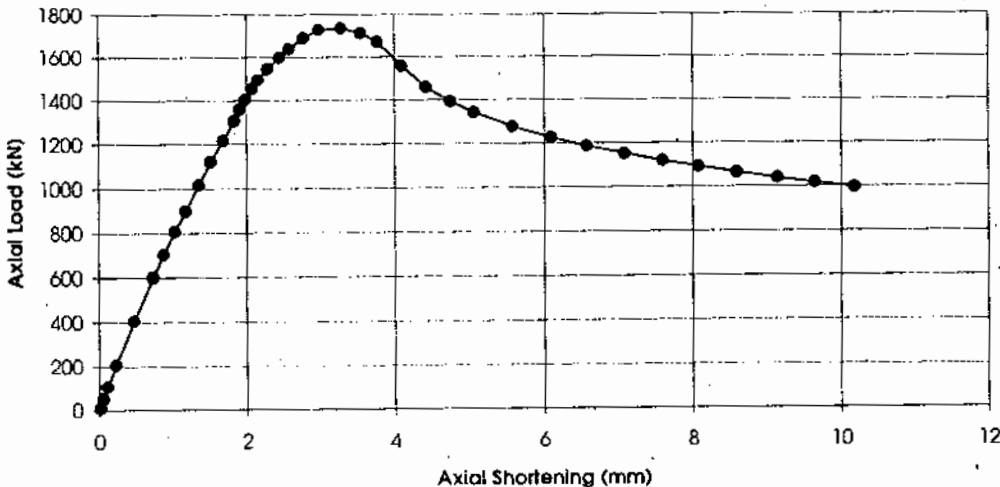
<p>Specimen Type: As-Built</p> <p>Type of Damage/Deformation: N/A</p> <p>Load Configuration: Axial compression with two 10 kN lateral loads. Plate in flexural compression.</p>	<p>Failure Mode: Plate Buckling</p> <p>Maximum Axial Load: 1572 kN</p>
<p style="text-align: center;">Test Summary</p> <p><i>Pre-ultimate:</i> Plate buckling waves initiate and amplify gradually. Stiffener remains straight.</p> <p><i>At ultimate:</i> No change in behavior at ultimate.</p> <p><i>Post-ultimate:</i> Gradual loss in capacity. Continued amplification of buckling waves. Stiffener does not trip.</p>	<p>Schematic:</p>  <p style="text-align: center;">Cross Section</p> <p style="text-align: center;">Front Elevation</p> <p style="text-align: center;">Side Elevation</p>
 <p style="text-align: center;">Load versus Axial Shortening Response</p>	

TABLE 4-3 TEST RESULTS OF SP1.2

<p>Specimen Type: As-Built</p> <p>Type of Damage/Deformation: N/A</p> <p>Load Configuration: Axial compression only.</p>	<p>Failure Mode: Plate Buckling</p> <p>Maximum Axial Load: 1736 kN</p>																																		
<p style="text-align: center;">Test Summary</p> <p><i>Pre-ultimate:</i> Plate buckling waves initiate and amplify gradually. Stiffener remains straight.</p> <p><i>At ultimate:</i> No change in behavior at ultimate.</p> <p><i>Post-ultimate:</i> Gradual loss in capacity. Continued amplification of buckling waves. Stiffener does not trip.</p>	<p>Schematic:</p>  <p style="text-align: center;">Cross Section</p> <p style="text-align: center;">Front Elevation Side Elevation</p>																																		
 <table border="1"> <caption>Approximate data points from the Load versus Axial Shortening Response graph</caption> <thead> <tr> <th>Axial Shortening (mm)</th> <th>Axial Load (kN)</th> </tr> </thead> <tbody> <tr><td>0</td><td>0</td></tr> <tr><td>0.5</td><td>400</td></tr> <tr><td>1.0</td><td>800</td></tr> <tr><td>1.5</td><td>1100</td></tr> <tr><td>2.0</td><td>1400</td></tr> <tr><td>2.5</td><td>1600</td></tr> <tr><td>3.0</td><td>1700</td></tr> <tr><td>3.5</td><td>1736</td></tr> <tr><td>4.0</td><td>1600</td></tr> <tr><td>4.5</td><td>1450</td></tr> <tr><td>5.0</td><td>1350</td></tr> <tr><td>6.0</td><td>1250</td></tr> <tr><td>7.0</td><td>1150</td></tr> <tr><td>8.0</td><td>1100</td></tr> <tr><td>9.0</td><td>1050</td></tr> <tr><td>10.0</td><td>1000</td></tr> </tbody> </table>		Axial Shortening (mm)	Axial Load (kN)	0	0	0.5	400	1.0	800	1.5	1100	2.0	1400	2.5	1600	3.0	1700	3.5	1736	4.0	1600	4.5	1450	5.0	1350	6.0	1250	7.0	1150	8.0	1100	9.0	1050	10.0	1000
Axial Shortening (mm)	Axial Load (kN)																																		
0	0																																		
0.5	400																																		
1.0	800																																		
1.5	1100																																		
2.0	1400																																		
2.5	1600																																		
3.0	1700																																		
3.5	1736																																		
4.0	1600																																		
4.5	1450																																		
5.0	1350																																		
6.0	1250																																		
7.0	1150																																		
8.0	1100																																		
9.0	1050																																		
10.0	1000																																		

Load versus Axial Shortening Response

TABLE 4-4 TEST RESULTS OF SP1.3

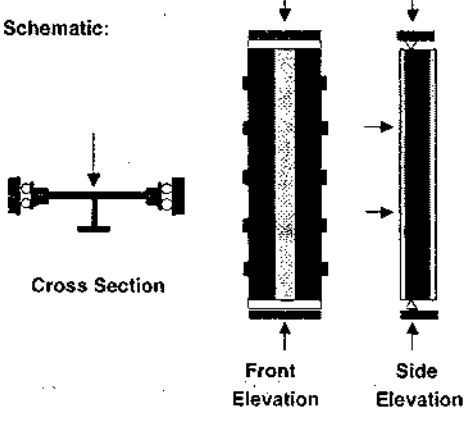
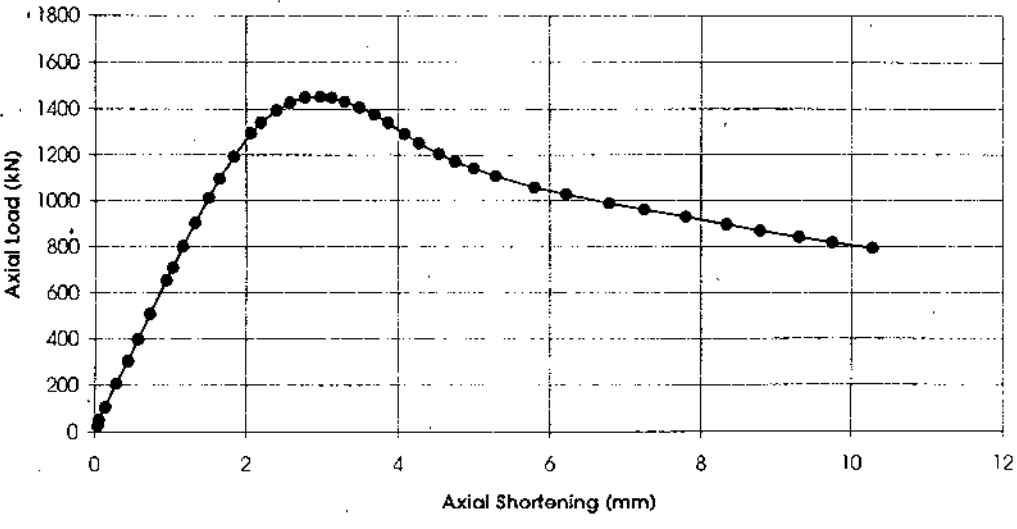
<p>Specimen Type: As-Built</p> <p>Type of Damage/Deformation: N/A</p> <p>Load Configuration: Axial compression with two 25 kN lateral loads. Plate in flexural compression.</p>	<p>Failure Mode: Plate Buckling</p> <p>Maximum Axial Load: 1453 kN</p>
<p style="text-align: center;">Test Summary</p> <p><i>Pre-ultimate:</i> Plate buckling waves initiate and amplify gradually. Stiffener remains straight.</p> <p><i>At ultimate:</i> No change in behavior at ultimate strength.</p> <p><i>Post-ultimate:</i> Gradual loss in capacity. Continued amplification of buckling waves. Stiffener does not trip.</p>	<p>Schematic:</p>  <p style="text-align: center;">Cross Section</p> <p style="text-align: center;">Front Elevation</p> <p style="text-align: center;">Side Elevation</p>
 <p style="text-align: center;">Load versus Axial Shortening Response</p>	

TABLE 4-5 TEST RESULTS OF SP1.4

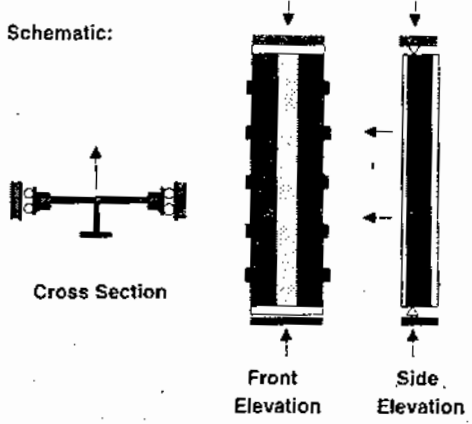
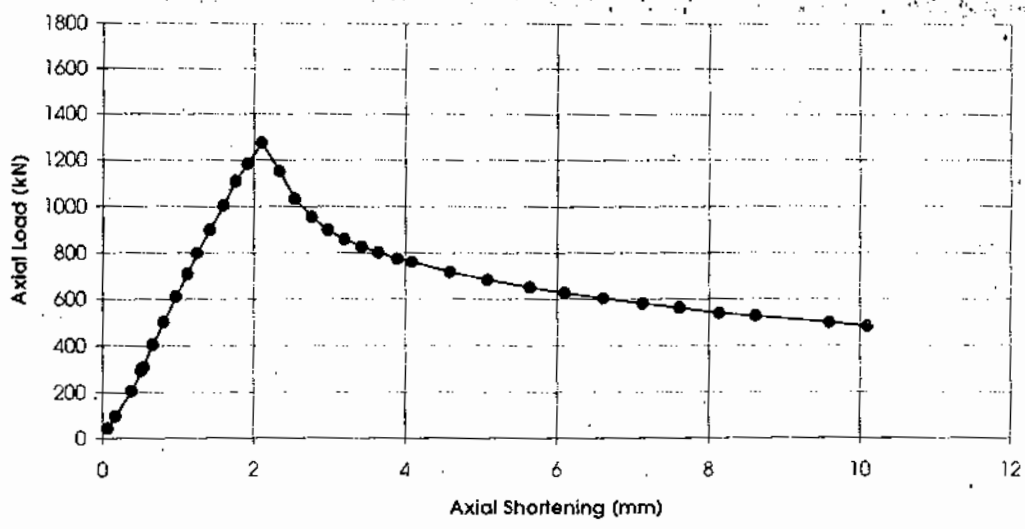
<p>Specimen Type: As-Built</p> <p>Type of Damage/Deformation: N/A</p> <p>Load Configuration: Axial compression with two 25 kN lateral loads. Plate is in flexural tension.</p>	<p>Failure Mode: Stiffener Tripping</p> <p>Maximum Axial Load: 1275 kN</p>
<p>Test Summary</p> <p><i>Pre-ultimate:</i> Stiffener tripping initiates and amplifies gradually. Plate remains flat.</p> <p><i>At ultimate:</i> Sudden increase in tripping deformation accompanied by sudden loss in capacity.</p> <p><i>Post-ultimate:</i> Gradual loss in capacity. Continued amplification of stiffener tripping. Plate does not buckle.</p>	<p>Schematic:</p>  <p>Cross Section</p> <p>Front Elevation</p> <p>Side Elevation</p>
 <p>Load versus Axial Shortening Response</p>	

TABLE 4-6 TEST RESULTS OF SP1.5

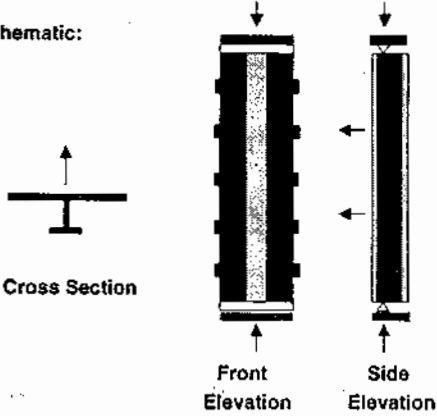
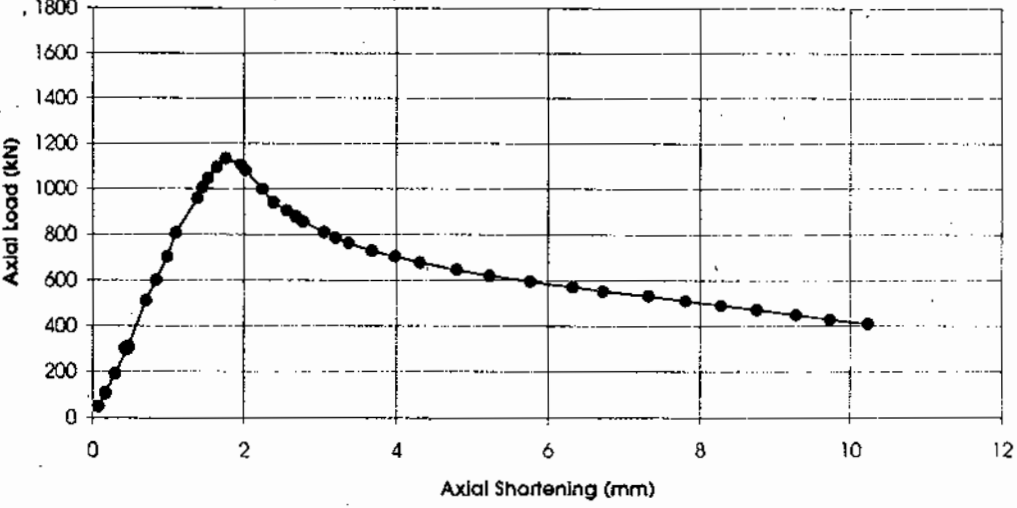
<p>Specimen Type: As-Built</p> <p>Type of Damage/Deformation: N/A</p> <p>Load Configuration: Axial compression with two 25 kN lateral loads. Plate in flexural tension. No edge restraint.</p>	<p>Failure Mode: Stiffener Tripping</p> <p>Maximum Axial Load: 1139 kN</p>
<p style="text-align: center;">Test Summary</p> <p><i>Pre-ultimate:</i> Stiffener tripping initiates and amplifies gradually. Plate remains flat.</p> <p><i>At ultimate:</i> Sudden increase in tripping deformation.</p> <p><i>Post-ultimate:</i> Gradual loss in capacity. Continued amplification of stiffener tripping. Plate does not buckle.</p>	<p>Schematic:</p>  <p style="text-align: center;">Cross Section</p> <p style="text-align: center;">Front Elevation Side Elevation</p>
 <p style="text-align: center;">Load versus Axial Shortening Response</p>	

TABLE 4-7 TEST RESULTS OF SP1.6

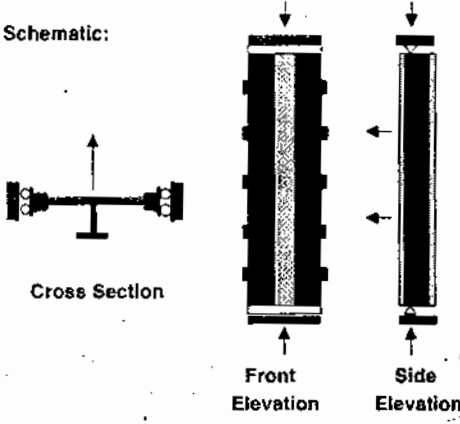
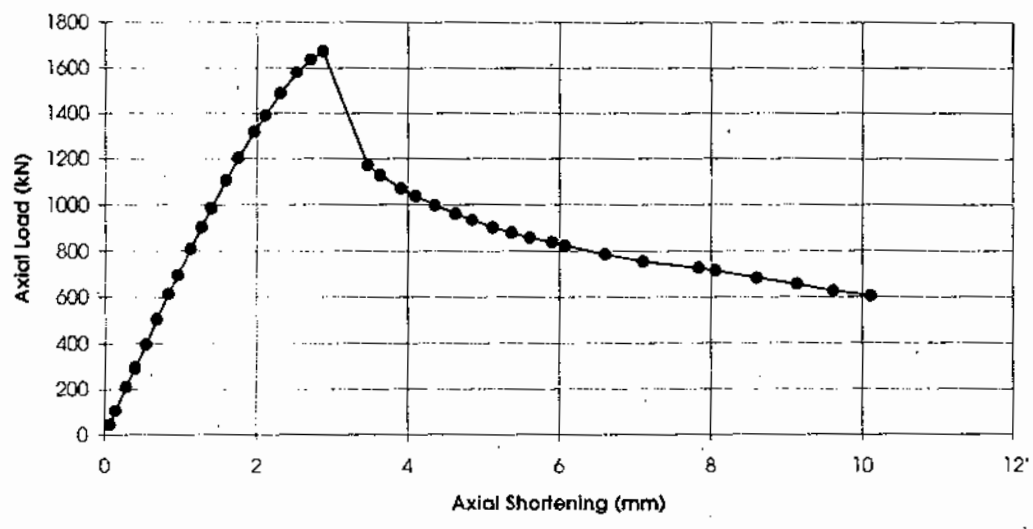
<p>Specimen Type: As-Built</p> <p>Type of Damage/Deformation: N/A</p> <p>Load Configuration: Axial compression with two 10 kN lateral loads. Plate is on the tension side.</p>	<p>Failure Mode: Stiffener Tripping</p> <p>Maximum Axial Load: 1673 kN</p>
<p style="text-align: center;">Test Summary</p> <p><i>Pre-ultimate:</i> Stiffener tripping initiates and amplifies gradually. Plate remains flat.</p> <p><i>At ultimate:</i> Sudden increase in tripping deformation accompanied by sudden, 30% loss in capacity.</p> <p><i>Post-ultimate:</i> Gradual loss in capacity. Continued amplification of stiffener tripping. Plate does not buckle.</p>	<p>Schematic:</p>  <p style="text-align: center;">Cross Section</p> <p style="text-align: center;">Front Elevation</p> <p style="text-align: center;">Side Elevation</p>
 <p style="text-align: center;">Load versus Axial Shortening Response</p>	

TABLE 4-8 TEST RESULTS OF SP1.7

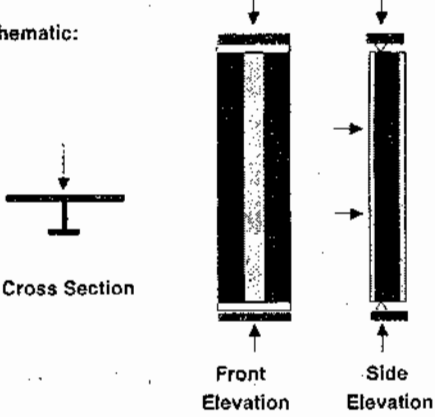
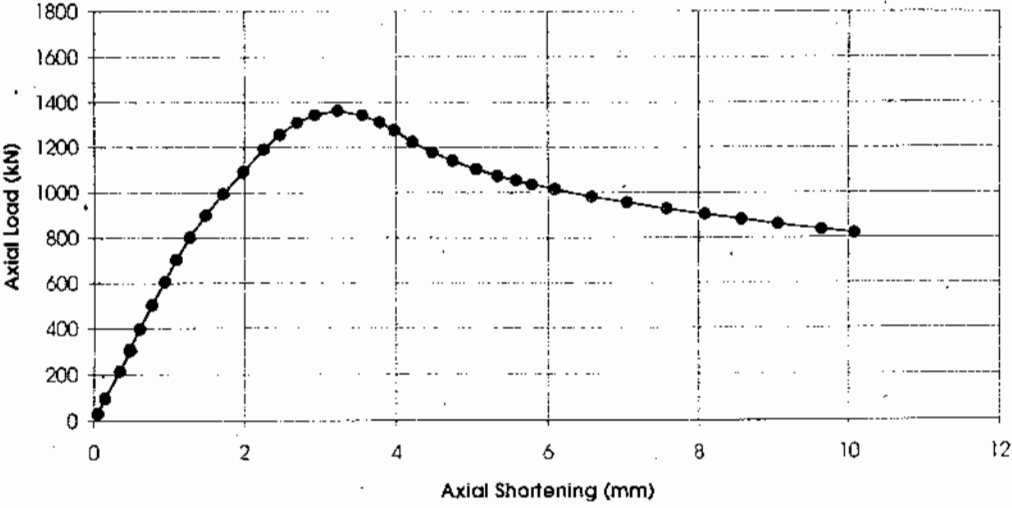
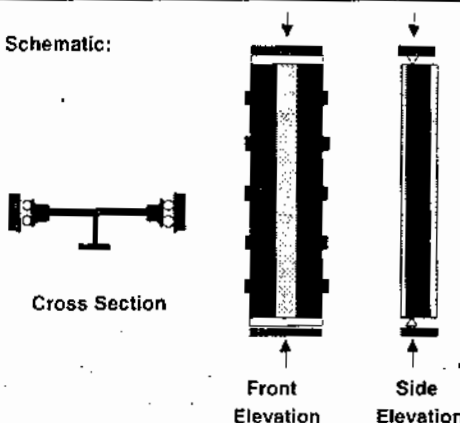
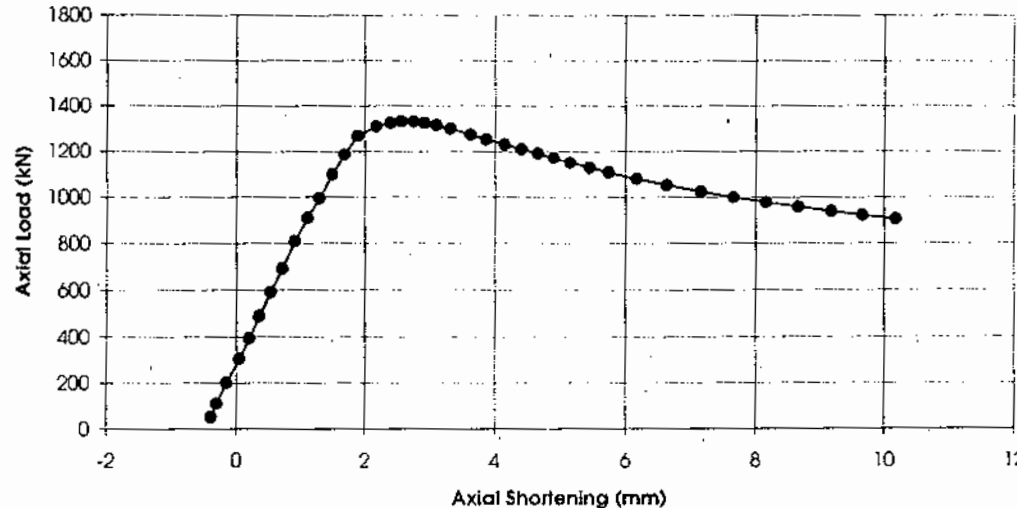
<p>Specimen Type: As-Built</p> <p>Type of Damage/Deformation: N/A</p> <p>Load Configuration: Axial compression with two 25 kN lateral loads. Plate in flexural compression.</p>	<p>Failure Mode: Plate Buckling</p> <p>Maximum Axial Load: 1361 kN</p>
<p style="text-align: center;">Test Summary</p> <p><i>Pre-ultimate:</i> Plate buckling waves initiate and amplify gradually. Stiffener remains straight.</p> <p><i>At ultimate:</i> No change in behavior at ultimate.</p> <p><i>Post-ultimate:</i> Gradual loss in capacity. Continued amplification of buckling waves. Stiffener does not trip.</p>	<p>Schematic:</p>  <p style="text-align: center;">Cross Section</p> <p style="text-align: center;">Front Elevation Side Elevation</p>
 <p style="text-align: center;">Load versus Axial Shortening Response</p>	

TABLE 4-9 TEST RESULTS OF SP2.1

<p>Specimen Type: Deformed</p> <p>Type of Damage/Deformation: Initial deformation of 20 mm at midspan.</p> <p>Load Configuration: Axial compression only.</p>	<p>Failure Mode: Plate Buckling</p> <p>Maximum Axial Load: 1331 kN</p>																														
<p style="text-align: center;">Test Summary</p> <p><i>Pre-ultimate:</i> Plate buckling waves initiate and amplify gradually. Stiffener remains straight.</p> <p><i>At ultimate:</i> No change in behavior at ultimate.</p> <p><i>Post-ultimate:</i> Gradual loss in capacity. Continued amplification of buckling waves. Stiffener does not trip.</p>	<p>Schematic:</p>  <p>The schematic shows three views of the specimen: a 'Cross Section' showing a horizontal beam with a central stiffener, a 'Front Elevation' showing a vertical beam with a central stiffener and buckling waves, and a 'Side Elevation' showing a vertical beam with a central stiffener and buckling waves. Arrows indicate the direction of load application.</p>																														
 <p>The graph plots Axial Load (kN) on the y-axis (0 to 1800) against Axial Shortening (mm) on the x-axis (-2 to 12). The curve shows a peak load of approximately 1331 kN at an axial shortening of about 2.5 mm. After the peak, the load gradually decreases to about 900 kN at 10 mm of axial shortening.</p> <table border="1"> <caption>Approximate data points from the Load versus Axial Shortening Response graph</caption> <thead> <tr> <th>Axial Shortening (mm)</th> <th>Axial Load (kN)</th> </tr> </thead> <tbody> <tr><td>0</td><td>0</td></tr> <tr><td>0.5</td><td>100</td></tr> <tr><td>1.0</td><td>200</td></tr> <tr><td>1.5</td><td>400</td></tr> <tr><td>2.0</td><td>1200</td></tr> <tr><td>2.5</td><td>1331</td></tr> <tr><td>3.0</td><td>1300</td></tr> <tr><td>4.0</td><td>1200</td></tr> <tr><td>5.0</td><td>1100</td></tr> <tr><td>6.0</td><td>1050</td></tr> <tr><td>7.0</td><td>1000</td></tr> <tr><td>8.0</td><td>950</td></tr> <tr><td>9.0</td><td>920</td></tr> <tr><td>10.0</td><td>900</td></tr> </tbody> </table>		Axial Shortening (mm)	Axial Load (kN)	0	0	0.5	100	1.0	200	1.5	400	2.0	1200	2.5	1331	3.0	1300	4.0	1200	5.0	1100	6.0	1050	7.0	1000	8.0	950	9.0	920	10.0	900
Axial Shortening (mm)	Axial Load (kN)																														
0	0																														
0.5	100																														
1.0	200																														
1.5	400																														
2.0	1200																														
2.5	1331																														
3.0	1300																														
4.0	1200																														
5.0	1100																														
6.0	1050																														
7.0	1000																														
8.0	950																														
9.0	920																														
10.0	900																														

Load versus Axial Shortening Response

TABLE 4-10 TEST RESULTS OF SP2.2

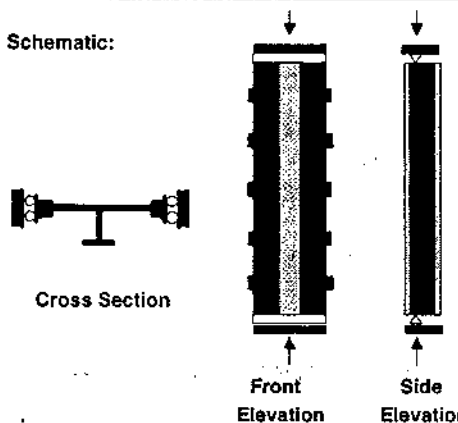
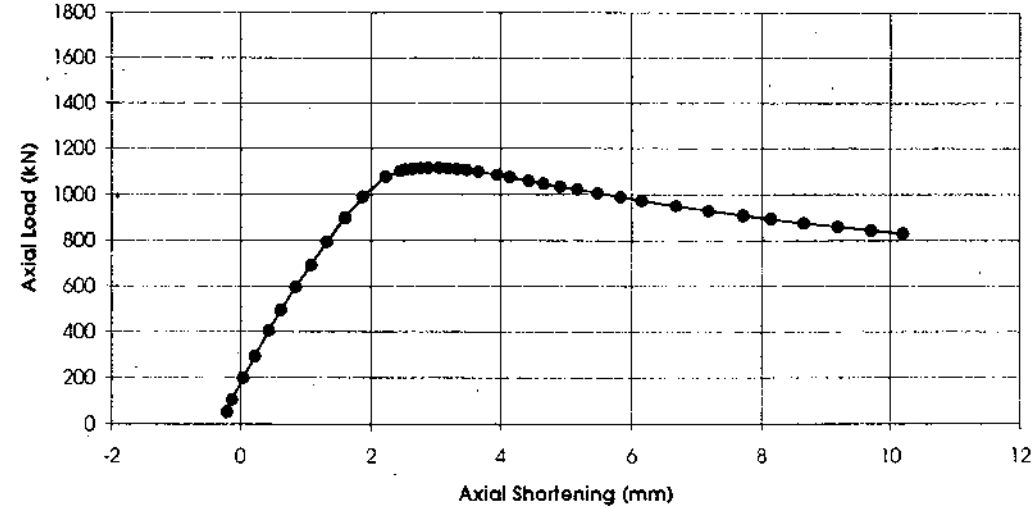
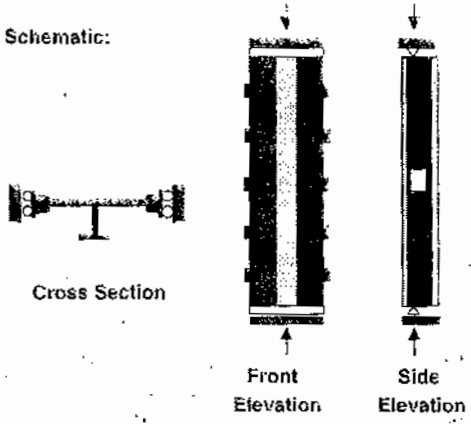
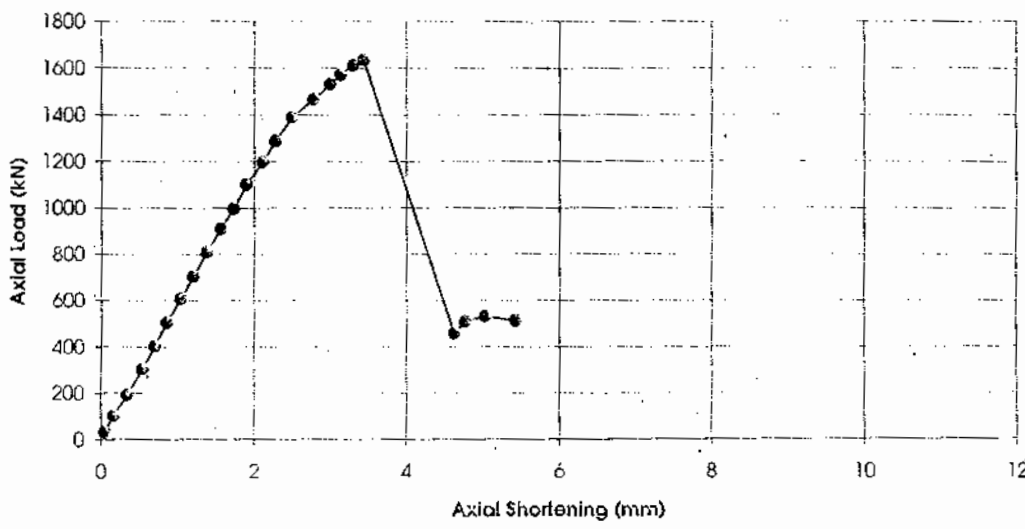
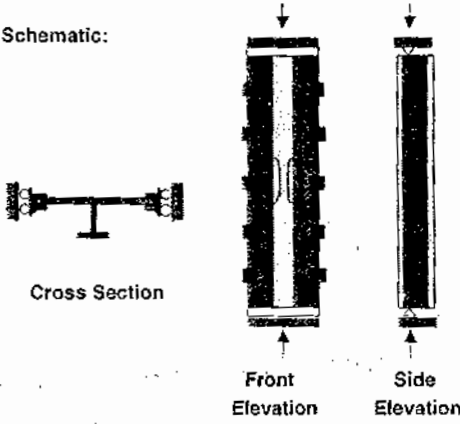
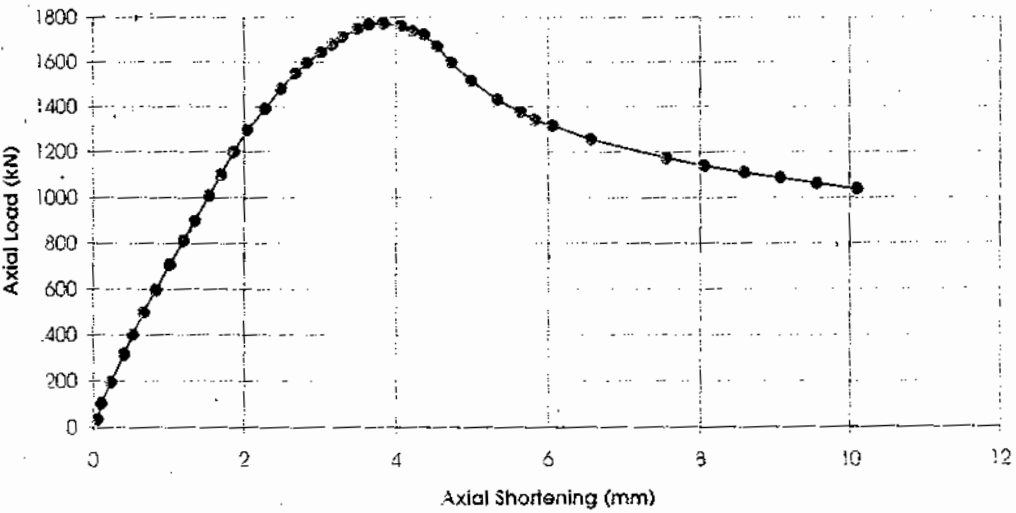
<p>Specimen Type: Deformed</p> <p>Type of Damage/Deformation: Initial deformation of 35 mm at midspan.</p> <p>Load Configuration: Axial compression only.</p>	<p>Failure Mode: Plate Buckling</p> <p>Maximum Axial Load: 1116 kN</p>
<p style="text-align: center;">Test Summary</p> <p><i>Pre-ultimate:</i> Plate buckling waves initiate and amplify gradually. Stiffener remains straight.</p> <p><i>At ultimate:</i> No change in behavior at ultimate.</p> <p><i>Post-ultimate:</i> Gradual loss in capacity. Continued amplification of buckling waves. Stiffener does not trip.</p>	<p>Schematic:</p>  <p style="text-align: center;">Cross Section</p> <p style="text-align: center;">Front Elevation</p> <p style="text-align: center;">Side Elevation</p>
 <p style="text-align: center;">Load versus Axial Shortening Response</p>	

TABLE 4-11 TEST RESULTS OF SP3.1

<p>Specimen Type: Damaged</p> <p>Type of Damage/Deformation: Local damage to stiffener web at midspan.</p> <p>Load Configuration: Axial compression only.</p>	<p>Failure Mode: Local failure (midspan portion buckles in the plane of the web).</p> <p>Maximum Axial Load: 1636 kN</p>																																																				
<p style="text-align: center;">Test Summary</p> <p><i>Pre-ultimate:</i> Plate buckling waves initiate and amplify gradually. Stiffener remains straight.</p> <p><i>At ultimate:</i> Midspan portion (about 200 mm long) suddenly buckles in the plane of the web. Plate buckling waves disperse.</p> <p><i>Post-ultimate:</i> Deformation concentrates at midspan in vicinity of web "damage". Specimen suffers dramatic loss in axial load capacity.</p>	<p>Schematic:</p>  <p style="text-align: center;">Cross Section</p> <p style="text-align: center;">Front Elevation Side Elevation</p>																																																				
 <table border="1"> <caption>Approximate data points from the Load versus Axial Shortening Response graph</caption> <thead> <tr> <th>Axial Shortening (mm)</th> <th>Axial Load (kN)</th> </tr> </thead> <tbody> <tr><td>0.0</td><td>0</td></tr> <tr><td>0.5</td><td>100</td></tr> <tr><td>1.0</td><td>200</td></tr> <tr><td>1.5</td><td>300</td></tr> <tr><td>2.0</td><td>400</td></tr> <tr><td>2.5</td><td>500</td></tr> <tr><td>3.0</td><td>600</td></tr> <tr><td>3.5</td><td>700</td></tr> <tr><td>4.0</td><td>800</td></tr> <tr><td>4.5</td><td>900</td></tr> <tr><td>5.0</td><td>1000</td></tr> <tr><td>5.5</td><td>1100</td></tr> <tr><td>6.0</td><td>1200</td></tr> <tr><td>6.5</td><td>1300</td></tr> <tr><td>7.0</td><td>1400</td></tr> <tr><td>7.5</td><td>1500</td></tr> <tr><td>8.0</td><td>1600</td></tr> <tr><td>8.5</td><td>1636</td></tr> <tr><td>9.0</td><td>1600</td></tr> <tr><td>9.5</td><td>1500</td></tr> <tr><td>10.0</td><td>1400</td></tr> <tr><td>10.5</td><td>1300</td></tr> <tr><td>11.0</td><td>1200</td></tr> <tr><td>11.5</td><td>1100</td></tr> <tr><td>12.0</td><td>1000</td></tr> </tbody> </table>		Axial Shortening (mm)	Axial Load (kN)	0.0	0	0.5	100	1.0	200	1.5	300	2.0	400	2.5	500	3.0	600	3.5	700	4.0	800	4.5	900	5.0	1000	5.5	1100	6.0	1200	6.5	1300	7.0	1400	7.5	1500	8.0	1600	8.5	1636	9.0	1600	9.5	1500	10.0	1400	10.5	1300	11.0	1200	11.5	1100	12.0	1000
Axial Shortening (mm)	Axial Load (kN)																																																				
0.0	0																																																				
0.5	100																																																				
1.0	200																																																				
1.5	300																																																				
2.0	400																																																				
2.5	500																																																				
3.0	600																																																				
3.5	700																																																				
4.0	800																																																				
4.5	900																																																				
5.0	1000																																																				
5.5	1100																																																				
6.0	1200																																																				
6.5	1300																																																				
7.0	1400																																																				
7.5	1500																																																				
8.0	1600																																																				
8.5	1636																																																				
9.0	1600																																																				
9.5	1500																																																				
10.0	1400																																																				
10.5	1300																																																				
11.0	1200																																																				
11.5	1100																																																				
12.0	1000																																																				

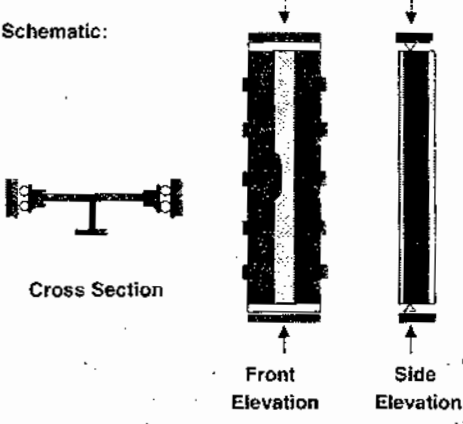
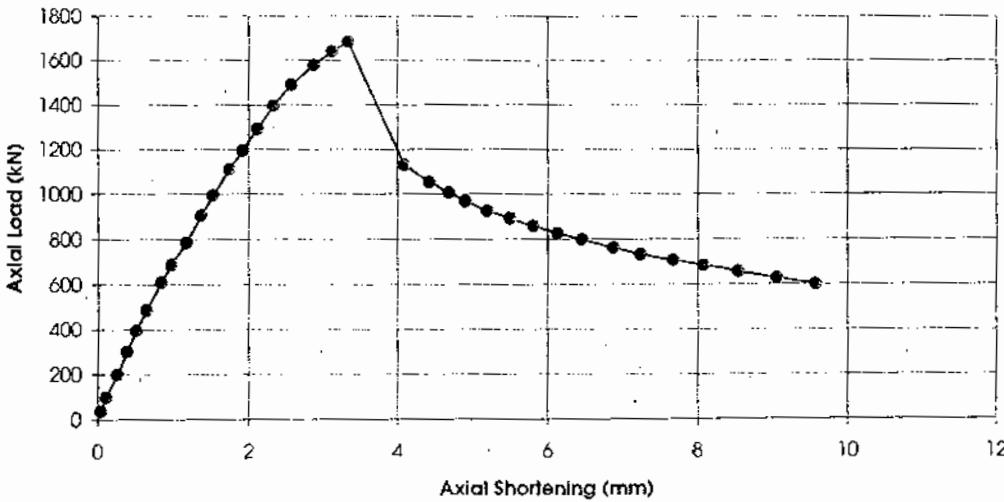
Load versus Axial Shortening Response

TABLE 4-12 TEST RESULTS OF SP3.2

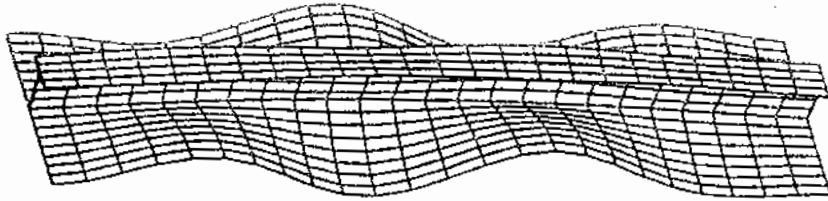
<p>Specimen Type: Damaged</p> <p>Type of Damage/Deformation: Local damage to stiffener flange at midspan (symmetric).</p> <p>Load Configuration: Axial compression only.</p>	<p>Failure Mode: Plate Buckling</p> <p>Maximum Axial Load: 1773 kN</p>																																		
<p>Test Summary</p> <p><i>Pre-ultimate:</i> Plate buckling waves initiate and amplify gradually. Stiffener remains straight.</p> <p><i>At ultimate:</i> No change in behavior at ultimate. Damage to flange has little impact on behavior and capacity.</p> <p><i>Post-ultimate:</i> Gradual loss in capacity. Continued amplification of buckling waves. Stiffener does not trip.</p>	<p>Schematic:</p>  <p>Cross Section</p> <p>Front Elevation</p> <p>Side Elevation</p>																																		
 <table border="1"> <caption>Approximate data points from the Load versus Axial Shortening Response graph</caption> <thead> <tr> <th>Axial Shortening (mm)</th> <th>Axial Load (kN)</th> </tr> </thead> <tbody> <tr><td>0</td><td>0</td></tr> <tr><td>0.5</td><td>300</td></tr> <tr><td>1.0</td><td>600</td></tr> <tr><td>1.5</td><td>900</td></tr> <tr><td>2.0</td><td>1200</td></tr> <tr><td>2.5</td><td>1400</td></tr> <tr><td>3.0</td><td>1550</td></tr> <tr><td>3.5</td><td>1650</td></tr> <tr><td>4.0</td><td>1773</td></tr> <tr><td>4.5</td><td>1700</td></tr> <tr><td>5.0</td><td>1550</td></tr> <tr><td>6.0</td><td>1350</td></tr> <tr><td>7.0</td><td>1250</td></tr> <tr><td>8.0</td><td>1150</td></tr> <tr><td>9.0</td><td>1100</td></tr> <tr><td>10.0</td><td>1050</td></tr> </tbody> </table>		Axial Shortening (mm)	Axial Load (kN)	0	0	0.5	300	1.0	600	1.5	900	2.0	1200	2.5	1400	3.0	1550	3.5	1650	4.0	1773	4.5	1700	5.0	1550	6.0	1350	7.0	1250	8.0	1150	9.0	1100	10.0	1050
Axial Shortening (mm)	Axial Load (kN)																																		
0	0																																		
0.5	300																																		
1.0	600																																		
1.5	900																																		
2.0	1200																																		
2.5	1400																																		
3.0	1550																																		
3.5	1650																																		
4.0	1773																																		
4.5	1700																																		
5.0	1550																																		
6.0	1350																																		
7.0	1250																																		
8.0	1150																																		
9.0	1100																																		
10.0	1050																																		

Load versus Axial Shortening Response

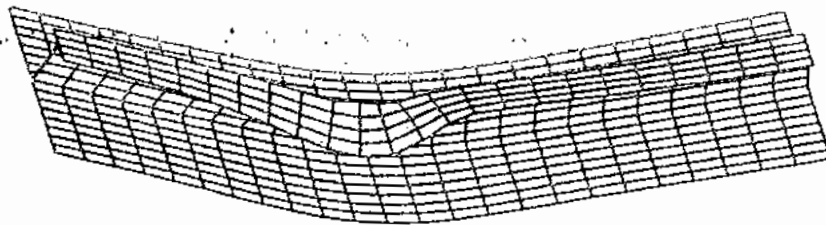
TABLE 4-13 TEST RESULTS OF SP3.3

<p>Specimen Type: Damaged</p> <p>Type of Damage/Deformation: Local damage to stiffener flange at midspan(unsymmetric).</p> <p>Load Configuration: Axial compression only.</p>	<p>Failure Mode: Stiffener Tripping</p> <p>Maximum Axial Load: 1683 kN</p>																																						
<p style="text-align: center;">Test Summary</p> <p><i>Pre-ultimate:</i> Plate buckling waves and stiffener tripping are observed. Both amplify gradually.</p> <p><i>At ultimate:</i> Sudden increase in tripping deformation accompanied by 30% loss in capacity. Plate buckling waves become insignificant.</p> <p><i>Post-ultimate:</i> Gradual loss in capacity. Tripping deformations in vicinity of local damage.</p>	<p>Schematic:</p>  <p style="text-align: center;">Cross Section</p> <p style="text-align: center;">Front Elevation Side Elevation</p>																																						
 <table border="1"> <caption>Approximate data points from the Load versus Axial Shortening Response graph</caption> <thead> <tr> <th>Axial Shortening (mm)</th> <th>Axial Load (kN)</th> </tr> </thead> <tbody> <tr><td>0.0</td><td>0</td></tr> <tr><td>0.5</td><td>100</td></tr> <tr><td>1.0</td><td>200</td></tr> <tr><td>1.5</td><td>400</td></tr> <tr><td>2.0</td><td>600</td></tr> <tr><td>2.5</td><td>800</td></tr> <tr><td>3.0</td><td>1000</td></tr> <tr><td>3.5</td><td>1200</td></tr> <tr><td>4.0</td><td>1400</td></tr> <tr><td>4.5</td><td>1500</td></tr> <tr><td>5.0</td><td>1600</td></tr> <tr><td>5.5</td><td>1683</td></tr> <tr><td>6.0</td><td>1500</td></tr> <tr><td>7.0</td><td>1000</td></tr> <tr><td>8.0</td><td>800</td></tr> <tr><td>9.0</td><td>700</td></tr> <tr><td>10.0</td><td>650</td></tr> <tr><td>11.0</td><td>600</td></tr> </tbody> </table>		Axial Shortening (mm)	Axial Load (kN)	0.0	0	0.5	100	1.0	200	1.5	400	2.0	600	2.5	800	3.0	1000	3.5	1200	4.0	1400	4.5	1500	5.0	1600	5.5	1683	6.0	1500	7.0	1000	8.0	800	9.0	700	10.0	650	11.0	600
Axial Shortening (mm)	Axial Load (kN)																																						
0.0	0																																						
0.5	100																																						
1.0	200																																						
1.5	400																																						
2.0	600																																						
2.5	800																																						
3.0	1000																																						
3.5	1200																																						
4.0	1400																																						
4.5	1500																																						
5.0	1600																																						
5.5	1683																																						
6.0	1500																																						
7.0	1000																																						
8.0	800																																						
9.0	700																																						
10.0	650																																						
11.0	600																																						

Load versus Axial Shortening Response



(a) Plate Buckling



(b) Stiffener Tripping

Figure 4-1 Buckling Mode for Stiffened Plate under Axial Compression



Figure 4-3 Specimen SP1.1 at Peak Load

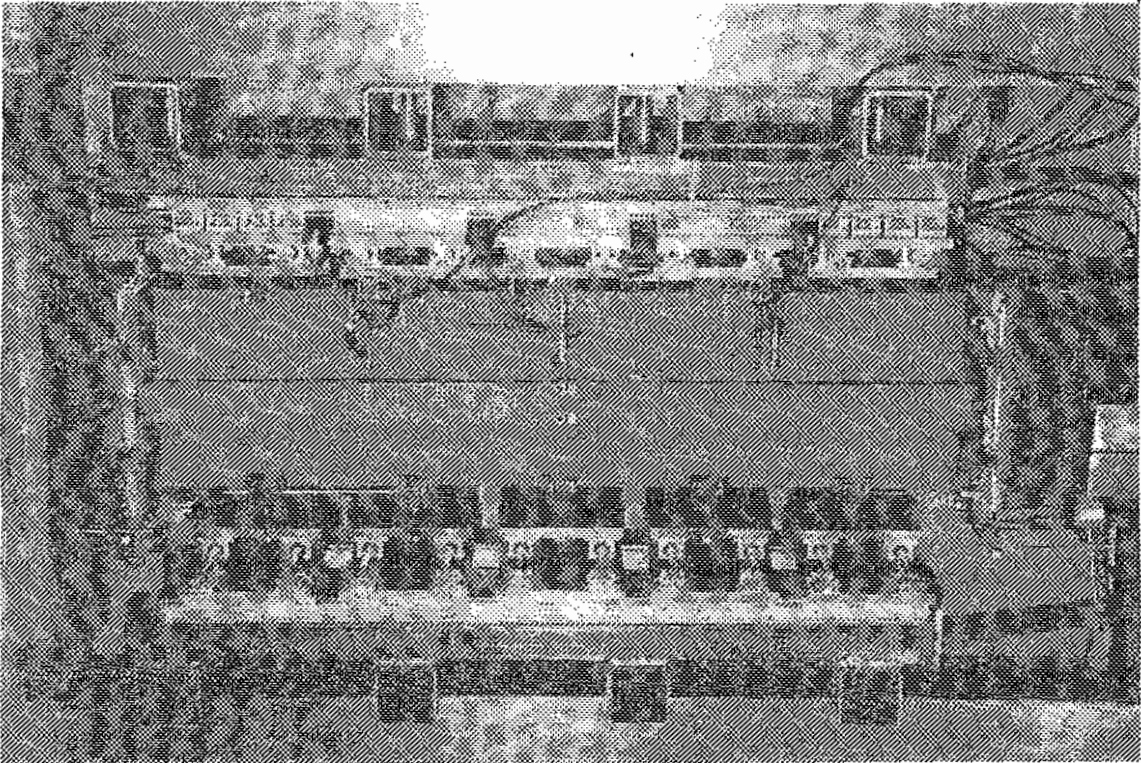


Figure 4-2 Specimen SP1.1 before Test

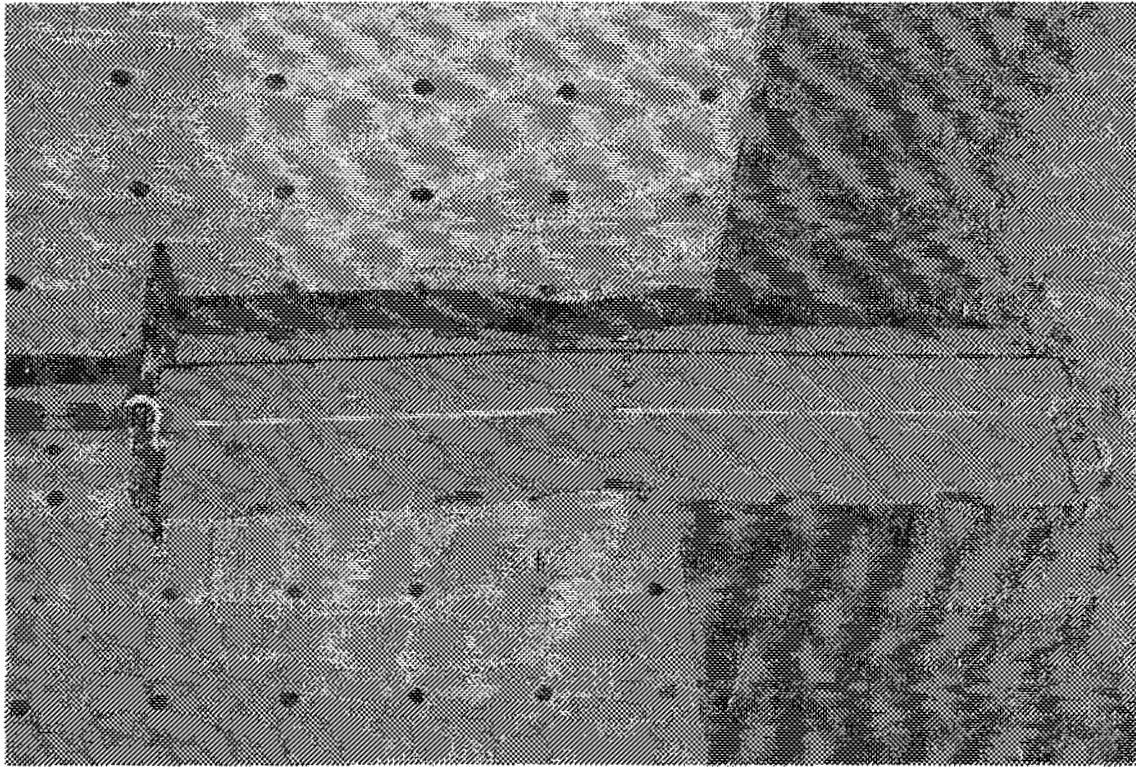


Figure 4-5 Deformed Shape of SP1.1 (front)

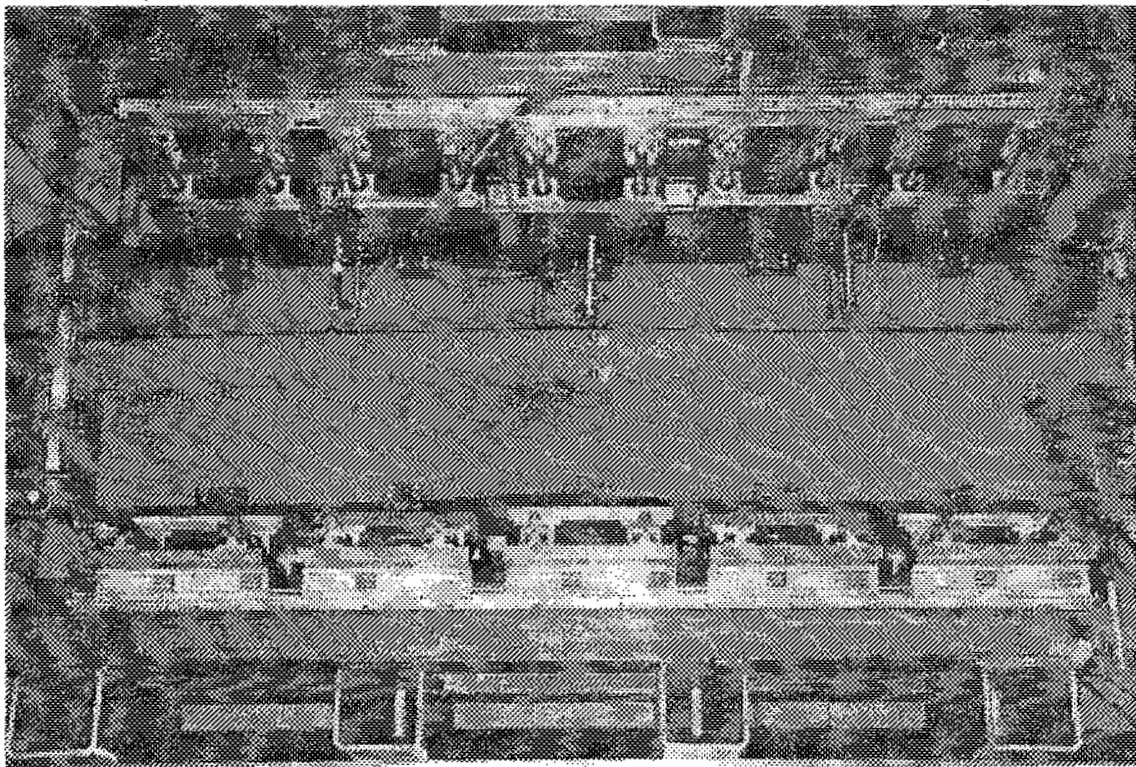


Figure 4-4 Specimen SP1.1 at the End of Test

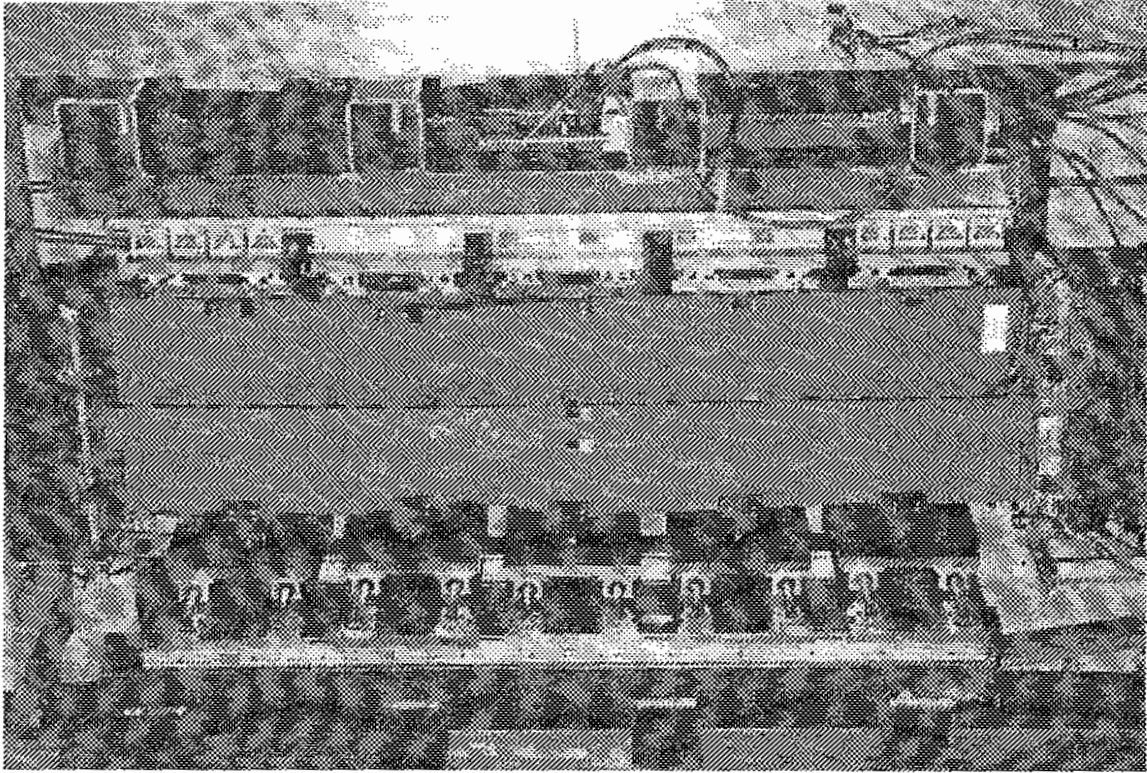


Figure 4-7 Deformed Shape of SP1.2

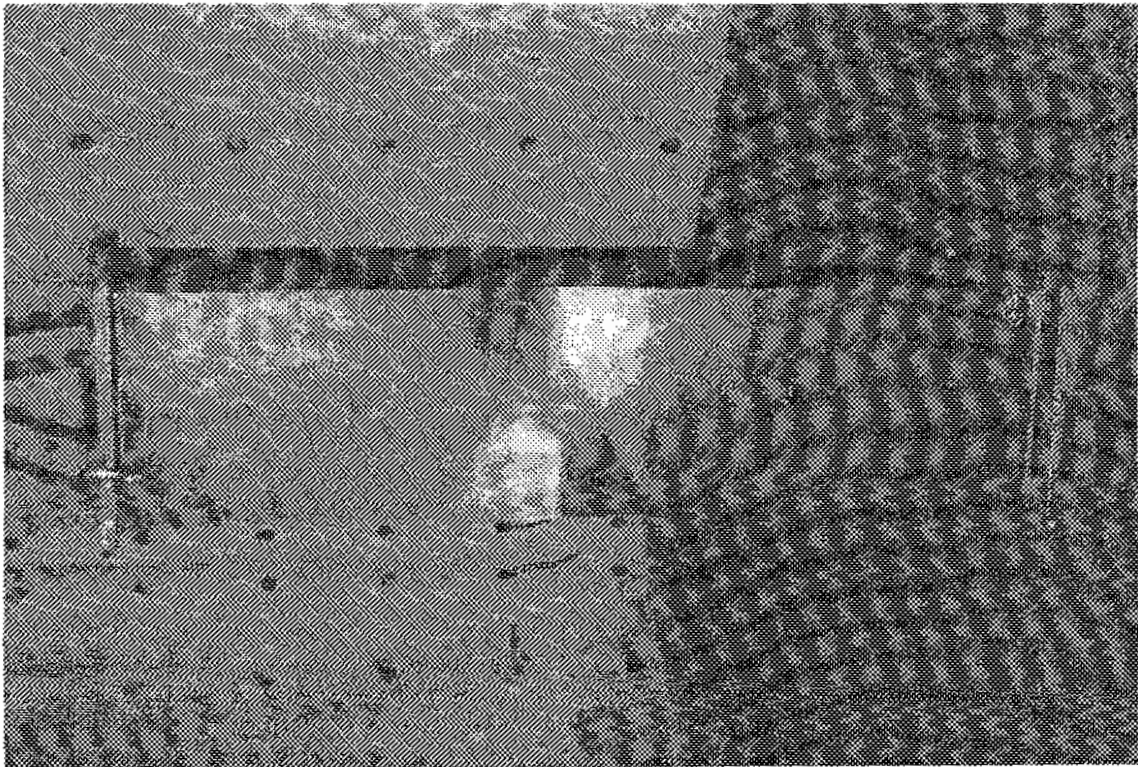


Figure 4-6 Deformed Shape of SP1.1 (back)

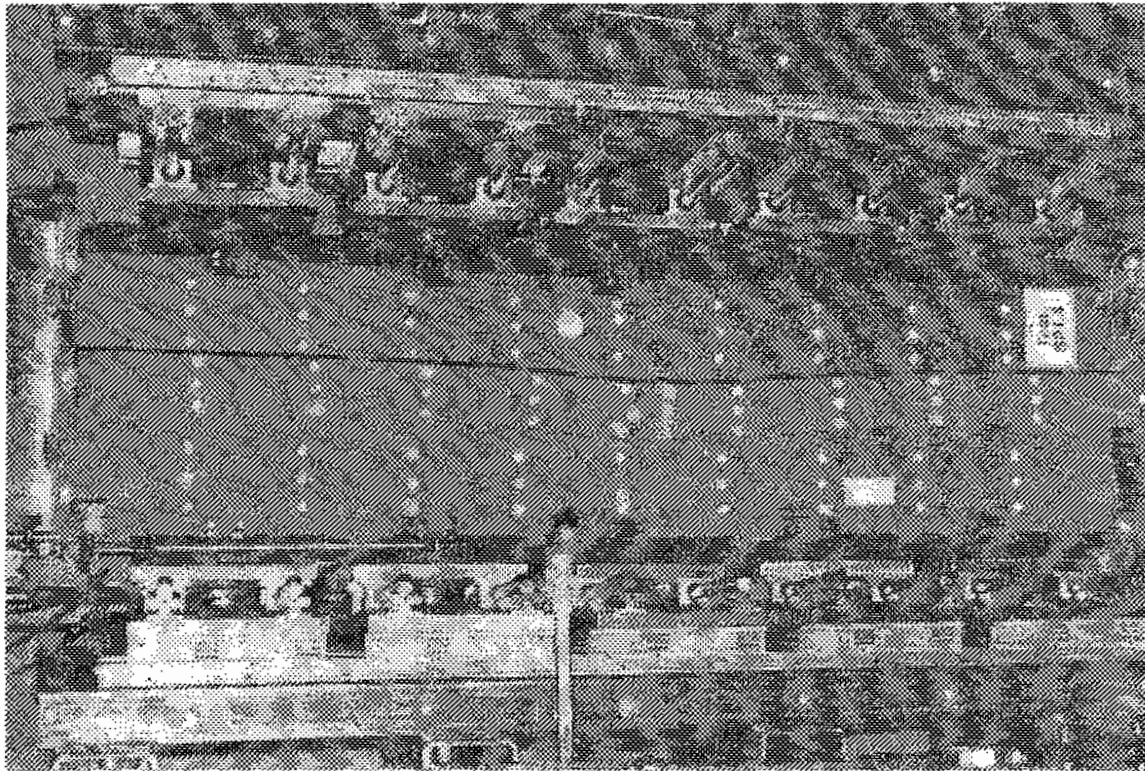


Figure 4-9 Deformed Shape of SP1.4

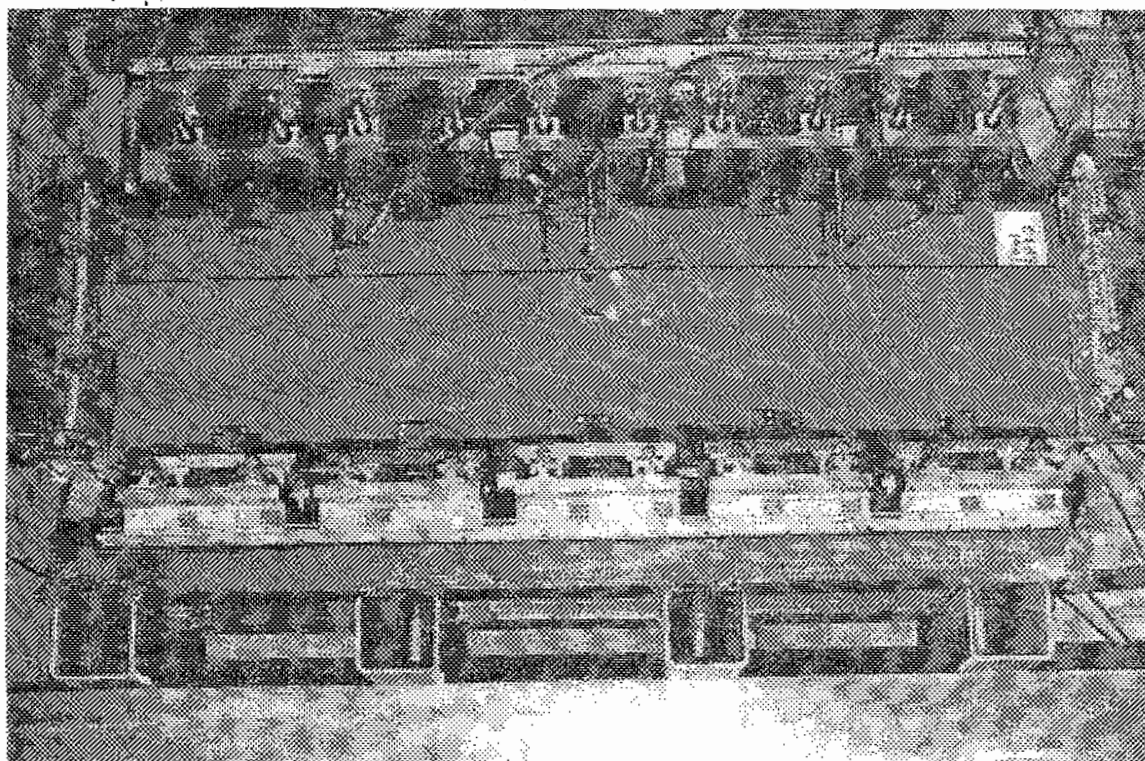


Figure 4-8 Deformed Shape of SP1.3

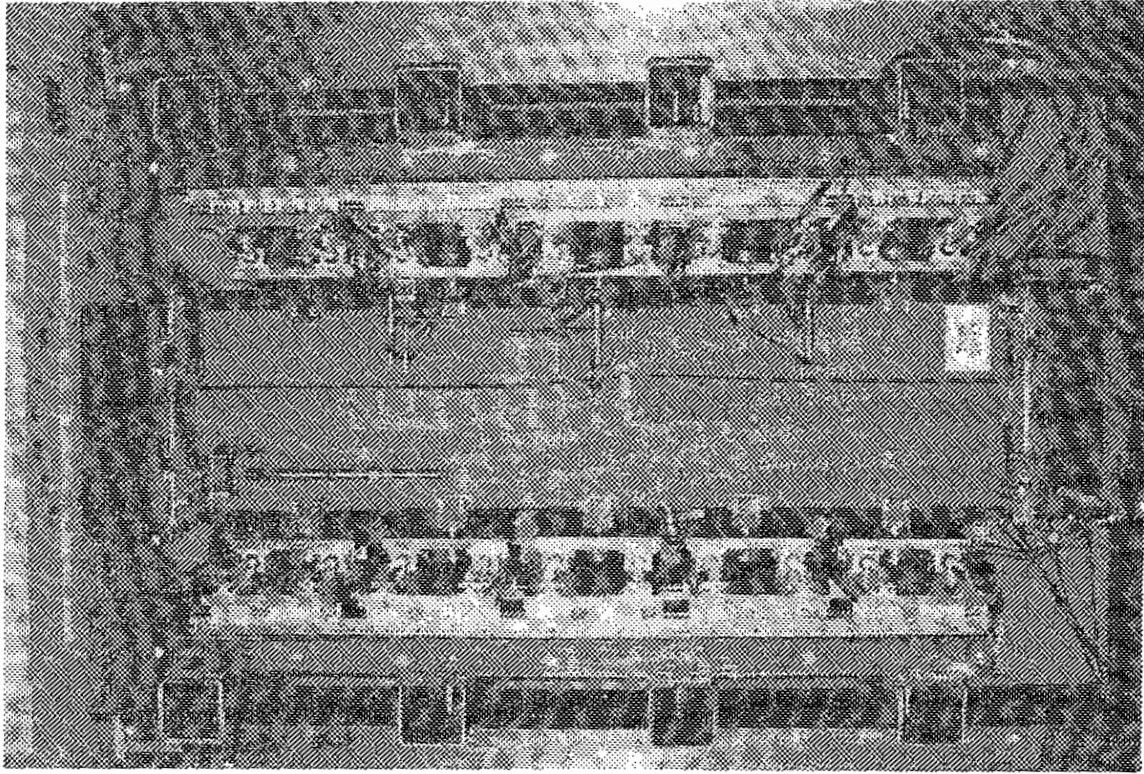


Figure 4-11 Deformed Shape of SP1.6

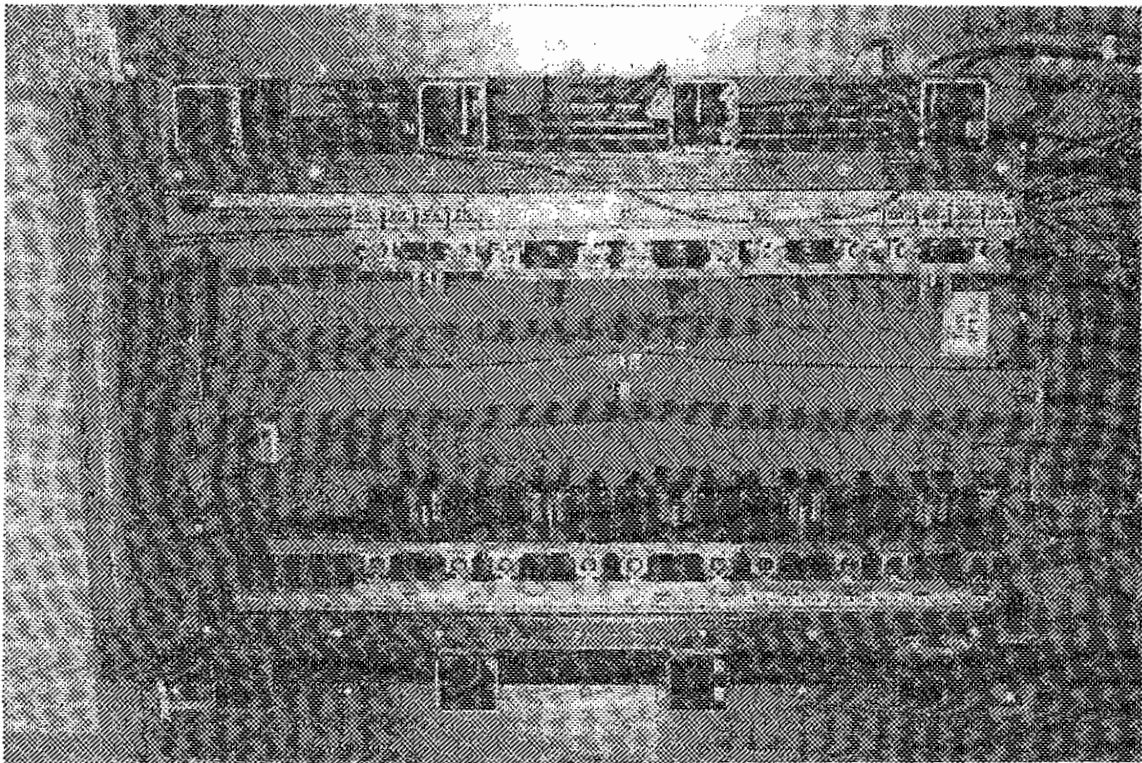


Figure 4-10 Deformed Shape of SP1.5

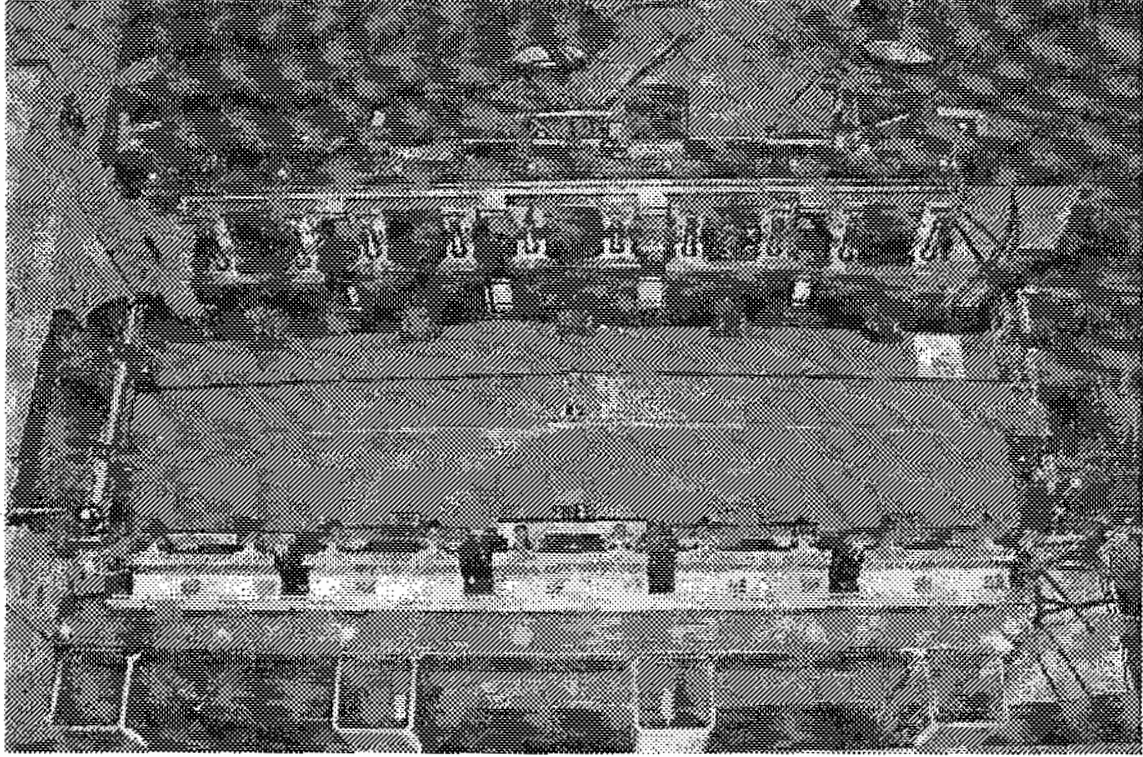


Figure 4-13 Deformed Shape of SP2.1

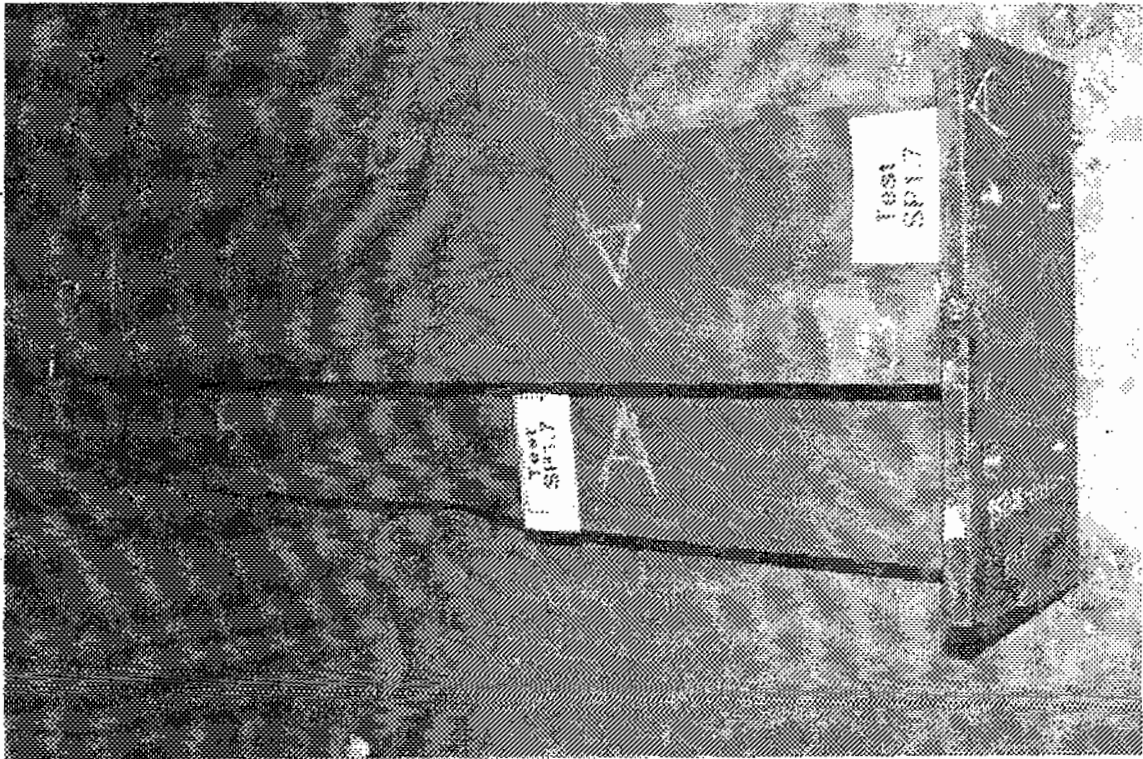


Figure 4-12 Deformed Shape of SP1.7

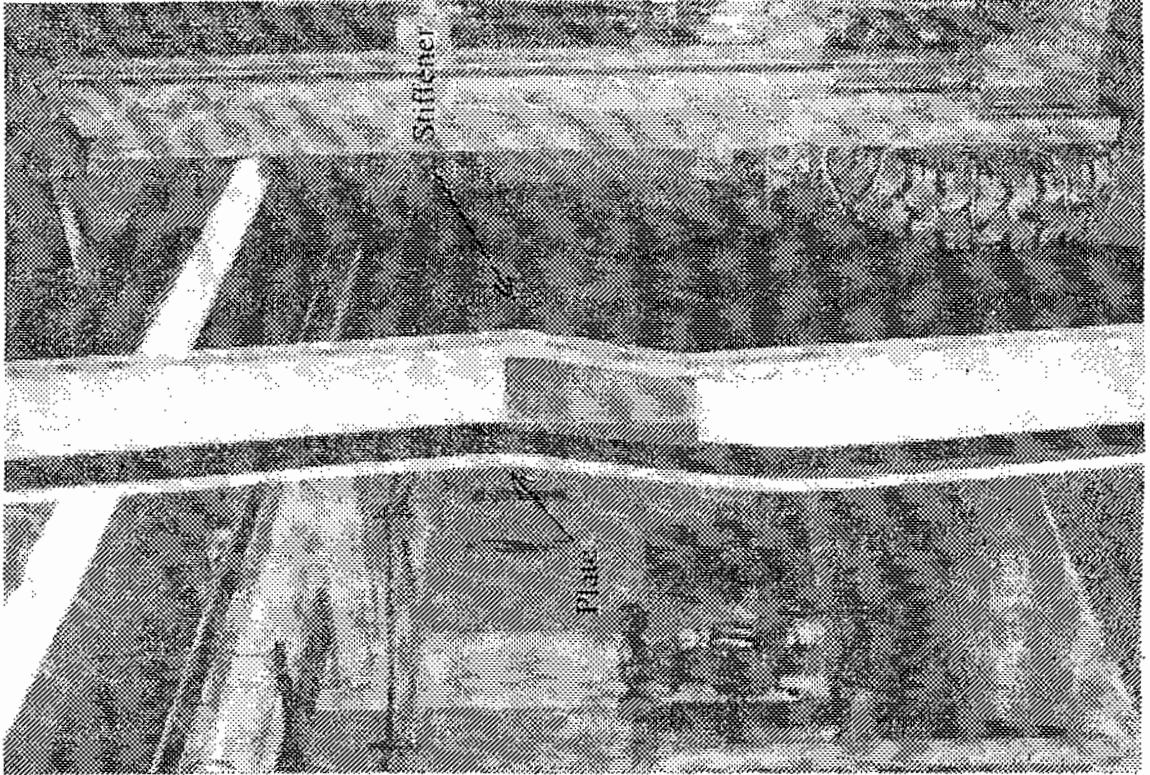


Figure 4-15 Deformed Shape of SP3.1

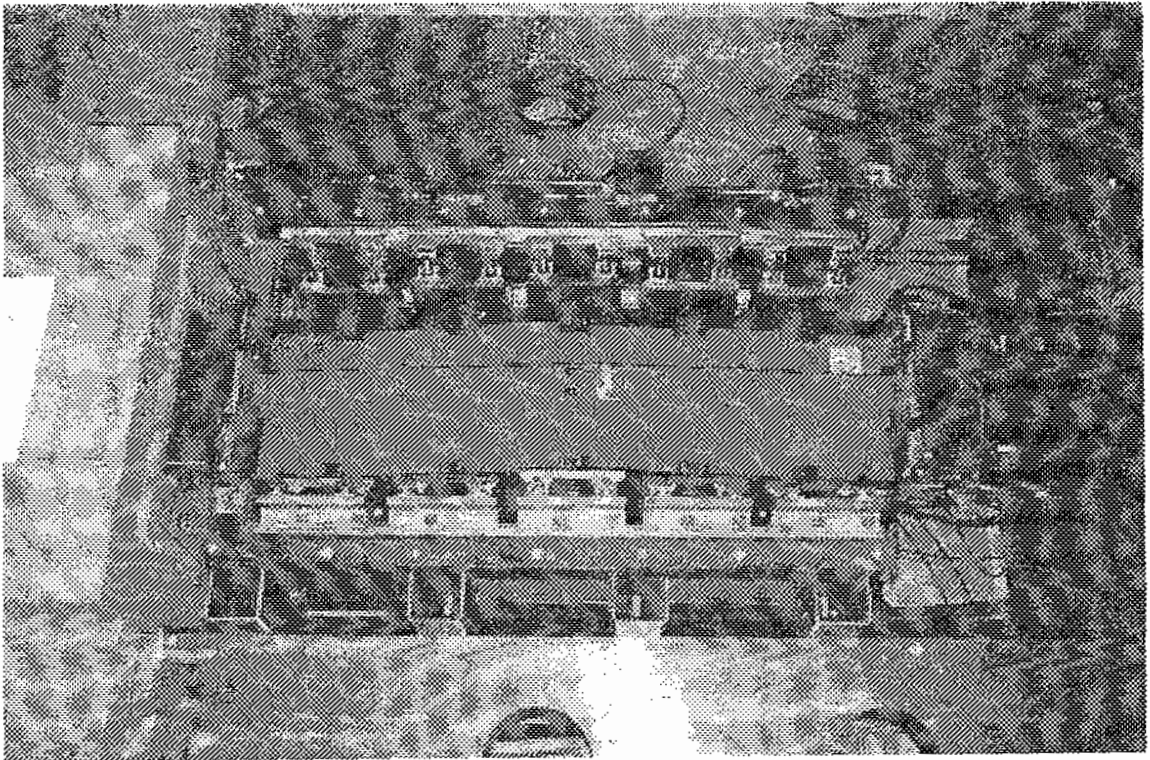


Figure 4-14 Deformed Shape of SP2.2

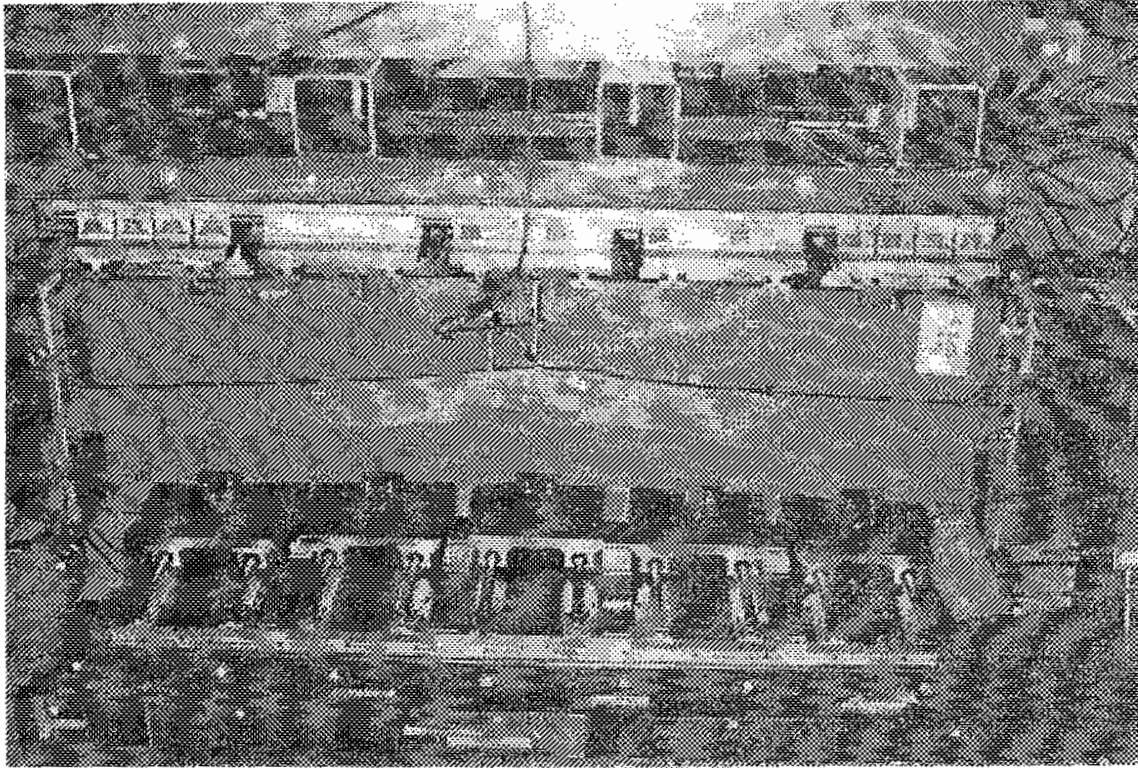


Figure 4-17 Deformed Shape of SP3.3

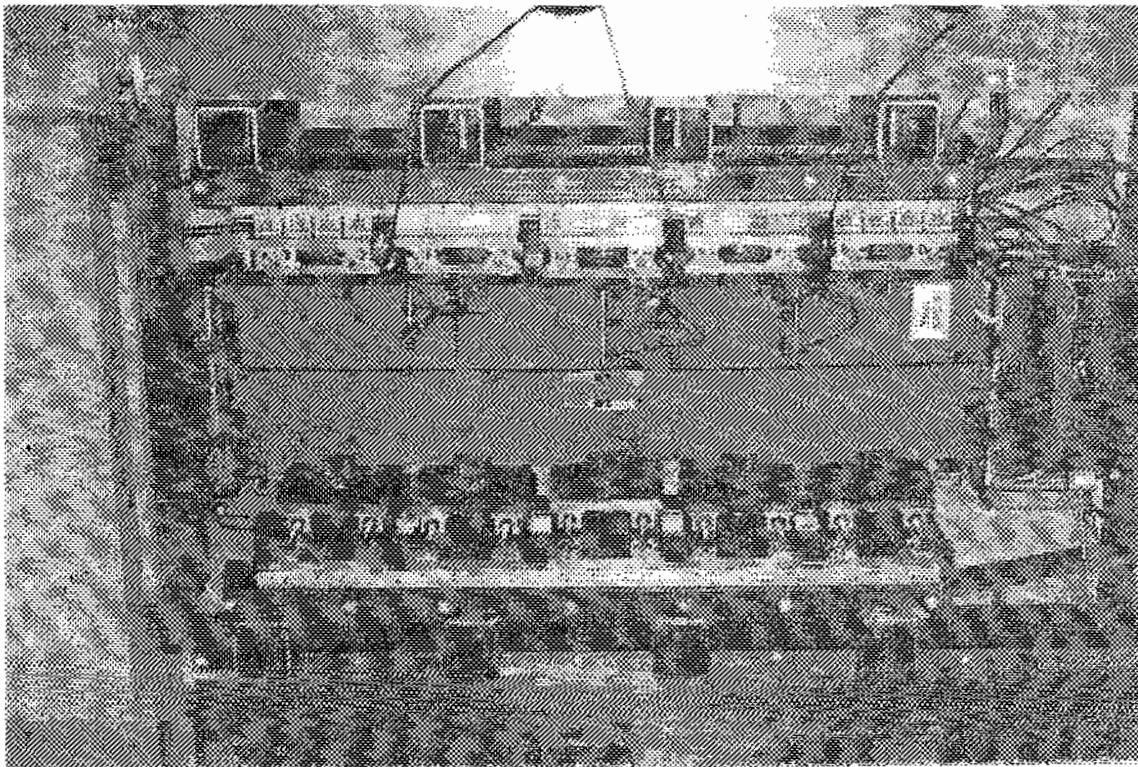


Figure 4-16 Deformed Shape of SP3.2

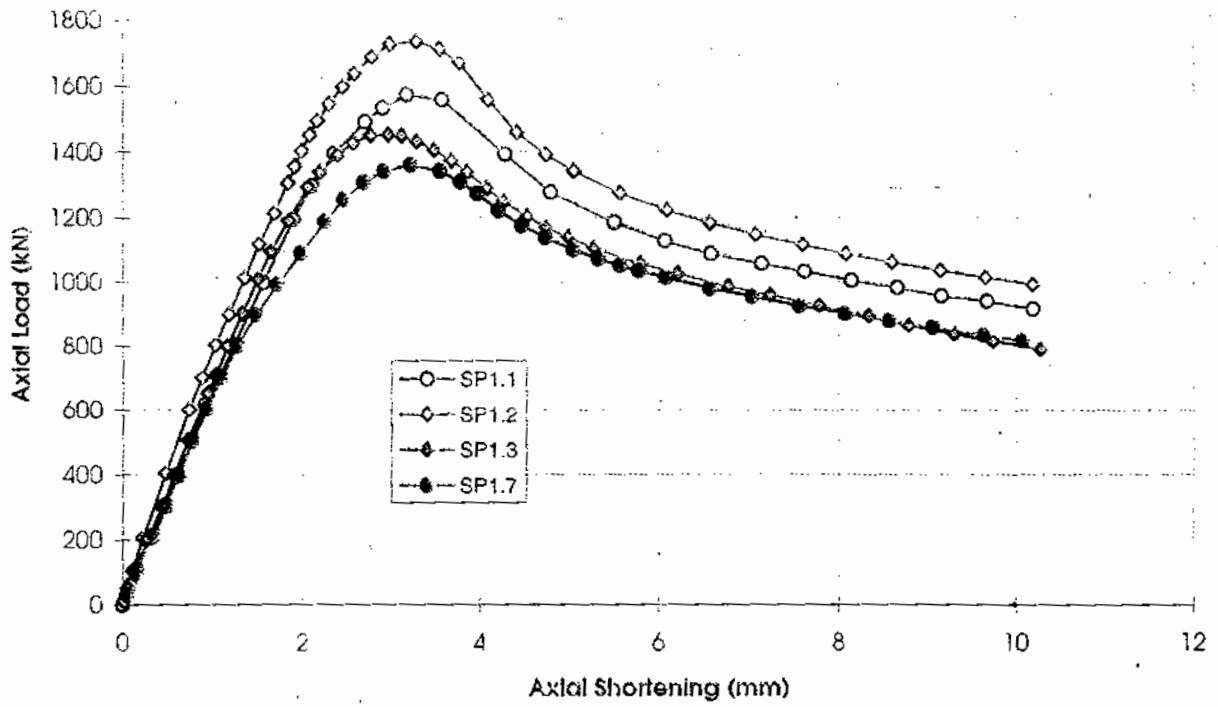


Figure 4-18 Axial Load versus Axial Shortening Response for Plate Buckling

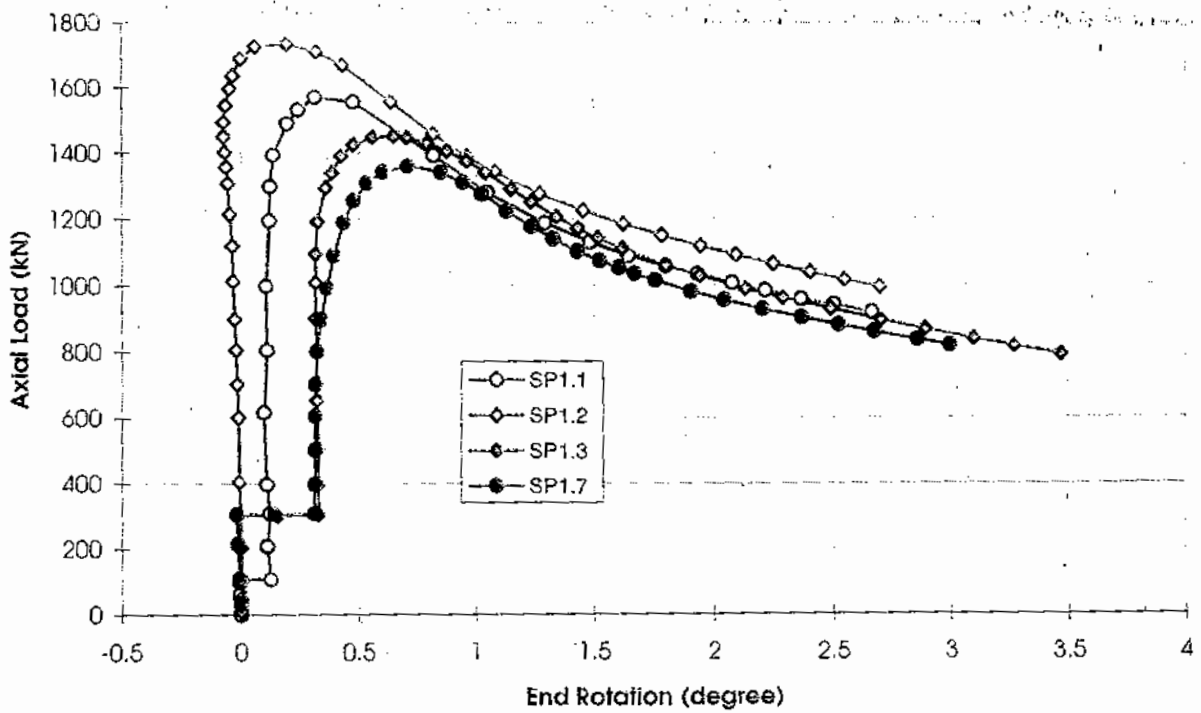


Figure 4-19 Axial Load versus End Rotation Response for Plate Buckling

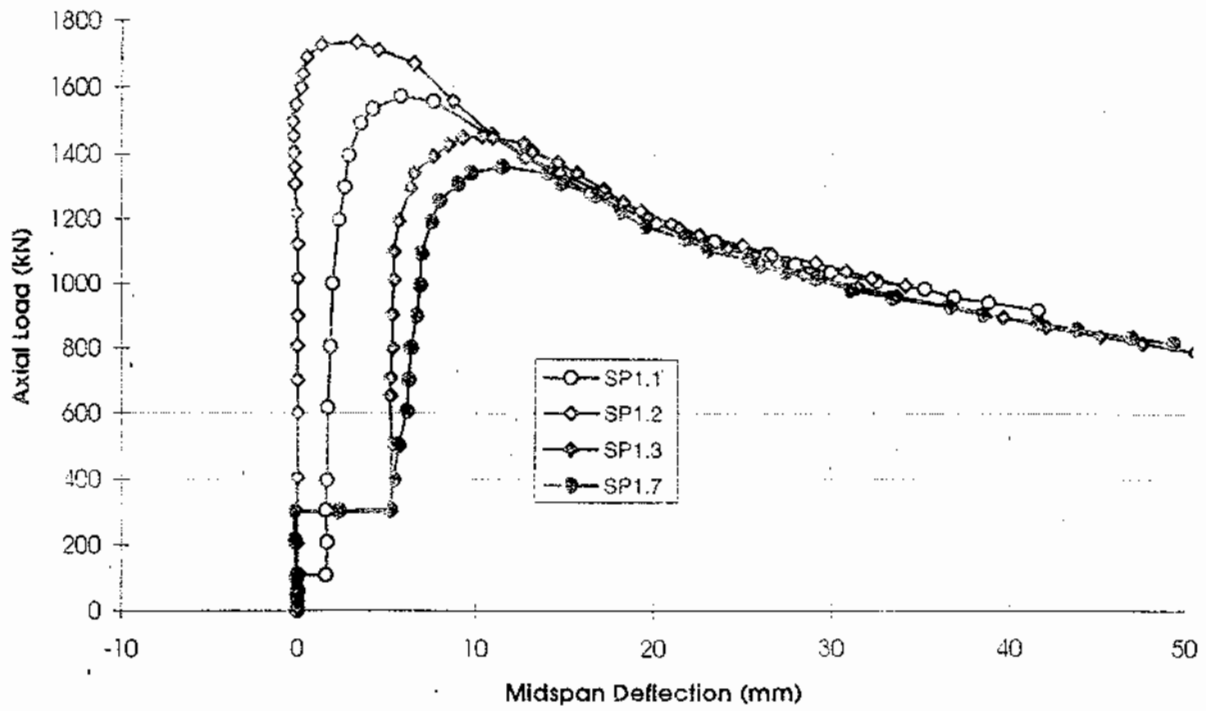


Figure 4-20 Axial Load versus Midspan Deflection Response for Plate Buckling

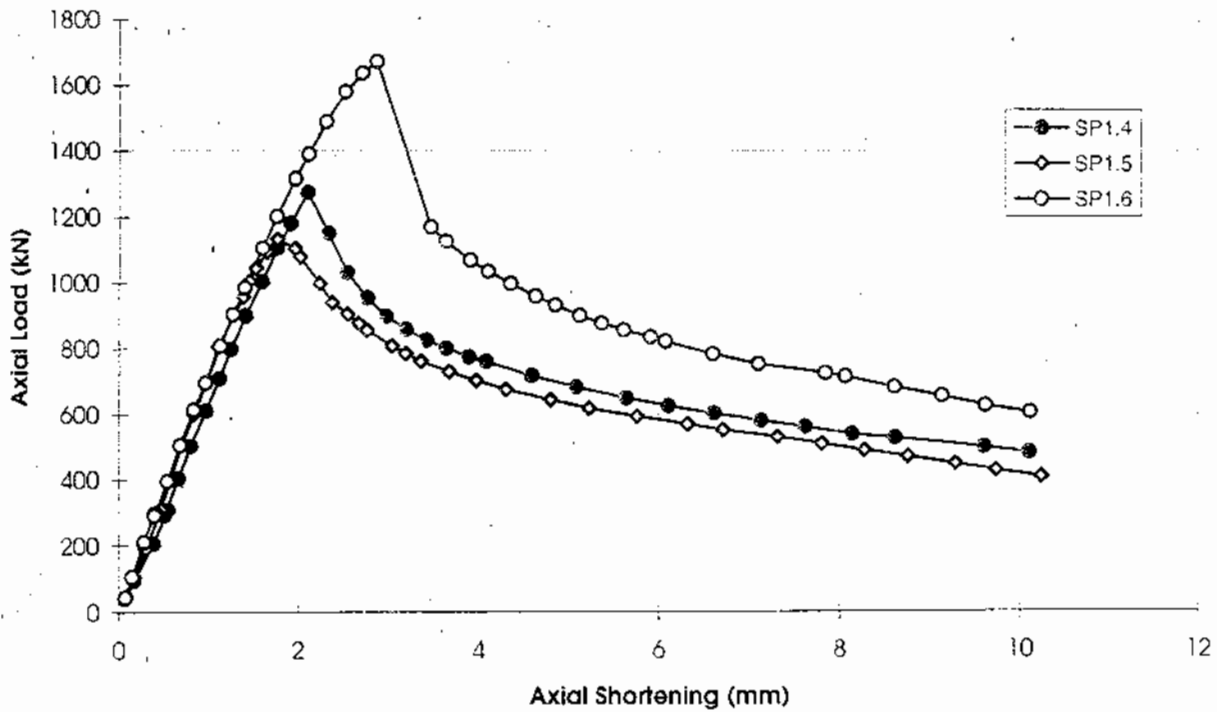


Figure 4-21 Axial Load versus Axial Shortening Response for Stiffener Tripping

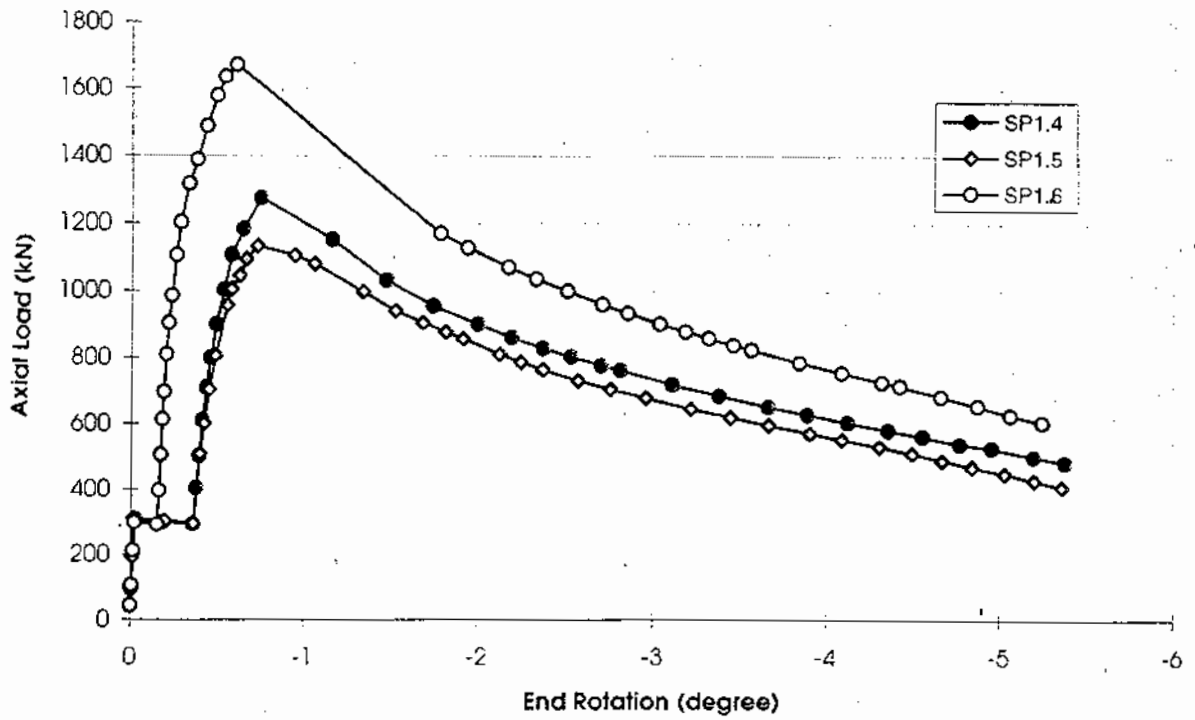


Figure 4-22 Axial Load versus End Rotation Response for Stiffener Tripping

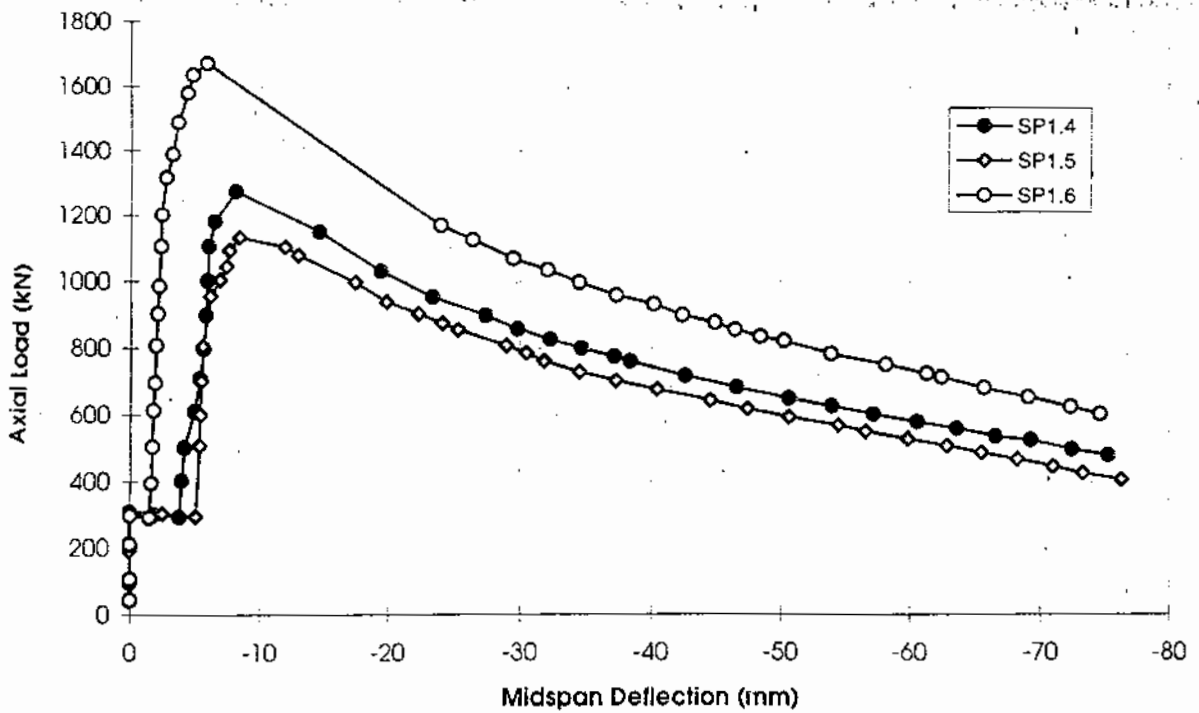


Figure 4-23 Axial Load versus Midspan Deflection Response for Stiffener Tripping

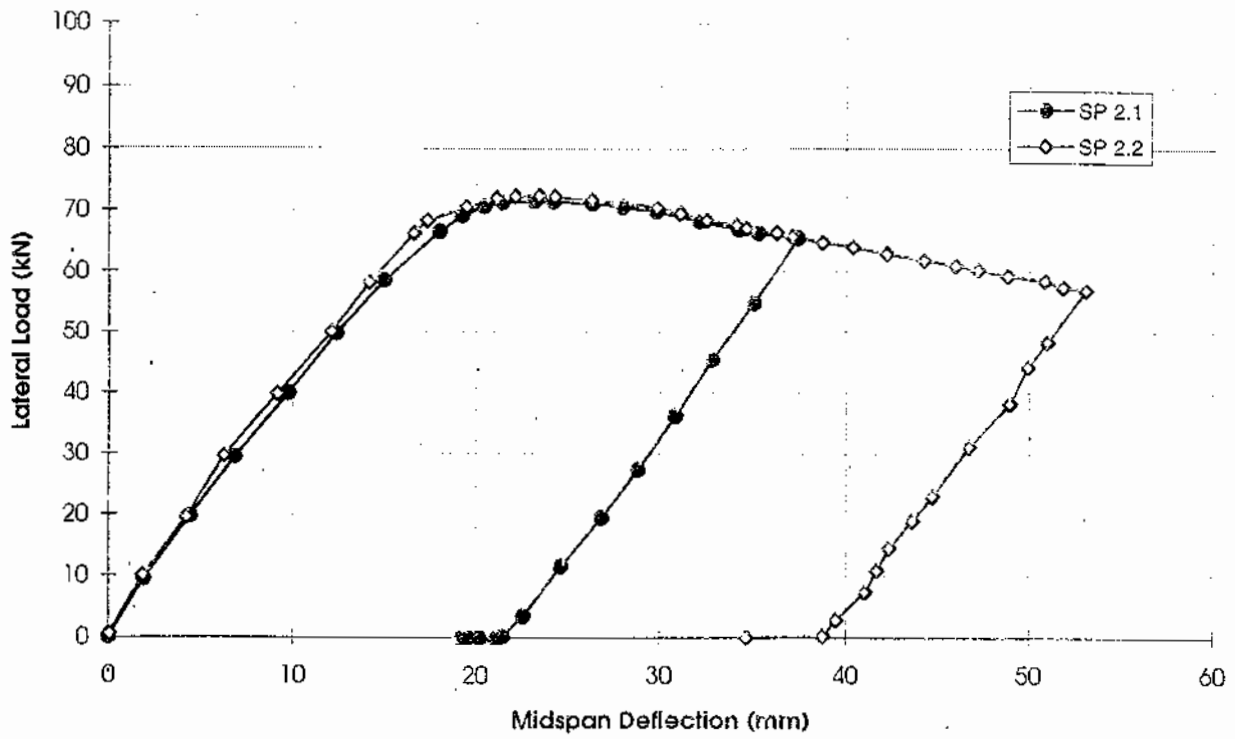


Figure 4-24 Lateral Load versus Midspan Deflection for "Deformation" Cycle

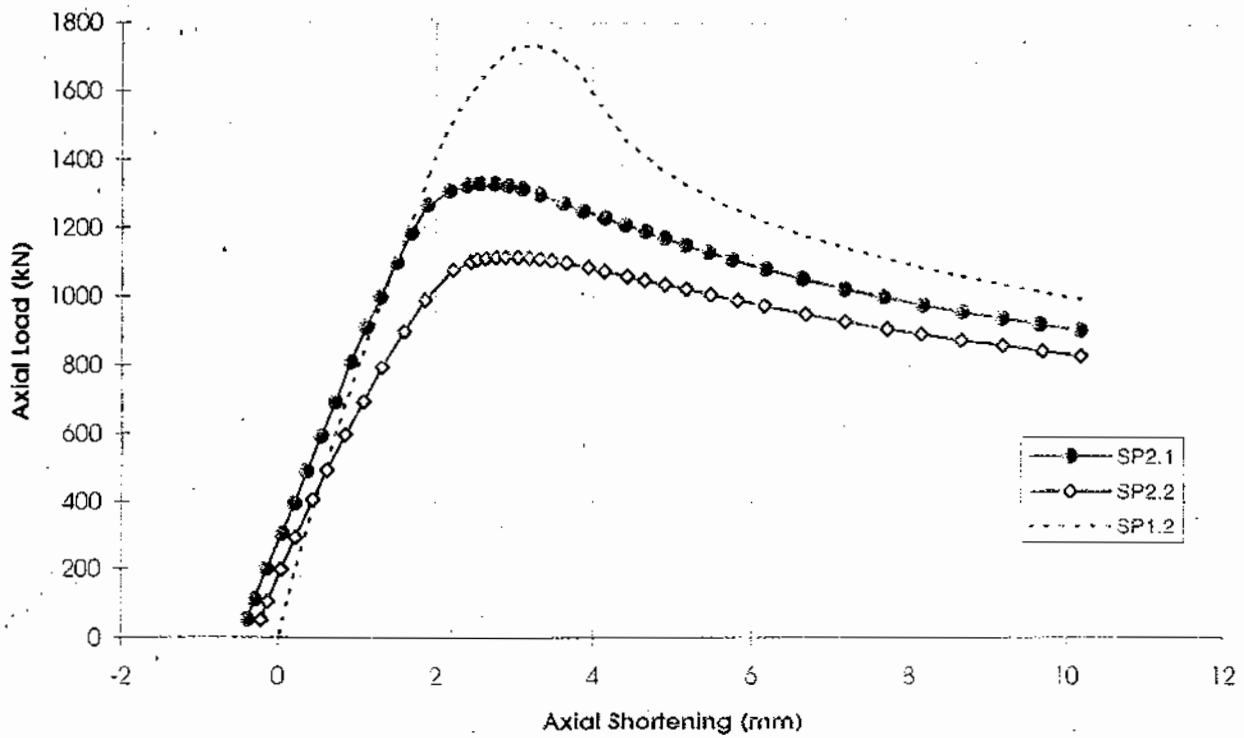


Figure 4-25 Axial Load versus Axial Shortening Response for Deformed Specimens

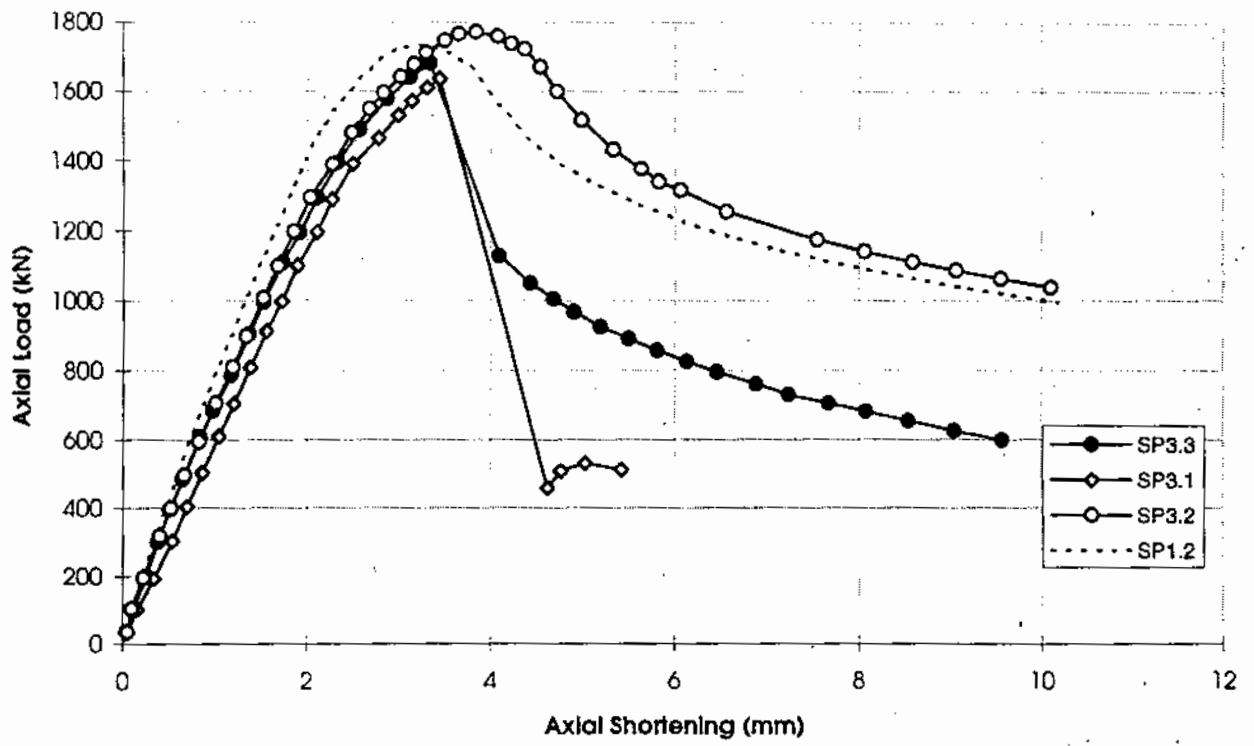


Figure 4-26 Axial Load versus Axial Shortening Response for Damaged Specimens

5.0 FINITE ELEMENT ANALYSIS

The purpose of the finite element work was to determine the accuracy with which a numerical model could predict the full-scale tests. Appropriate load combinations, boundary conditions, residual stresses and initial imperfections were all taken into account. Details of the model and analyses are given in Appendix A. This section provides an overview of the numerical model and compares the results of the finite element analyses with the test results.

5.1 Numerical Model

The finite element work was conducted using ABAQUS, a general purpose finite element program with advanced nonlinear analysis capabilities. ABAQUS is well suited for work in which global and local stability are key factors in determining ultimate capacity and where both material and geometric nonlinearities are important.

Key elements of the finite element model included:

- Elements: The model consisted of 512 S4R shell elements (Figure 5-1). The S4R is a four-noded shell element based on a finite strain formulation.
- Material Model: The input stress-strain relationship was defined using true stresses and strains, converted from the engineering stresses and strains obtained from the material tests. Metal plasticity was modelled by a tri-linear stress-strain curve with a von Mises yield surface and isotropic hardening.
- End Supports: A rigid segment, 38 mm in length, was used to connect the specimen ends to a simple support which represented the center of the cylindrical bearing. This accurately modelled the axial load which always passed through that center (Figure 2-5). Since the lateral load acted at the bearing circumference and not the center, however, the lateral reaction was modelled with a force and an end moment, which equaled the product of the force and the radius of the bearing.
- Plate Edge Restraints: To restrain θ_η in a deformed configuration (Section 2.2.1), short rigid beams perpendicular to the plate edge were attached to the plate via rigid connections. Y-displacements of these rigid beams were restrained to prevent tangential rotation θ_η . This approach was adapted because ABAQUS does not permit direct reference to rotations in a deformed system. In other finite element programs, such as ADINA, a direct restraint for θ_η could be used.
- Imperfections: The X-Y-Z coordinates of the specimen were defined by the imperfection measurements described in Section 3.2. The interpolation and extrapolation of the measurement grid to the finite element nodes assumed linear variations longitudinally in the specimen and transversely in the stiffener web and flange. Quadratic curves were used transversely across the plate.
- Residual Stresses: Axial residual stresses were generated by specifying a fictitious temperature field prior to applying loads, and by specifying orthotropic thermal material properties for the specimens. Displacements caused by this temperature field were recorded and then subtracted from the initial coordinates so that the model contained

measured imperfections and residual stresses that were consistent with those measured in the specimens.

- **Loading:** Loading procedures were analogous to those used in the physical tests. Lateral loads were applied first using the Newton-Raphson method and then held constant. Axial load was applied using displacement control.

The effect of large displacements was accounted for by using a Total Lagrange Formulation. An effective solution for capturing the nonlinear post-buckling behavior was achieved using the modified Ricks algorithm.

5.2 Comparison with Test Results

Five full-scale tests were selected for comparative analysis purposes. The five cases analyzed were:

- Specimens SP1.1 and SP1.3, two “as-built” specimens which failed by plate buckling;
- Specimen SP1.4, an “as-built” specimen which failed by stiffener tripping;
- Specimen SP1.5, an “as-built” specimen without plate edge restraints; and
- Specimen SP2.1, a “deformed” specimen.

By comparing the post-test deformed shape of the test specimens with the finite element analysis predictions shown in Appendix A, it was apparent that all analyses successfully identified the correct buckling mode. Good agreement was also found between test and predicted capacity, as shown in Table A-1. On average, the analysis over-estimated the ultimate capacity by less than 3%.

Figures 5-2 to 5-4 present comparisons of the finite element analyses to the observed behavior of specimens SP1.1 and SP1.3. In both cases the numerical results predicted the ductile failure behavior with satisfactory accuracy. Test to predicted ratios of 0.99 and 1.01 were obtained for these two specimens respectively.

Results comparisons for specimens SP1.4 and SP1.5 are shown graphically in Figures 5-5 to 5-7. These specimens were subjected to the same lateral load as SP1.4, but were restrained by discrete supports, while SP1.5 had free boundaries. The finite element predictions reproduced the main characteristics of the load-displacement curve for these specimens, such as the sharp drop in load capacity immediately following attainment of the peak load.

For the “deformed” specimen (SP2.1), the analysis included both the test and the pre-test “deformation” cycle. Figures 5-9 and 5-10 illustrate that the tests are well predicted by the model. For the “deformation” cycle, Appendix A shows that the prediction of both maximum lateral load and the residual displacement agreed with the test results.

5.3 Summary

The finite element work clearly demonstrates the ability of state-of-the-art finite element analytical techniques to accurately predict both failure mode and failure load of stiffened steel plate components of the type tested in this research program. This will allow future parametric FEA work to proceed with some confidence that the results are accurate and meaningful.

6.0 CONCLUSIONS AND RECOMMENDATIONS

6.1 Conclusions

This project successfully developed an experimental testing system for conducting buckling tests of single stiffened steel plate components representative of those used in ship structure design. The high capacity testing system provides the capability to test stiffened steel plate specimens under combined in-plane and out-of-plane loads, while maintaining an accurate representation of the actual boundary conditions applicable to a unidirectional stiffened plate within a grillage system.

The twelve full-scale tests conducted, demonstrated the use and functionality of the system and the importance of accurately representing plate edge boundary conditions. Test data, useful in its own right for establishing load-shortening curves, was obtained for a number of different loading conditions and specimen damage configurations.

Finally, the analytical phase of work clearly demonstrated the ability of current nonlinear finite element analyses techniques to accurately model structures of this type. For the test specimens analyzed, both the buckling mode and the failure load were accurately predicted.

6.2 Recommendations for Future Research

The focus of the work described in this report was the development of a testing system for studying the buckling response of stiffened steel plate systems. Only limited experimental work was conducted, basically to provide proof-of-concept. The first, and most obvious, recommendation for future research work is to conduct additional experiments using this setup in order to study different aspects of stiffened panel strength and behaviour.

The experimental work in this study considered only a few combinations of the various parameters that affect strength and behaviour (loading combination and direction, geometry, boundary restraint, initial imperfections and residual stresses, and location and pattern of damage). Additional experimental work can be used to more fully explore the effect of the various parameters and to generate a broad spectrum of load-displacement response for various initial conditions. In particular, more “damaged” specimens need to be tested. Depending on the type of damage sustained, behaviour can change radically. This is an important consideration in assessing the fitness-for-purpose of damaged ship hulls. Large-scale tests of multiple panels, or grillage systems, are also desirable in order to study the interaction between panels and the effect on ultimate strength and post-buckling response.

Additional parametric numerical analysis work is also recommended. The finite element model developed in this study provided accurate predictions of the test results, which suggests that it can be used with confidence to analytically study stiffened plate behaviour under a variety of different conditions. The results of a parametric FEA study could be used

to augment the experimental database. This would greatly facilitate the further development and verification of other analytical approaches, including reliability-based design approaches with the ability to take parameter and model uncertainties into account in determining probabilities of failure.

7.0 ACKNOWLEDGMENTS

The work of Professors J. J. Cheng, A. E. Elwi, G. Y. Grondin and G. L. Kulak, of the University of Alberta, is gratefully acknowledged, as is the helpful assistance of the DREA project manager, Thomas Hu.

APPENDIX A

Finite Element Analysis

Centre for Frontier Engineering Research

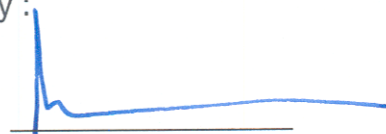
Finite Element Analysis of Stiffened Plates

Final Report — Project 95026.008

Prepared by :



J.J.R. Cheng, P. Eng.



A. E. Elwi, P.Eng.



G. Y. Grondin, P. Eng.



G. L. Kulak, P.Eng.

Acting as a Sub-Contractor

to

Centre for Frontier Engineering Research

February 16, 1996

Finite Element Analysis of Stiffened Steel Plates

Introduction

This document is the final report on the finite element analysis of stiffened ship plate carried out for the Centre for Frontier Engineering Research (C-FER). The report contains five sections, each of which deals with a different aspect of the analysis. The finite element analysis dealt with three major issues. The first task was to develop a finite element plate model that was capable of including both measured initial imperfections and residual stresses and was also capable of reproducing the different modes of failure of a stiffened plate in compression.

The plate under consideration is a single stiffened panel taken out of a repeated, continuous assembly of such panels. Since it is difficult experimentally to simulate the continuous boundary conditions along the longitudinal edge of the panel, the second task was to use the finite element model to determine the optimum number of longitudinal edge restraint devices necessary to simulate the continuous boundaries.

Once the functional model containing all these aspects had been developed, the remaining task was to use the finite element model to predict, *a priori*, a limited number of test results from the physical tests carried out by C-FER.

The report begins with a description of the finite element model. This is followed by a short section that discusses simulation of the different failure modes. The investigation of the boundary conditions is then presented, followed by a discussion of the different aspects of modeling the test specimens, including the boundary conditions, the initial imperfections, and the residual stresses. Finally, the finite element model predictions of the physical tests are presented.

Preliminary Finite Element Modeling

The stiffened plate panel was modeled and analyzed using the commercial finite element code ABAQUS, distributed by HKS Inc. of Providence, Rhode Island. ABAQUS is a high-level code, probably the most capable and popular in North America at this time. The analysis was carried out on a SUN SPARCS IPX workstation at the University of Alberta. License fees were paid to HKS Inc.

The geometry of the plate was modeled with a total of 384 plate bending SR4 elements. The SR4 element is a powerful four-node standard ABAQUS element that allows for changes in the thickness as well as finite membrane strains. The model invoked large displacements using a Total Lagrangian formulation. The plate material behaviour was modeled by an elastic-plastic von Mises kinematic strain-hardening constitutive model.

In order to model the full range of behaviour of the panel, including both the pre-buckling and post-buckling regimes, the solution strategy started with a load control standard Newton-Raphson iterative procedure in the initial stage of loading, then shifted to a Modified Ricks procedure as the ultimate load was approached. This procedure permits tracing the behaviour in the softening post-buckling regime.

Figure A-1 shows the finite element mesh used in the initial stages of the investigation. The rotations about the longitudinal axis 1 were suppressed, either at all the nodes along the unloaded edges or at a selected number of nodes, in order to simulate full or partial continuity. A frame of rigid beams was attached at both of the profile of the stiffened plate to model the loading plate end constraints. This frame suppresses distortion of the end cross-sections, but allows for rigid body rotations about axes 2 and 3 and/or rigid body translations.

Further aspects of the model will be elaborated later on in the report in the appropriate places.

Behaviour of Stiffened Plates in Compression

In practice, the stiffened plates under consideration can be loaded in a variety of ways. The scope of this project covers the cases of axial compressive loads coupled with out-of-plane loads. A number of failure modes or combinations thereof are possible. These include over-all Euler column buckling, plate buckling followed by a form of Euler buckling, and stiffener tripping. The plate and stiffener proportions under examination precluded failure by the first of the three possible failure modes.

It was expected that a lateral load producing a flexural compressive strain in the plate and tensile strain in the stiffener flange would result in plate buckling followed by a form of Euler buckling. In this case, a peak longitudinal compressive load is reached first, followed by a rapid increase in the lateral deflection and a corresponding drop in the axial load-carrying capacity.

Figure A-2 shows two stages in the behaviour of a panel loaded in the fashion described above. Two lateral third-point loads were first applied in the plane of the web and held constant at a value of 7.5 kN each. This was followed by application of an axial compressive load. Figure A-2a shows plate buckling (magnified 20 times) which started before the ultimate axial compressive load of 1880 kN was achieved. Figure A-2b shows localization of the plate buckle in the post-buckling regime when the load had dropped to 489 kN. The figure shows large lateral deformation of the entire panel, which indicates that a plastic hinge formed at the location of the plate buckle.

Figure A-3 shows a panel that has been loaded laterally in the reverse direction to that described for the panel of Figure A-2. Now, the flange of the stiffener is in flexural compression. A plate buckle is also seen in the prebuckling regime (magnified 20 times). The peak load is reached at 1990 kN. Tripping of the stiffener is clearly seen in Figure A-3b, which shows the deformation in the postbuckling regime.

Although the ultimate load capacity in each of these two cases is nearly the same, there are distinct differences in the deformation responses. The behaviour of the first assembly is very ductile, while that of the second is characterized by a sharp peak followed by a rapid drop in the load-carrying capacity. This distinction in behaviour will be shown more clearly later.

The analysis showed that the tripping mode (second assembly, Figure A-3) in stiffened plates with a discrete number of unloaded edge restraints is triggered only if the lateral load is greater than a certain threshold value. At lateral loads lower than this threshold the buckling mode reverts to that of Figure A-2.

Investigation of Boundary Conditions

Two sets of boundary conditions had to be modeled, corresponding to the loaded ends and to the unloaded (longitudinal) plate edges. Since it is expected that in actual practice the stiffeners would be welded to massive bulkheads that are stiff in their own planes but flexible in the out-of-plane condition, an ideal test would allow the ends of the specimen to rotate locally but maintain the shape of the cross-section. This implies a test in which half circular grooves are performed in the end bearing plates. Specimens with similarly rounded edges would be seated in the grooves but not welded to the end plates, as shown in Figure A-4a. This configuration presents certain difficulties in the assembly and test procedures, however. Fully welded ends, as shown in Figure A-4b, provide the most expedient and reliable test configuration.

If fully welded ends were to be used, it was necessary first to explore the effect of the boundary conditions presented by the physical arrangements shown in Figure A-4a and Figure A-4b. Therefore, the analyses presented in Figures A-2 and A-3 were repeated with and without local constraint on the rotation between the end plates and specimens. Figure A-5 shows that the differences in end conditions had no significant effect on the axial load versus longitudinal displacement.

The boundary condition along the unloaded edge proved to be more difficult to treat, and a large number of analyses had to be carried out. These used a varying number of discrete restraints on the unloaded edges. (In each case, the restraint imposed is that on rotation about axis 1.) Different magnitudes and direction of the lateral load were explored.

Figure A-6 shows the behaviour of a stiffened plate for three different conditions of restraint at the longitudinal edge; fully-restrained, totally unrestrained, and a model that uses five discrete restraints along each edge. All models were analyzed with the stiffener flange initially in flexural tension. It is clear that the behaviour in the region of the peak load softens if there is less than a fully-restrained longitudinal boundary.

Figure A-7a shows the behaviour of the stiffened plate when the stiffener flange is initially in moderate flexural compression. There are three models—restraint at five, six, and eight points—and their behaviour is compared with that of the fully-restrained case. There was no difference in the behaviour between the three partially restrained models. Whereas failure of the fully restrained model occurred by tripping of the stiffener, failure of the partially restrained models occurred by plate buckling and subsequent Euler buckling. Figure A-8 shows a similar comparison for the condition that the stiffener is under high flexural strain. Here no distinction can be made between the fully restrained and the partially restrained models.

Based on the examinations reported above, it was decided to use a welded detail for the loaded ends (Figure A-4b) and rotational restraint at five discrete locations along each unloaded edge in the numerical model.

Modeling of The Test Specimens

Completion of the numerical model required knowledge of the residual stresses and the initial imperfections in the as-fabricated specimens and the details of the restraint device that would be

used at the longitudinal boundaries. When this information became available, it was possible to complete the model and then use it to predict the behaviour of the test specimens.

Geometry and Boundary Conditions

In order to incorporate the rotational restraint devices into the numerical model, it was necessary to provide a more refined mesh than had been used to this point. This mesh, shown in Figure A-8, now has a total of 512 SR4 plate bending elements. In order to model the effect of the restraint device, short rigid beam elements were attached at the centre of each such device. In addition, the bending stiffness of the two plate elements surrounding each short beam was increased by an order of magnitude and assumed to be linearly elastic. In this way, the stiffening effect of a finite size gripping device was incorporated into the numerical model. The rotational restraint was applied by constraining the translation along direction 2 at the tip of each short beam. This allowed for accurate modeling of a constraint of the rotation about an axis tangential to the edge of the plate. This is considered to be more realistic than a direct restraint of the rotation about axis 1.

Adjustments to the model were also required to reflect the loading device that was to be used at each end of the stiffened plate assembly. Since the loaded end plate was to rest on a half-cylinder roller at each end (Figure A-9), the point of rotation would be shifted longitudinally away from the actual end of the stiffened plate. In addition, the lateral reaction to the lateral loads would also be shifted by an amount approximately equivalent to the radius of the end roller. Thus, end moments would also be generated. To account for both effects, the rigid beam element frames used to model the end plates were shifted away from the actual end of the stiffened panel, as shown in Figure A-8, and end moments equal to the lateral reaction times the radius of the cylindrical bearing were added at each loaded end. The rigid beam elements were shifted by an amount equal to the thickness of the end plate and grout layer.

Material Properties

As mentioned above, an elasto-plastic material model with a von Mises yield criterion and kinematic strain-hardening rule was used to model the material constitutive behaviour. Since large deformations and finite strain could be reached during the analysis, particularly after the buckle formation, true stress vs. true strain properties derived from coupon tests were input into the model. Figure A-10 shows the stress vs. strain relationships and other hardening parameters used in the simulation.

Initial Imperfections

Up to this point in the modeling, the specimen had been assumed to be free of initial stresses and arbitrary initial imperfections had been used. The next step, then, was to map the measured initial imperfections onto each perfect specimen. The measured initial imperfection data were supplied by C-FER. Subsequently, the residual stresses were introduced. The residual stress information was obtained by measurement, as described in Appendix B. Both aspects will be discussed in detail in the context of Specimen SP1.1, the first specimen to be examined.

Figures A-11 and A-13 show the measured imperfections of the plate and flange, respectively, for specimen SP1.1. The imperfections were mapped onto the mesh shown in Figure A-8. The mapping process was based on a least squares fit of the imperfect surface and was carried out using the MacGridzo code¹.

The mapped initial imperfections are shown for the plate of SP1.1 in Figure A-12 and the and the flange of the stiffener from the same specimen in Figure A-14. The slight chattering seen in Figures A-12 and A-14 was deemed to be of no importance relative to the major pattern of imperfections.

Residual Stresses

The only residual stresses introduced into the model were the longitudinal stresses arising in the specimens because of the manufacturing process of the plate and tee stiffener and the longitudinal welding process during the fabrication of the specimens. The modeling was done by imposing initial strains in the form of a temperature distribution. In order to model the initial strains only in the longitudinal direction, an orthotropic temperature material property was used that had zero thermal expansion coefficients in directions 2 and 3. The initial strains introduce initial stresses, upon which an iteration is carried out in order to establish equilibrium. A complication arises because this process introduces a distortion in the specimen. Therefore, the application of residual stresses went through two stages. First a set of strains equal in magnitude but opposite in sign to those measured and attributed to residual stresses were introduced in the model with the mapped initial imperfections. The resulting displacements were recorded and then superimposed on the initial imperfections. A new deformed, stress-free, mesh was thus generated. The proper initial strains were then reapplied on the newly generated model. At this stage the model incorporates initial imperfections consistent with those measured and residual stresses as measured.

Figure A-15 shows a set of measured residual stresses reported in Appendix B. Figure A-16 presents a comparison between the measured residual strains and the input and output residual strains from the ABAQUS model for the plate of specimen SP1.1. Figures A-17 and A-18 show similar comparisons for the web and flange of the tee section of the same specimen. It is concluded that the reconstructed residual stress picture is successful. Similar simulations were conducted for all of the following analyses.

Prediction of Test Results

The numerical model described above was used to predict the behaviour of five test specimens that were tested subsequently at C-FER. Four of these belonged to series SP1 and one belonged to series SP2. The first four specimens, SP1.1, SP1.3, SP1.4, and SP1.5, were loaded both axially and laterally (with third-point loads). Specimens SP1.1 and SP1.3 were loaded so that the tee stiffener flange was in flexural tension, whereas SP1.4 and SP1.5 were loaded such that the tee stiffener flange was in compression. The lateral loads were held constant while the axial compressive load was applied by imposing deformations (stroke control) until failure was reached. Specimen SP2.1, on the other hand, was first loaded laterally in a damage cycle, the

¹ "MacGridzoTM – Contour Mapping and Base Map Plotting for the Macintosh," Version 2, Rockware, Inc., Wheat Ridge, CO, 1988.

lateral load removed, and then the specimen reloaded to failure with an axial compressive load. The predicted values of the peak load and the values obtained in the physical tests carried out subsequently are shown in Table 1.

The predictions and physical test results for the first four tests are shown in pairs of figures. Figures A-19, A-21, A-23, and A-25 show the axial load versus axial shortening predictions and the physical test results for specimens SP1.1, SP1.3, SP1.4, and SP1.5, respectively. Figures A-20, A-22, A-24, and A-26 show corresponding deformed configurations for the following conditions; before loading, after application of the lateral load, at peak load, and just before the end of each test. The eight figures show that the predictions of the pre-peak behaviour, the peak load value, the post-peak behavior, and the buckling mode were all excellent.

Figures A-27, A-28, and A-29 show the finite element predictions and the actual test results for the damage cycle of specimen SP2.1. These figures show, respectively, the axial load versus axial shortening, lateral load versus lateral deflection, and lateral load versus end rotation. There is excellent agreement between prediction and test results for the case of axial load versus axial shortening (Figure A-27) and for the case of lateral load versus end rotation (Figure A-29). However, the initial stiffness is not predicted very well for the case of lateral load versus lateral deflection (Figure A-28).

The next three figures, Figures A-30, A-31, and A-32 show the axial load versus axial shortening, mid-span lateral deflection, and end rotation for specimen SP2.1 during the test cycle. Figures A-33 and A-34 show the deformed shape of this specimen at various stages of loading. As was the case for the other specimens, the numerical model provided good predictions of the response of specimen SP2.1.

Summary

This work has shown that the stiffened steel plates that form the main structural component of a ship hull can be modeled with a high level of confidence. The numerical model developed for the examination reported herein used measured initial deformations and residual stresses typical for the stiffened plate configuration under examination. If other arrangements are to be explored, the magnitude and distribution of both initial imperfections and residual stresses must be examined on a case basis.

Table A-1

Comparison of Test Peak Load with Predicted Peak Load

Specimen No.	Test Peak Load (kN)	Predicted Peak Load (kN)	$\frac{\text{Test Load}}{\text{Predicted Load}}$
SP1.1	1573	1593	0.99
SP1.3	1453	1436	1.01
SP1.4	1275	1321	0.97
SP1.5	1134	1255	0.90
SP2.1	1331	1340	0.99

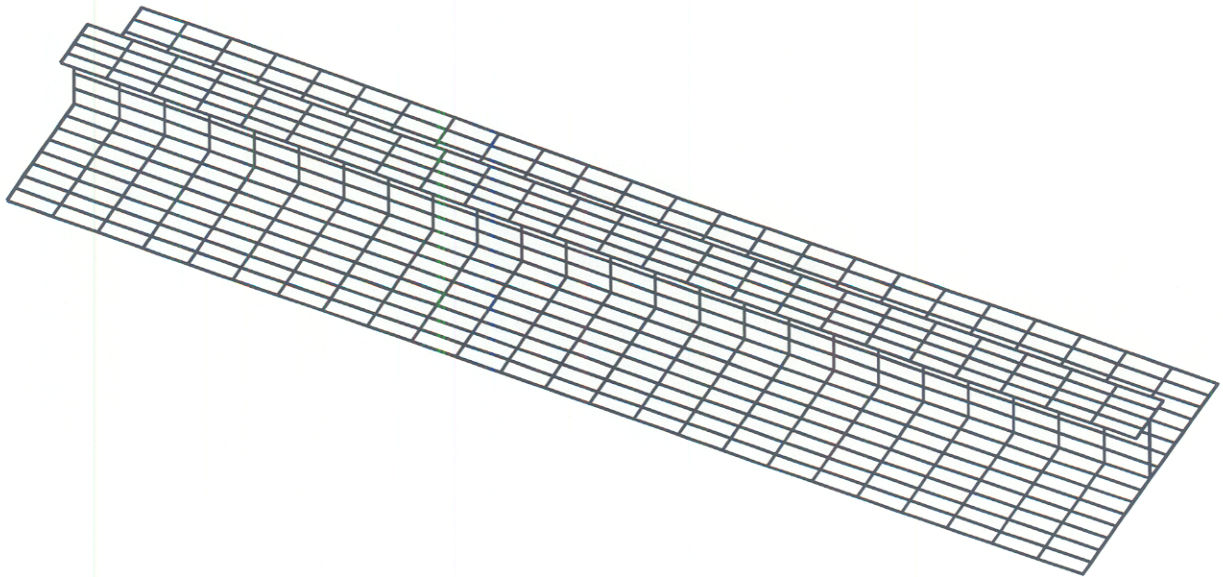
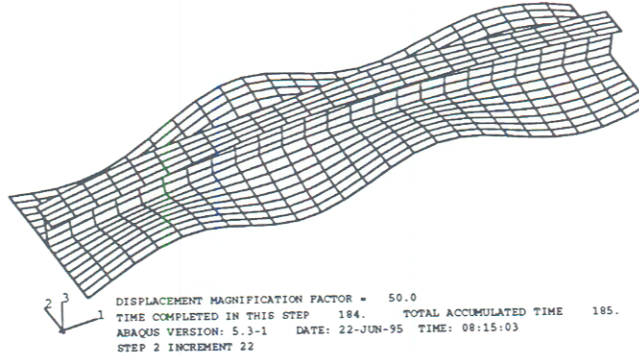


Figure A-1. Finite Element Mesh of Stiffened Plate

ABAQUS

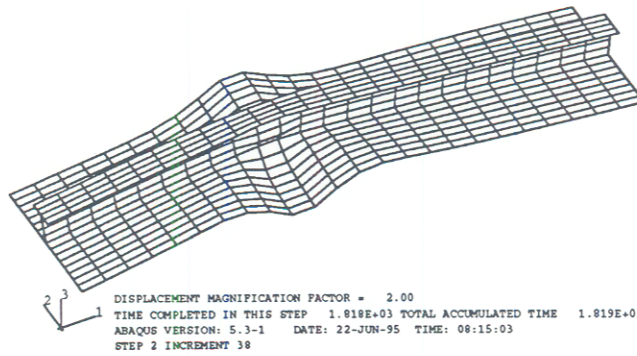
Axial Load = 2036 kN (peak load)



(a) Stiffened Plate Configuration at Peak Load
(displacements magnified by a factor of 50)

ABAQUS

Axial Load = 682 kN; Axial Deflection = 14.0 mm

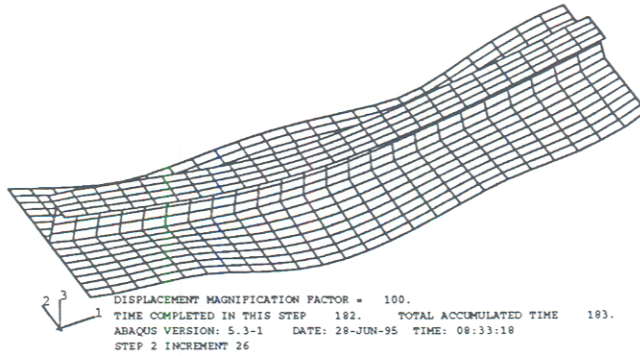


(b) Stiffened Plate Configuration in the Post Peak Load Region

Figure A-2. Failure of Stiffened Plate by Plate Buckling

ABAQUS

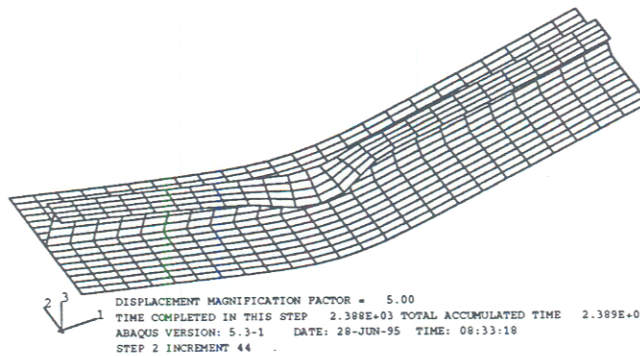
Axial load = 1943 kN (peak load)



(a) Stiffened Plate Configuration at Peak Load
(displacements magnified by a factor of 100)

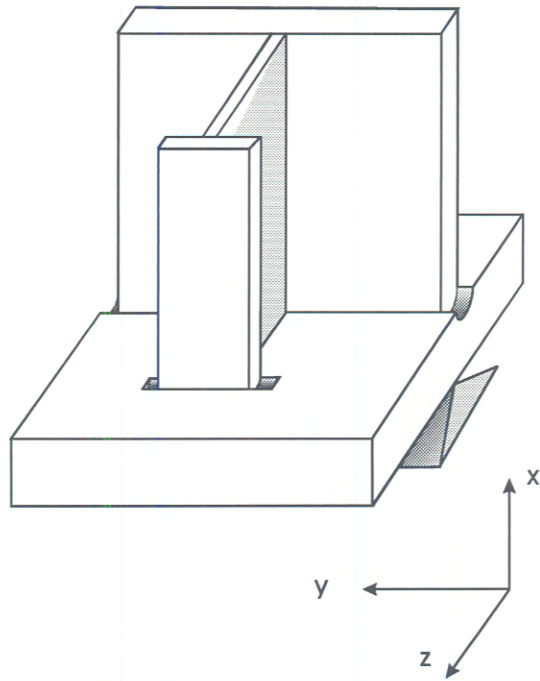
ABAQUS

Axial Load = 750 kN; Axial displacement = 5.0 mm

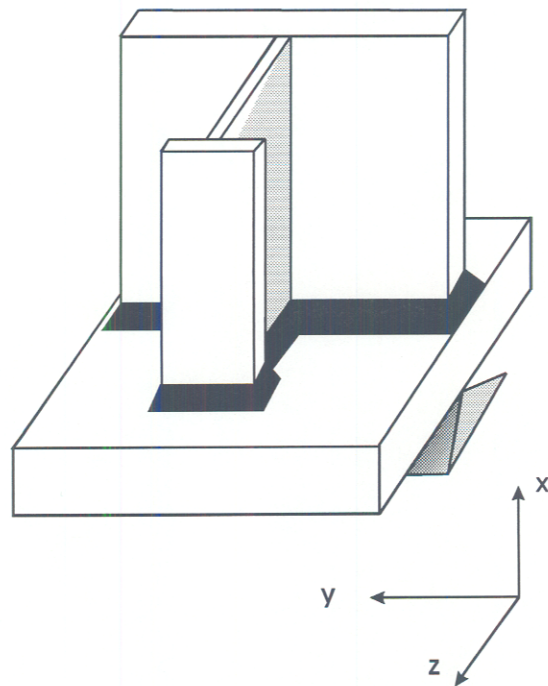


(b) Stiffened Plate Configuration in the Post Peak Load Region
(displacements magnified by a factor of 5)

Figure A-3. Failure of Stiffened Plate by Stiffener Tripping



(a) End of Stiffened Plate Supported in Groove



(b) End of Stiffened Plate Welded to the Loading Plate

Figure A-4. Loaded Ends Support Conditions

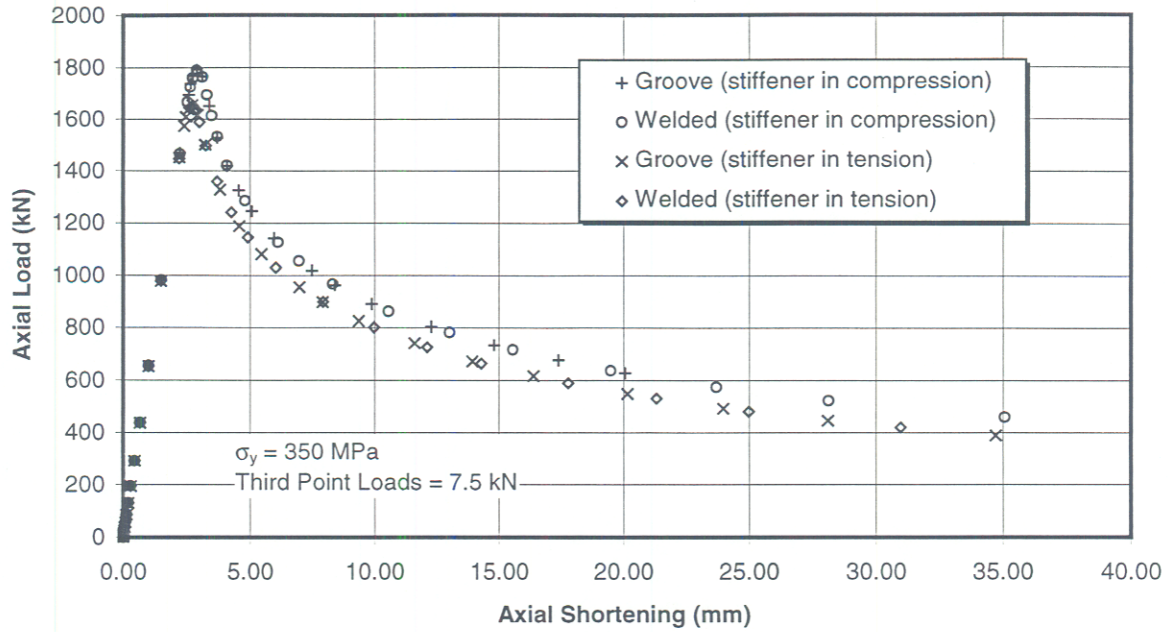


Figure A-5. Effect of Restraint at the Loaded Ends

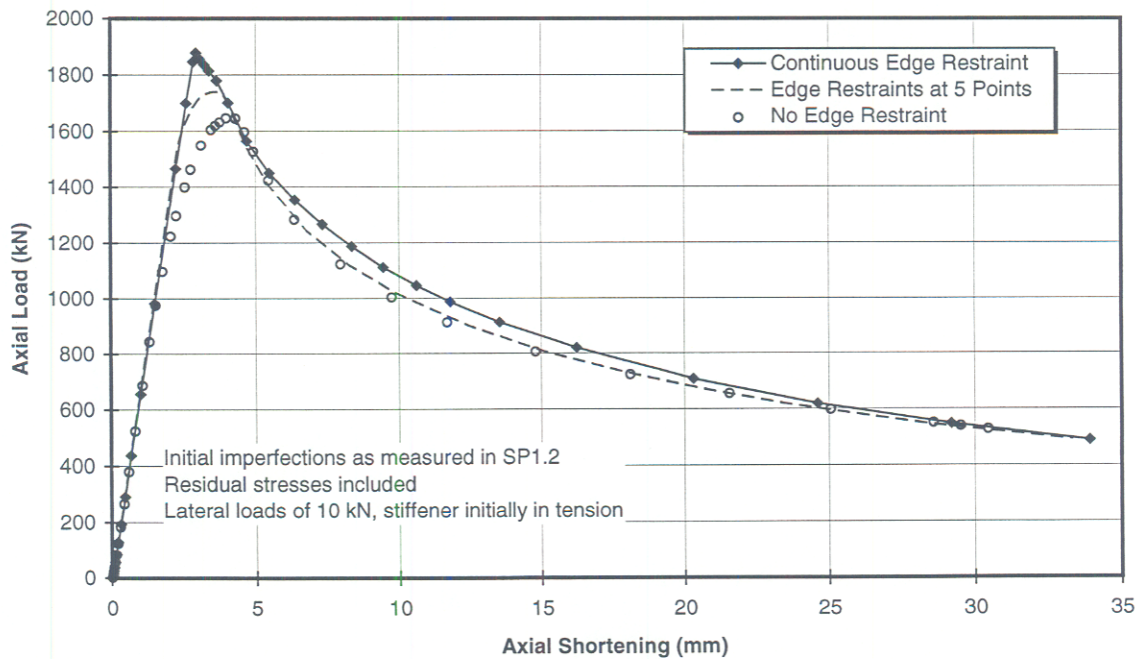
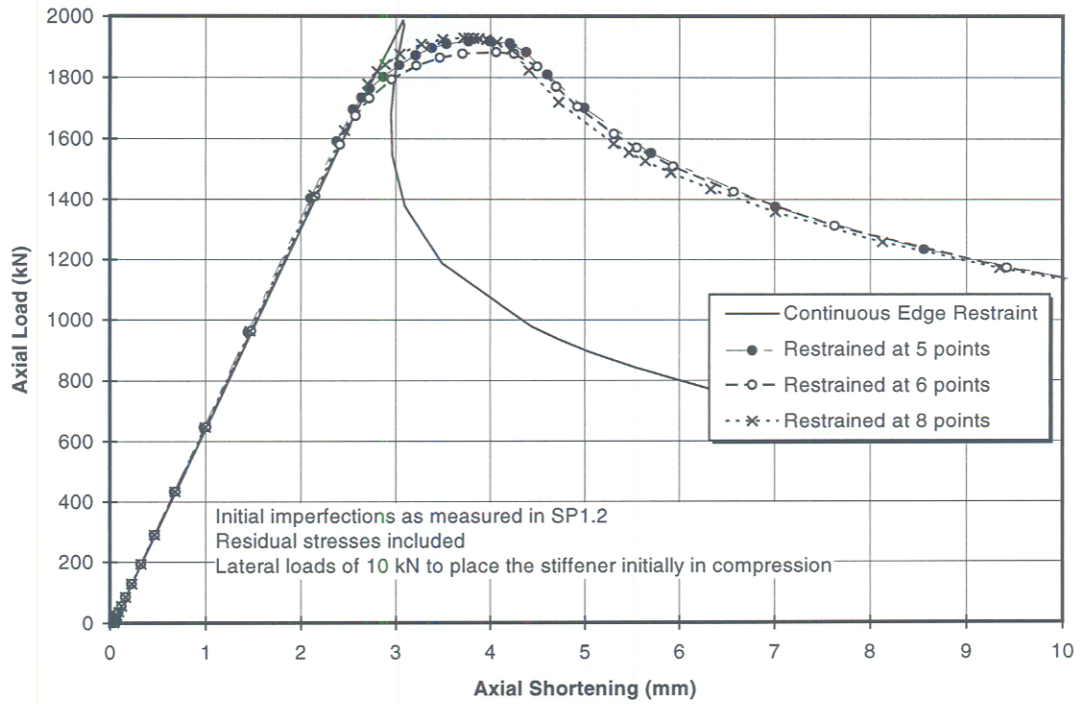
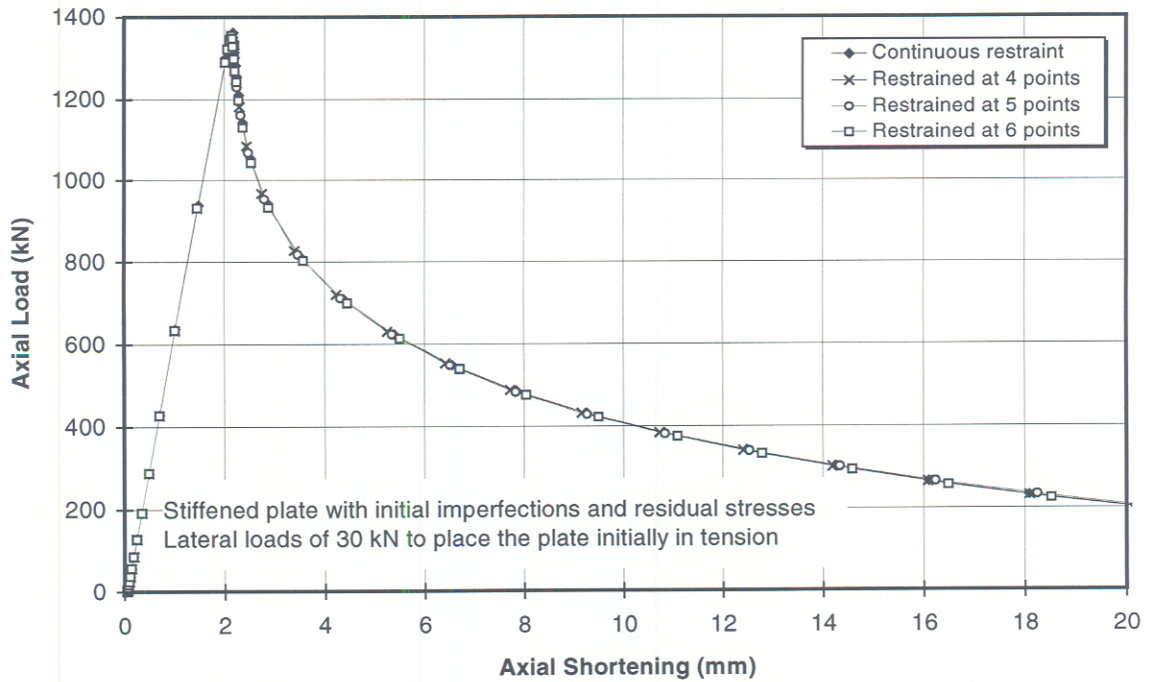


Figure A-6. Effect of Boundary Conditions Along the Unloaded Edges (Stiffener on the Tension Side)



(a) Stiffener in Compression Under 10 kN Lateral Loads



(b) Stiffener in Compression Under 30 kN Lateral Loads

Figure A-7. Effect of Boundary Conditions along the Unloaded Edges (Stiffener on the Compression Side)

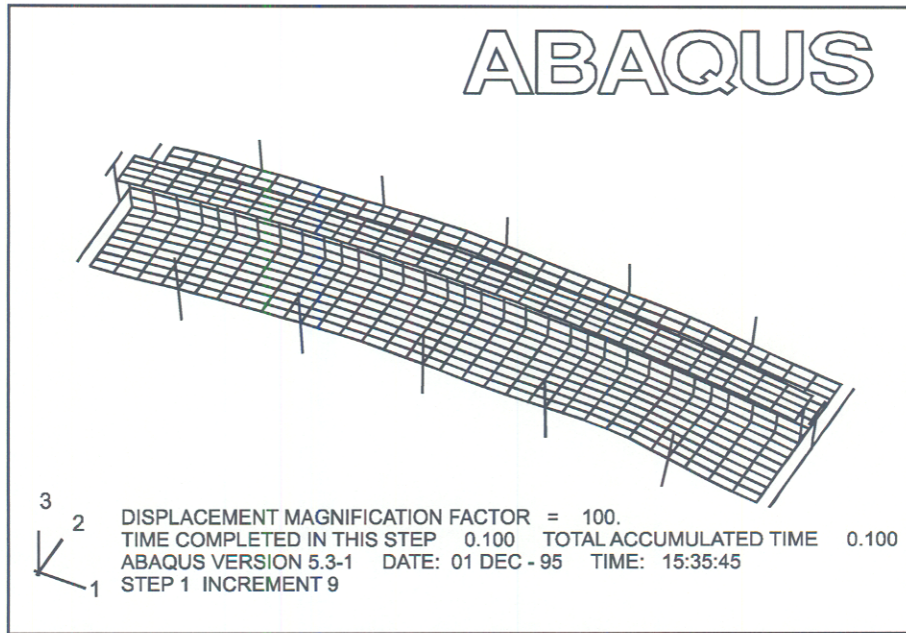


Figure A-8. Modified Finite Element Mesh Used for the Prediction of the Test Results

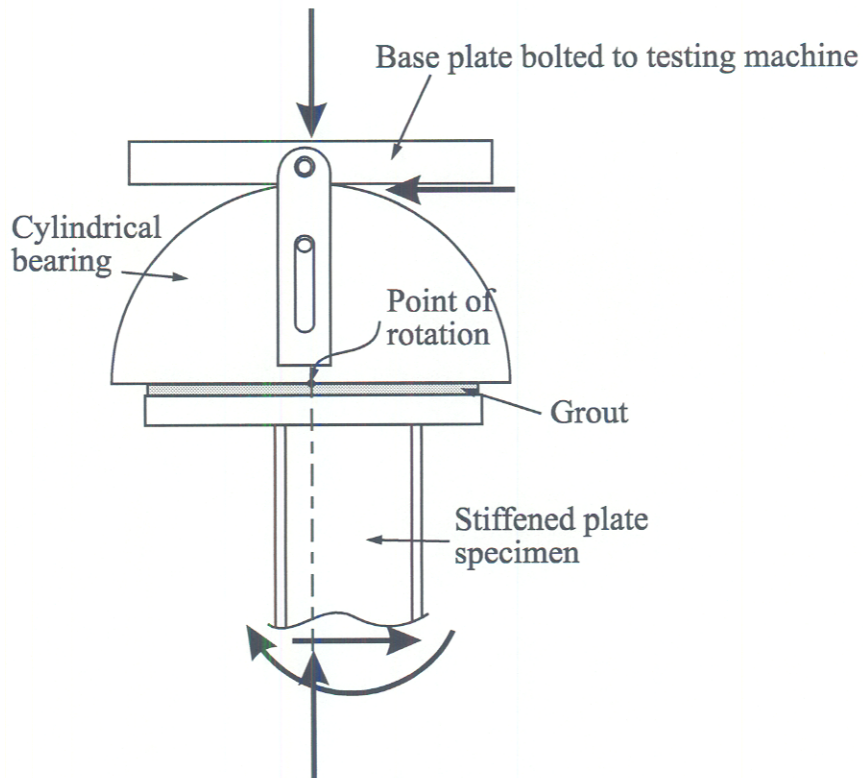
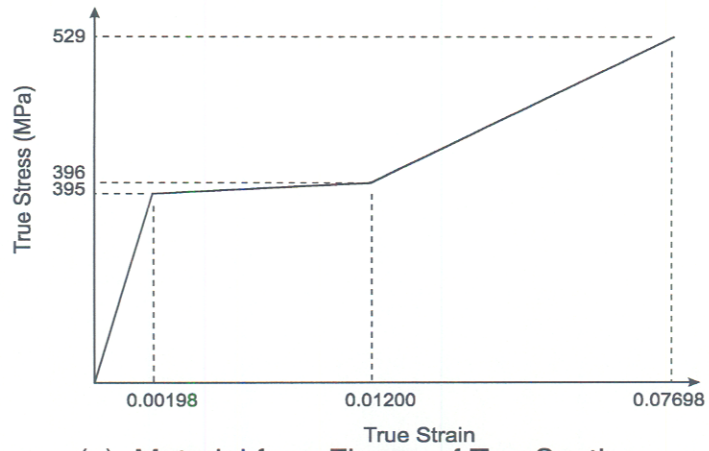
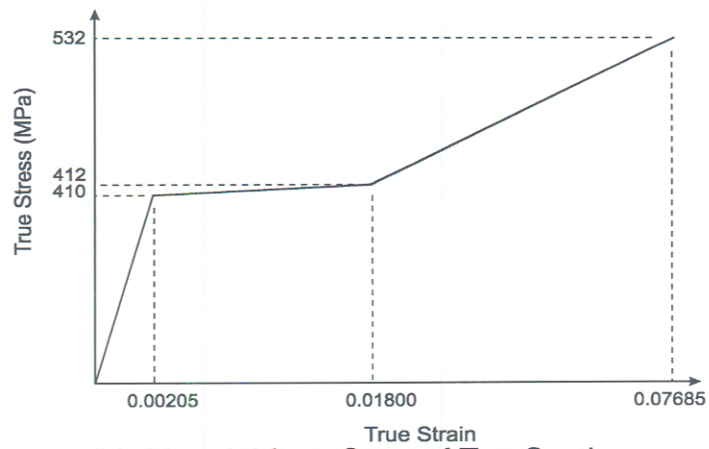


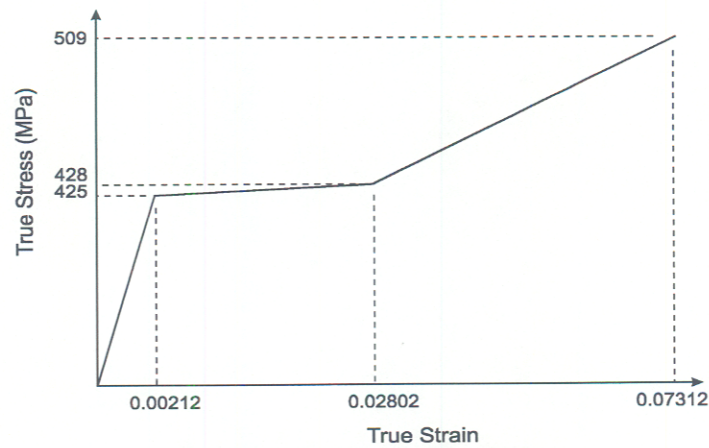
Figure A-9. Schematic of End Bearing



(a) Material from Flange of Tee Section



(b) Material from Stem of Tee Section



(c) Material from the Plate

Figure A-10. Material Models Used in the Analysis

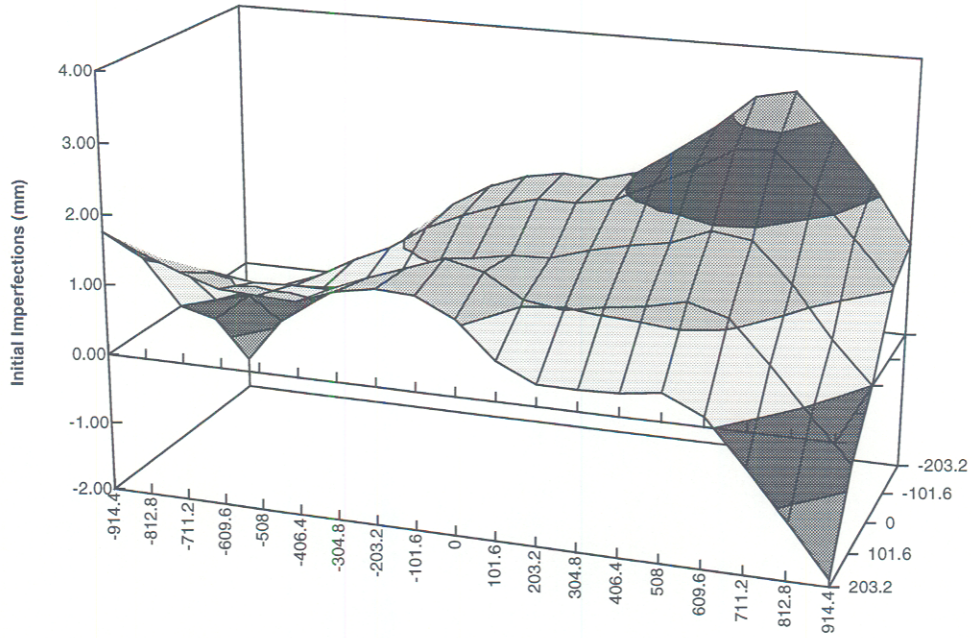


Figure A-11. Measured Initial Imperfections in the Plate of SP1.1

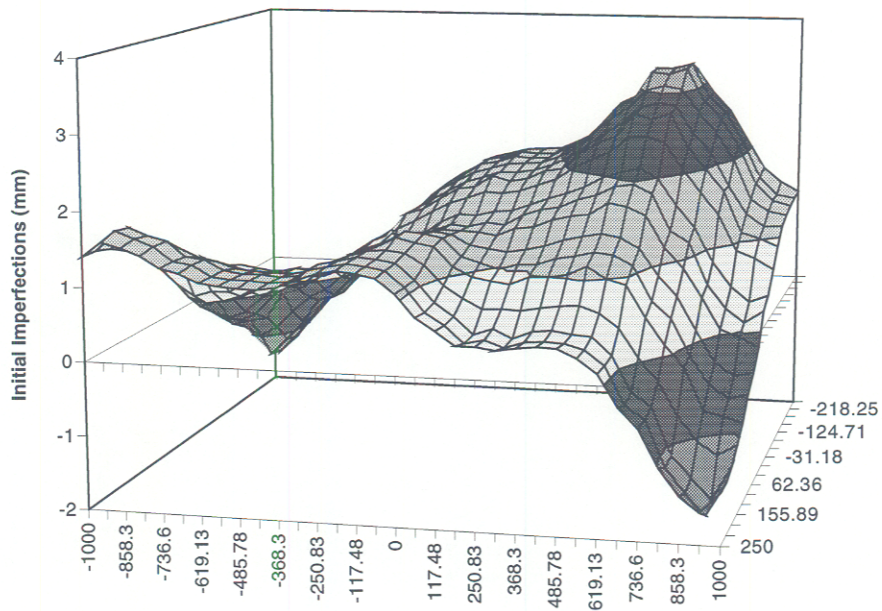


Figure A-12. Mapped Initial Imperfections in the Plate of SP1.1

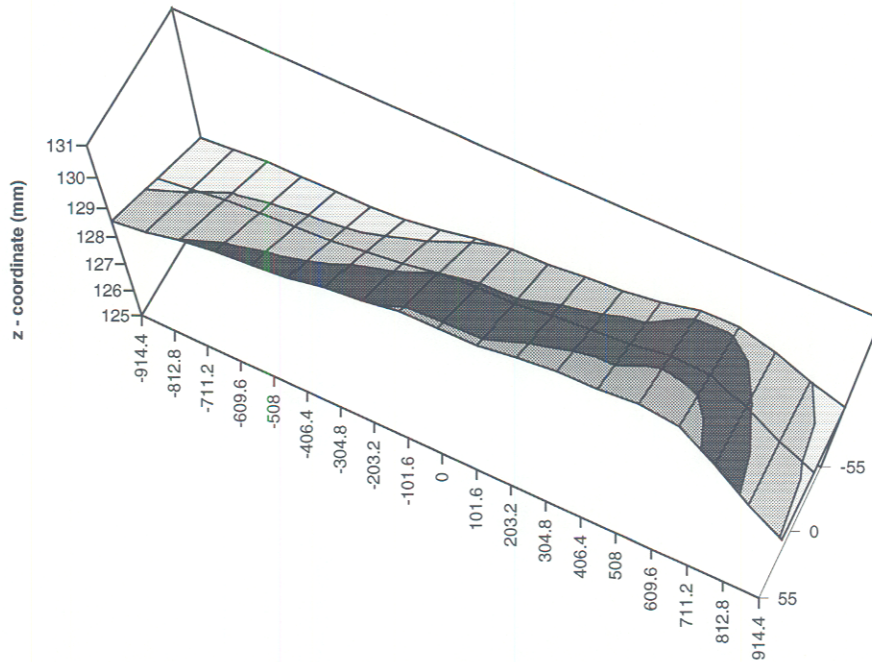


Figure A-13. Measured Initial Imperfections in Flange of Tee Section from SP1.1

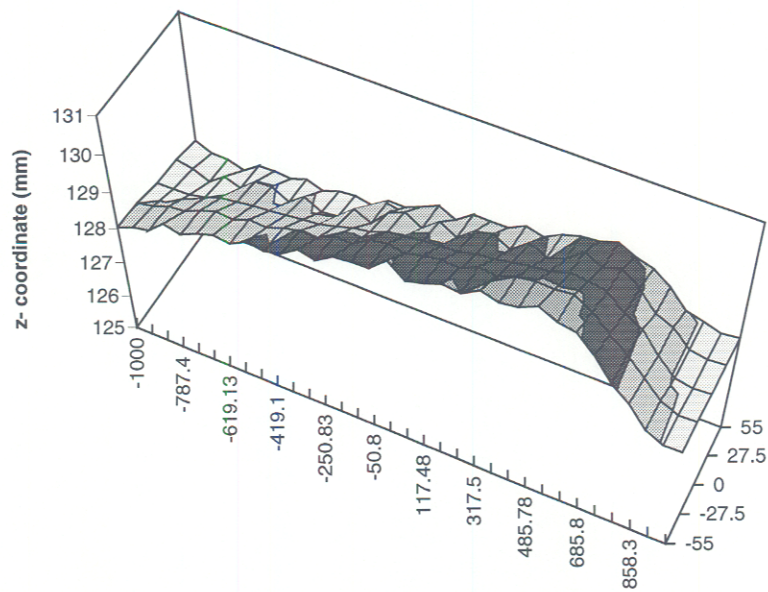


Figure A-14. Mapped Initial Imperfections in Flange of Tee Section from SP1.1

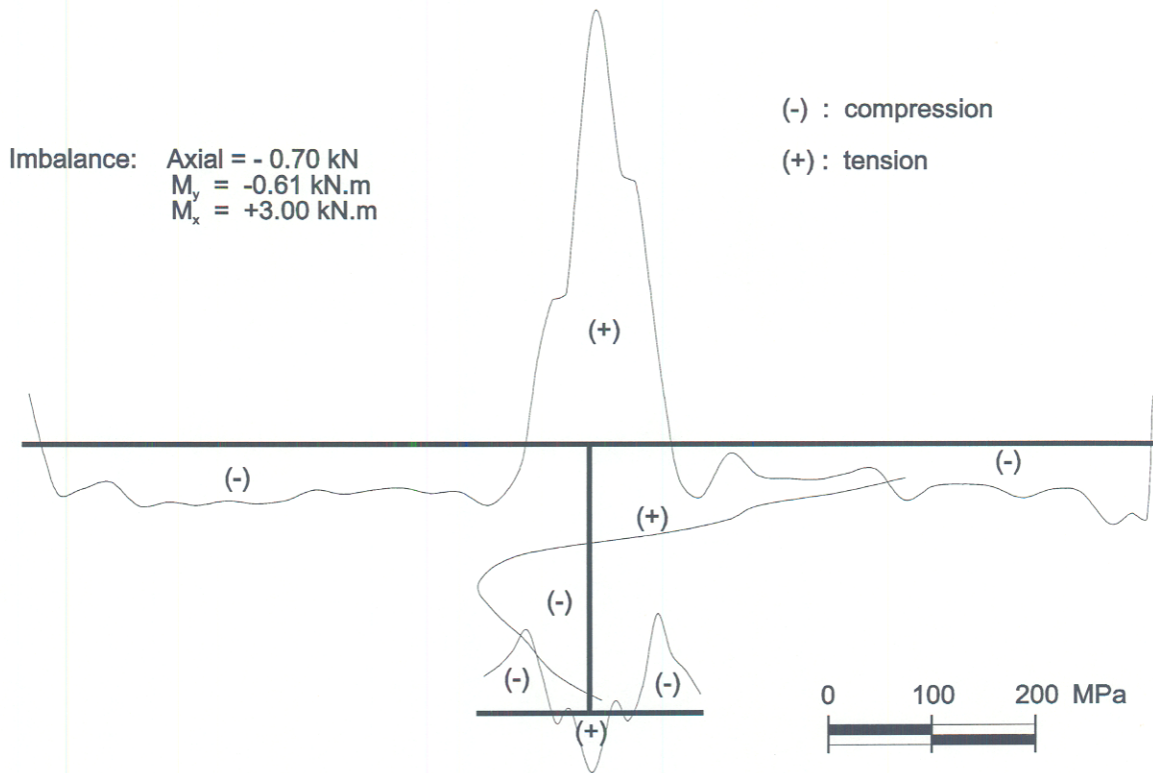


Figure A-15. Measured Longitudinal Residual Stresses in a Stiffened Steel Plate

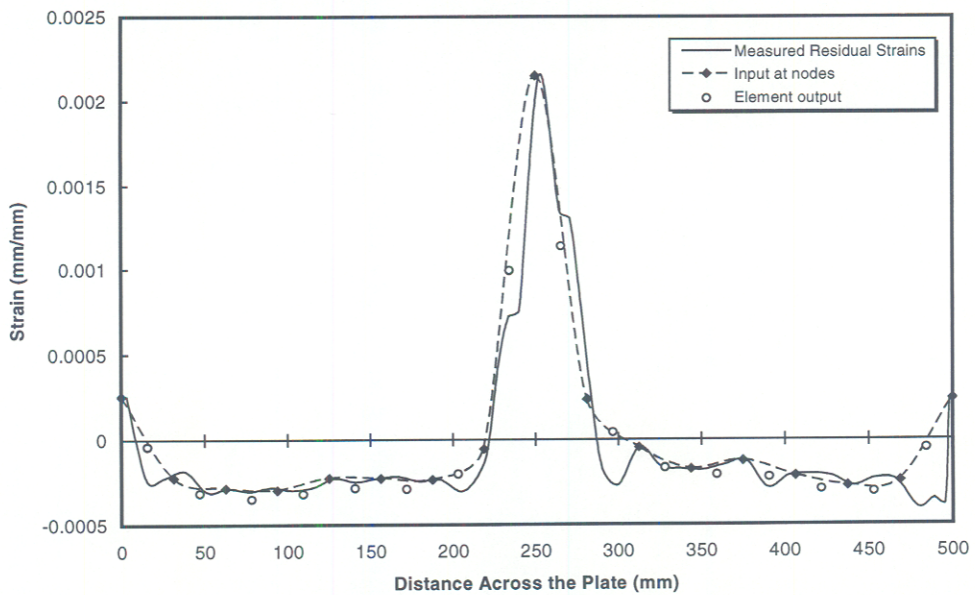


Figure A-16. Comparison Between the Measured and Modeled Residual Stresses in the Plate of Test Specimen SP1.1

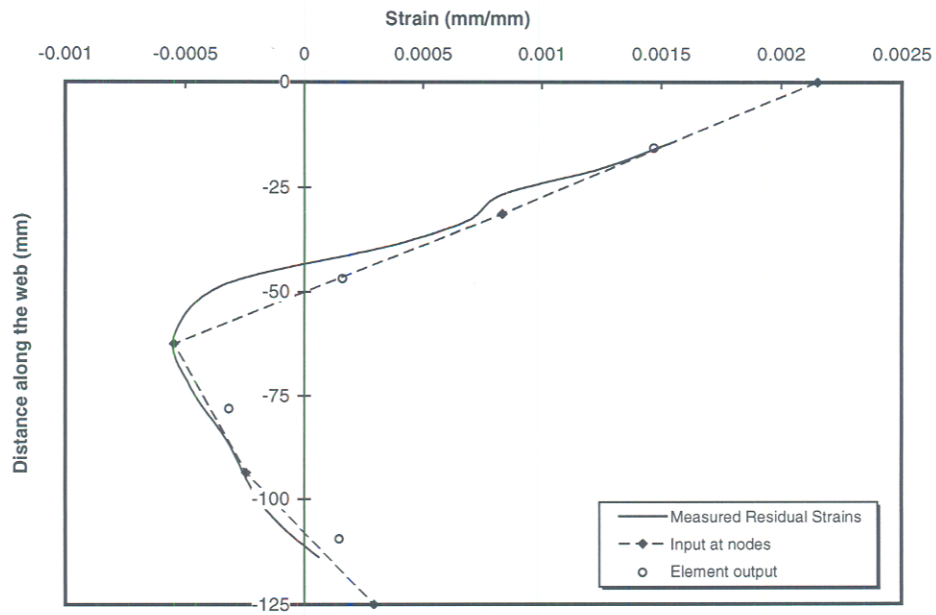


Figure A-17. Comparison Between the Measured and Modeled Residual Stresses in the Stem of Tee Section from SP1.1

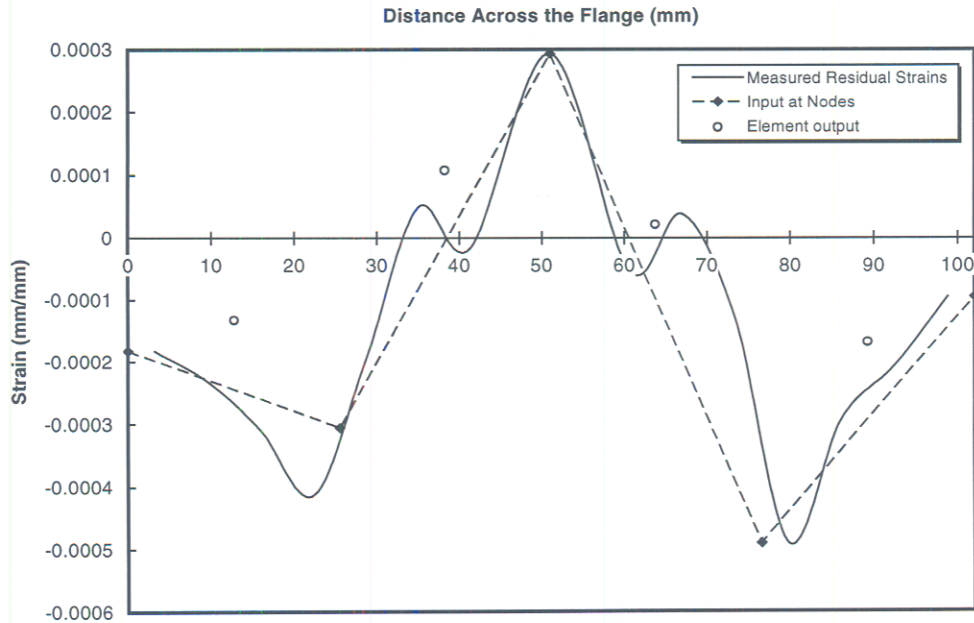


Figure A-18. Comparison Between the Measured and Modeled Residual Stresses in the Flange of Tee Section from SP1.1

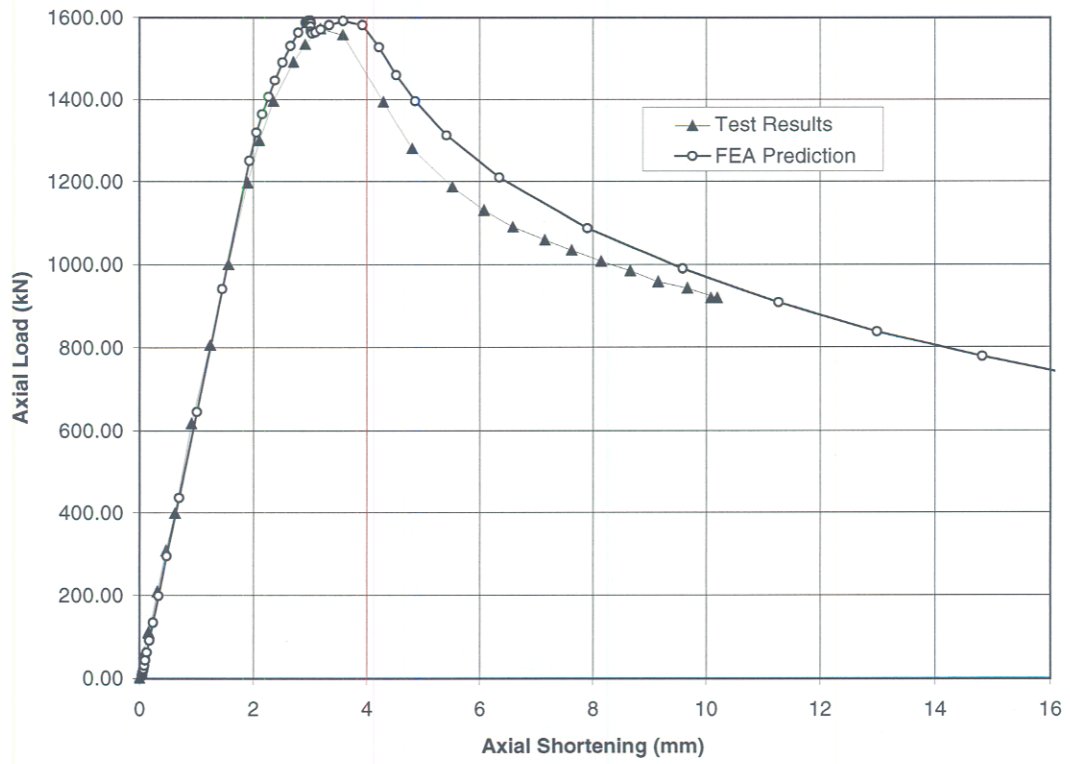
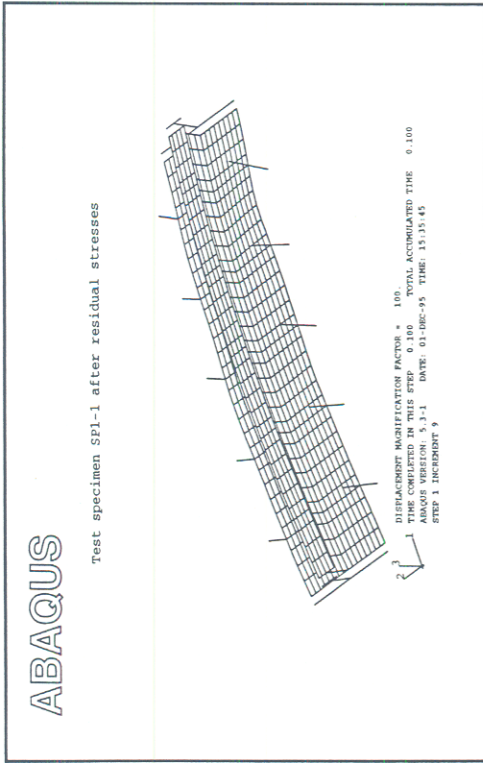
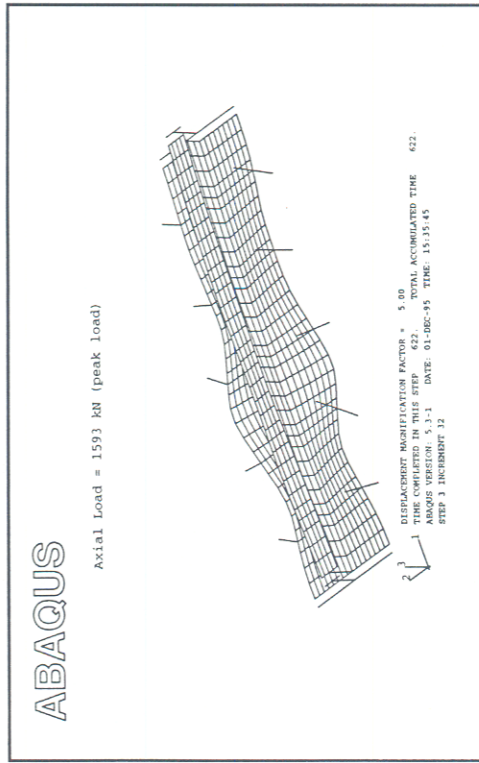


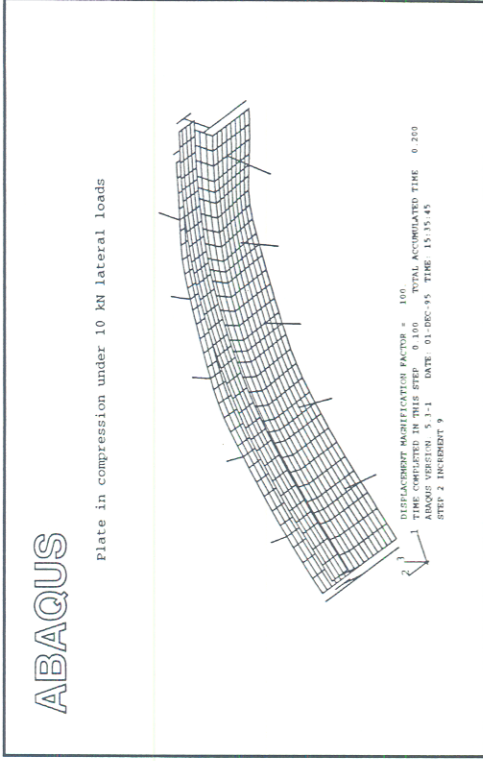
Figure A-19. Axial Load vs. Axial Shortening for Test SP1.1



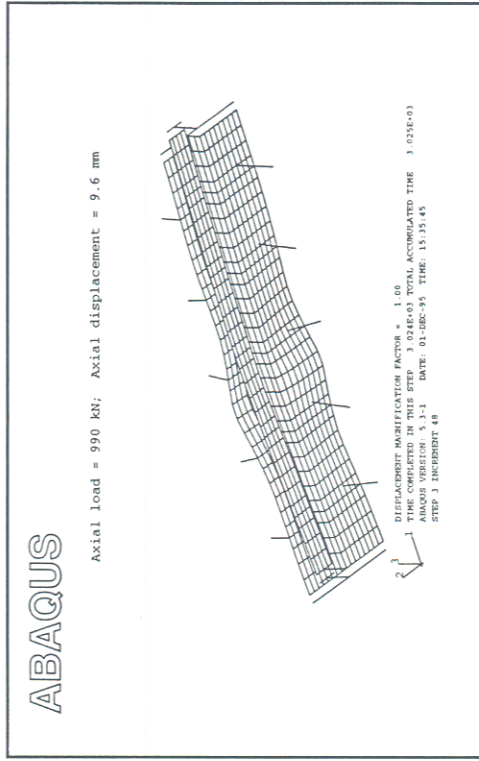
(a) Plate before loading
 (displacements magnified by 100)



(c) Plate configuration at peak load
 (displacements magnified by 5)



(b) Plate configuration with 25 kN lateral loads
 (displacements magnified by 100)



(d) Plate configuration at end of test

Figure A-20. Deformed Shape of SP1.1 at Various Stages of Loading

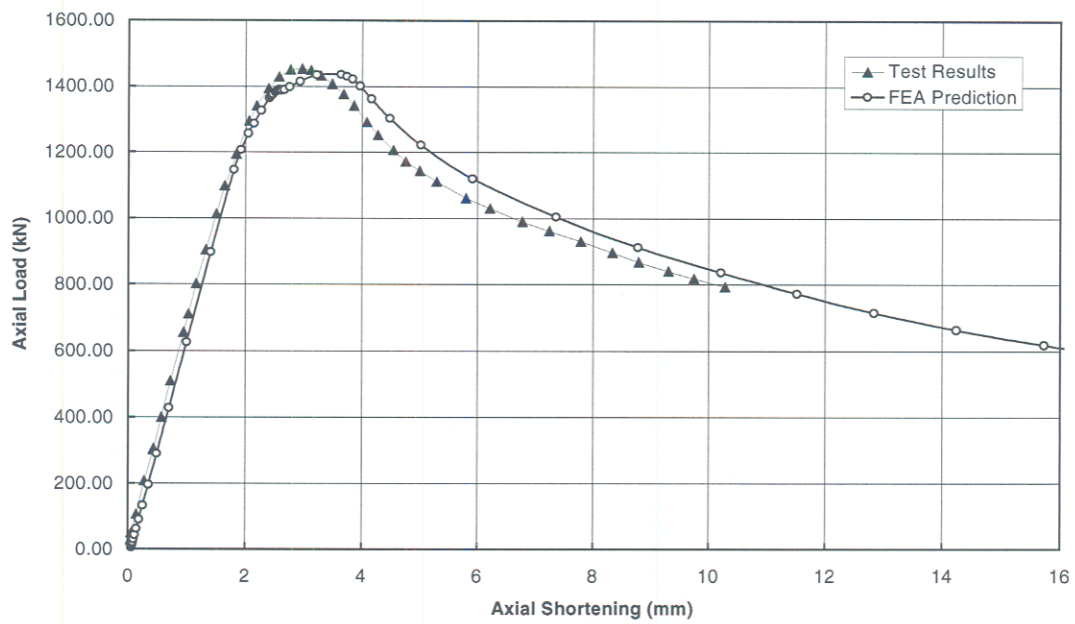
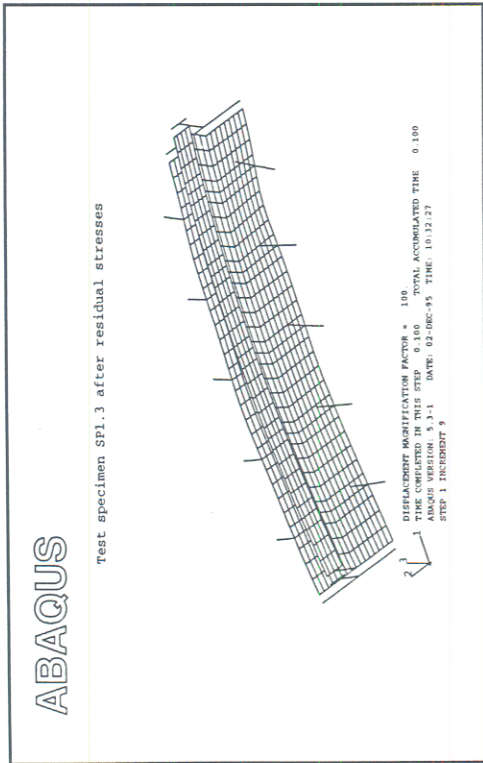
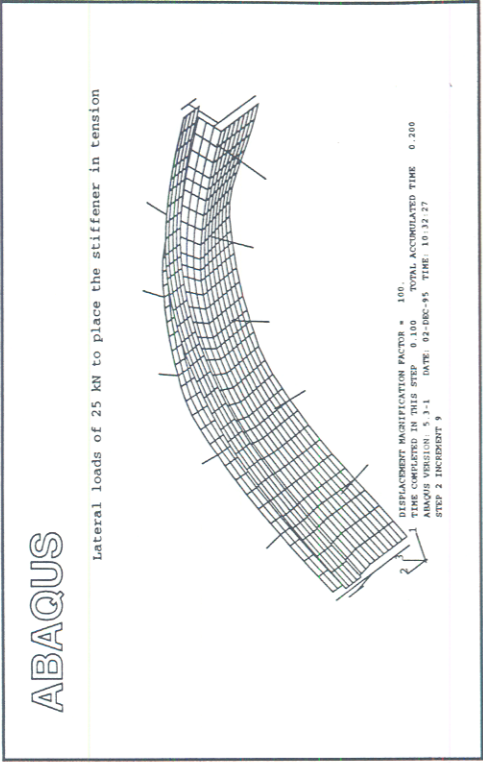


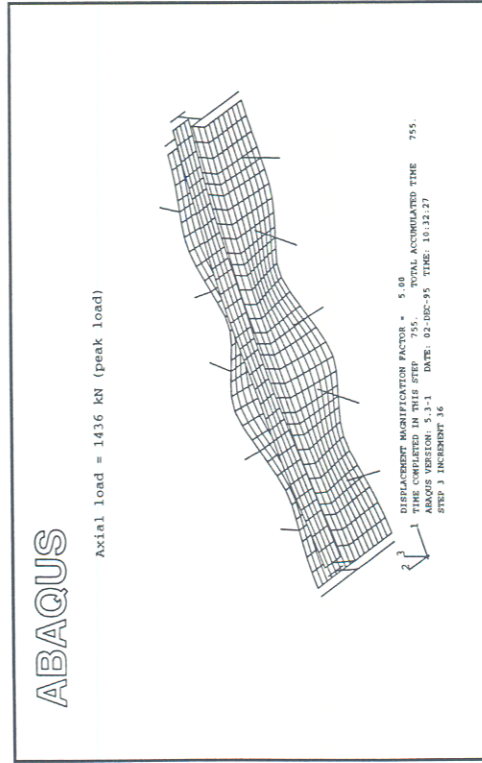
Figure A-21. Axial Load vs. Axial Shortening for Test SP1.3



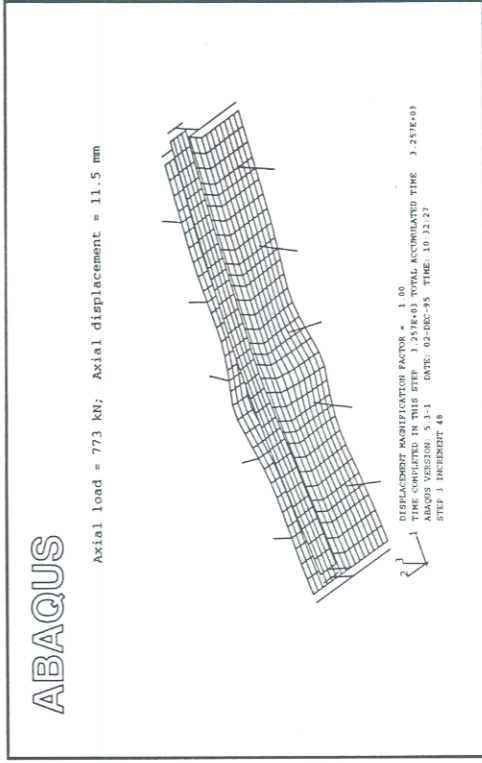
(a) Plate before loading
 (displacements magnified by 100)



(b) Plate configuration with 25 kN lateral loads
 (displacements magnified by 100)



(c) Plate configuration at peak load
 (displacements magnified by 5)



(d) Plate configuration at end of test

Figure A-22. Deformed Shape of SP1.3 At Various Stages of Loading

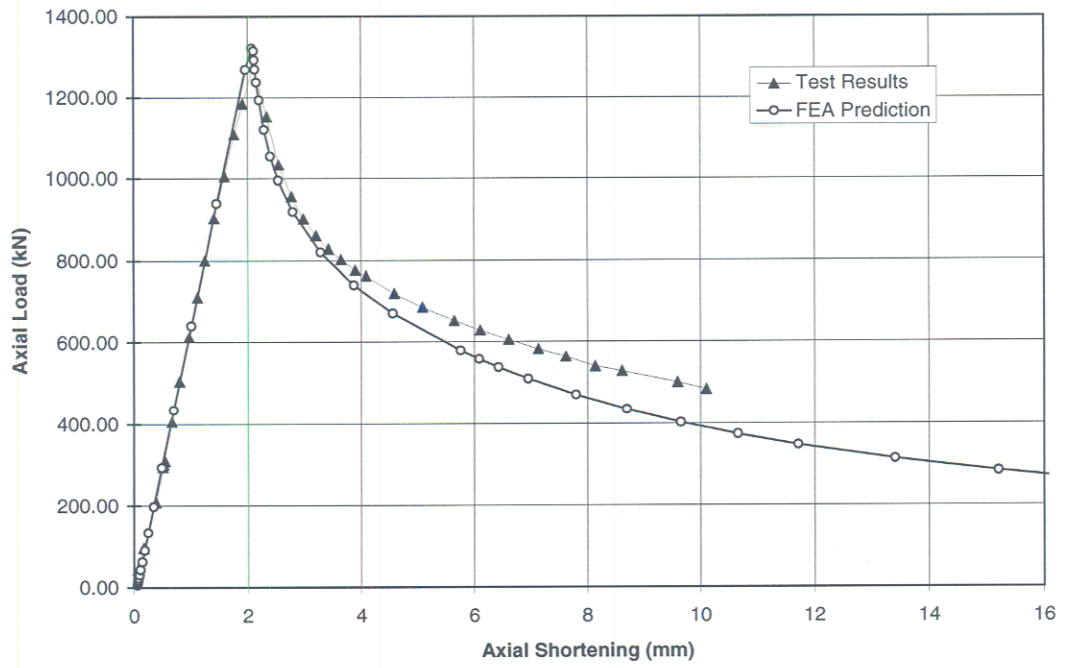
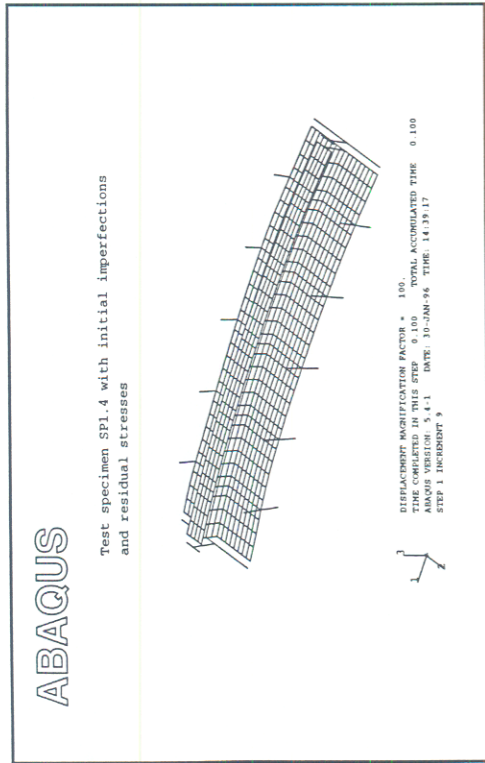
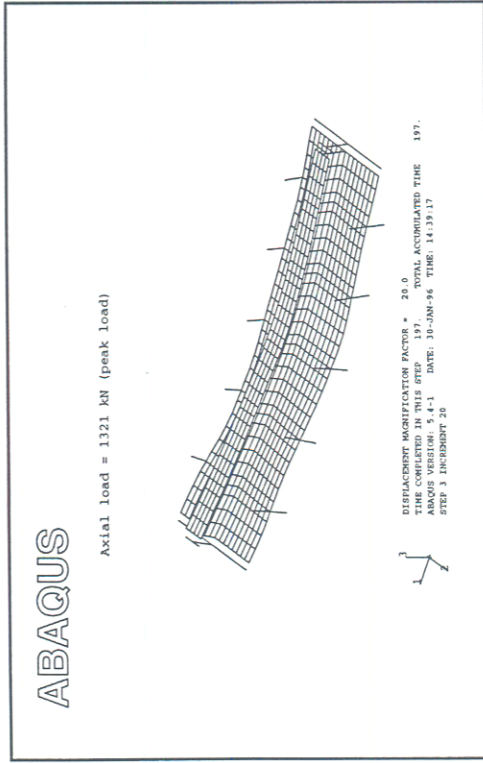


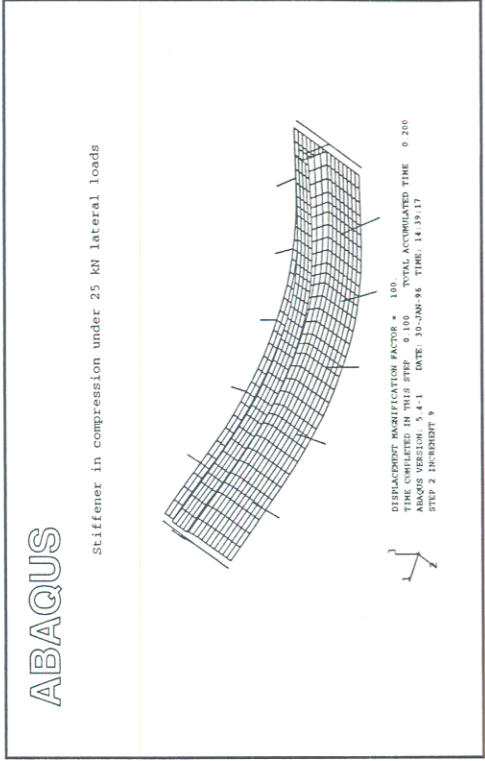
Figure A-23. Axial Load vs. Axial Shortening for Test SP1.4



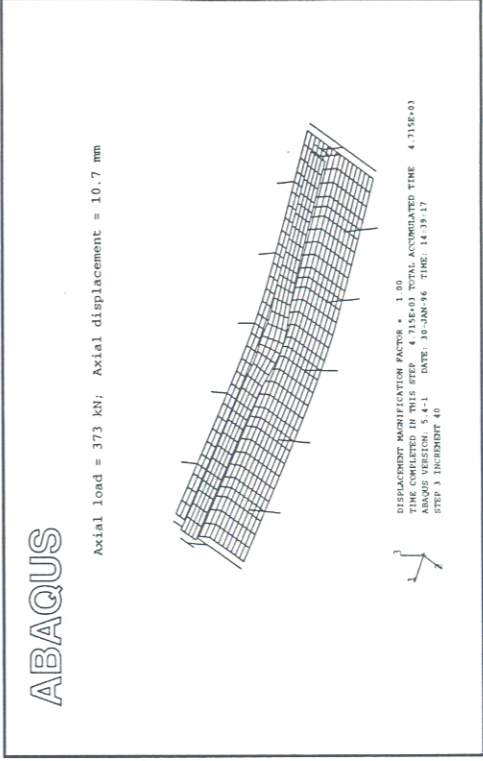
(a) Plate before loading (displacements magnified by 100)



(c) Plate configuration at peak load (displacements magnified by 20)



(b) Plate configuration with 25 kN lateral loads (displacements magnified by 100)



(d) Plate configuration at end of test

Figure A-24. Deformed Shape of SP1.4 at Various Stages of Loading

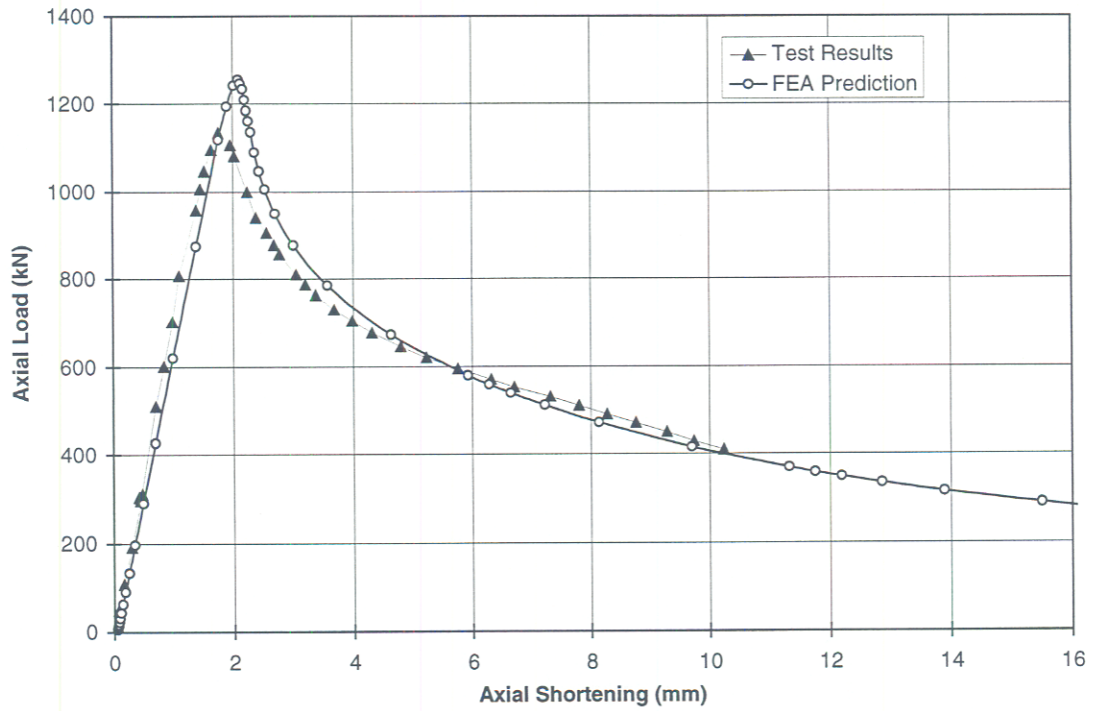
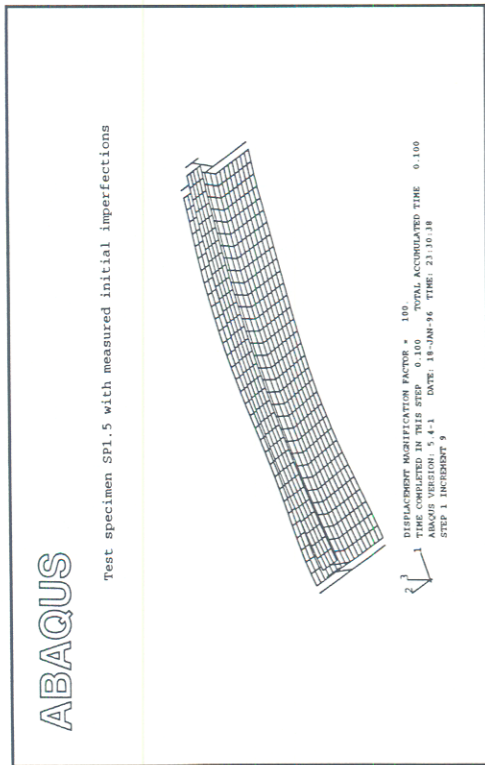
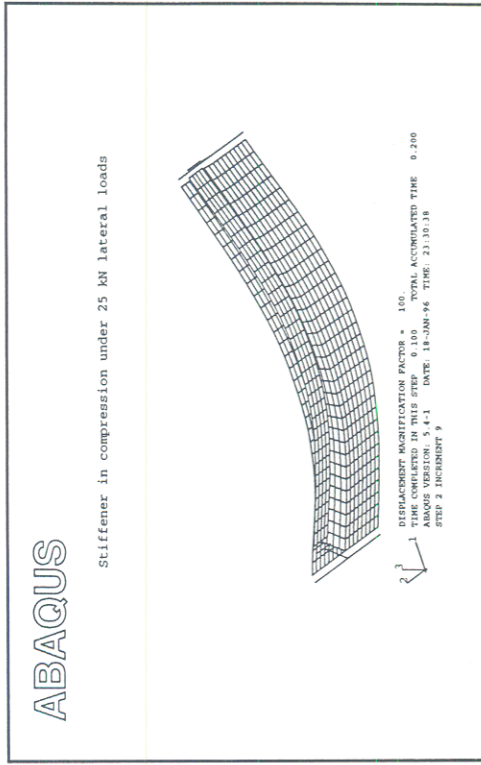


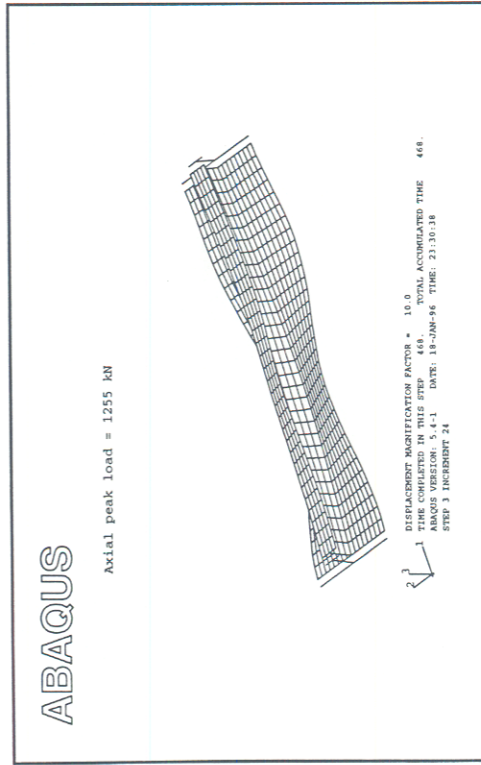
Figure A-25. Axial Load vs. Axial Shortening for Test SP1.5



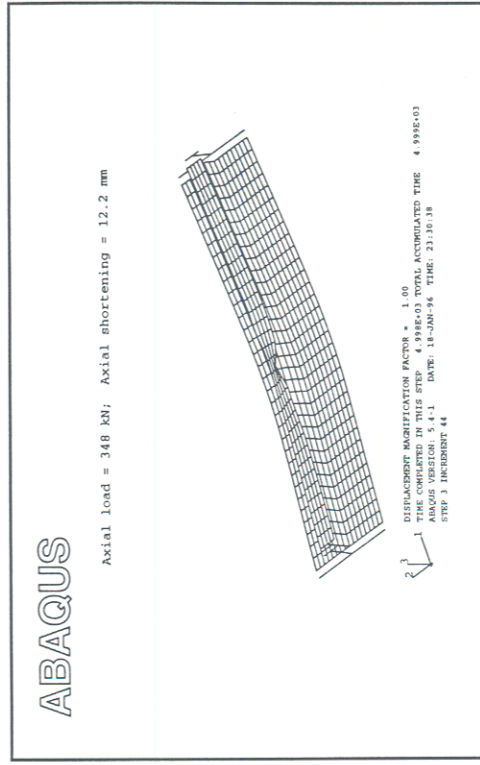
(a) Plate before loading
(displacements magnified by 100)



(b) Plate configuration with 25 kN lateral loads
(displacements magnified by 100)



(c) Plate configuration at peak load
(displacements magnified by 10)



(d) Plate configuration at end of test

Figure A-26. Deformed Shape of SP1.5 at Various Stages of Loading

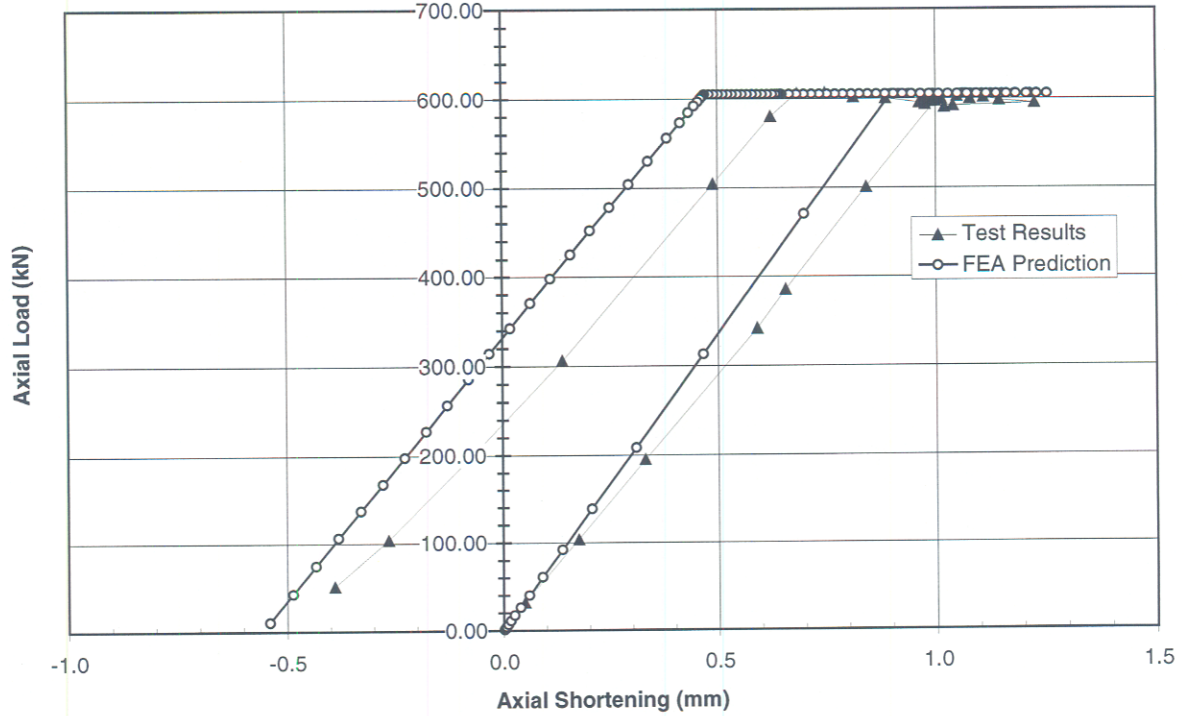


Figure A-27. Axial Load vs. Axial Shortening During the Damage Cycle of Test SP2.1

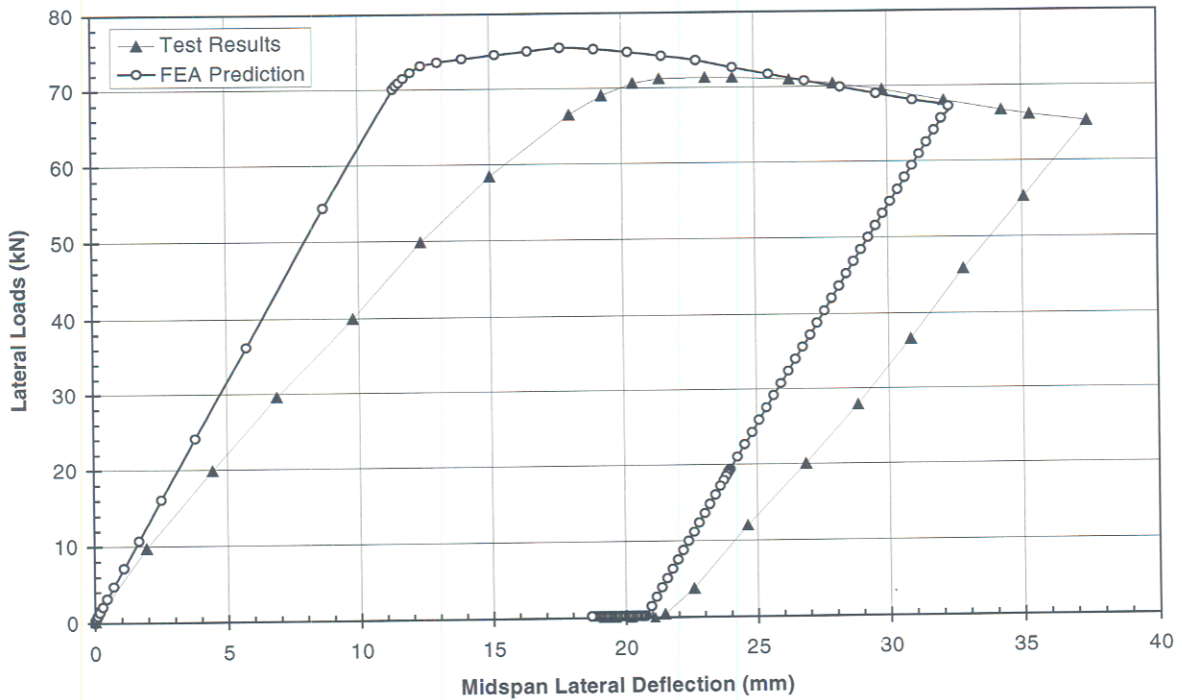


Figure A-28. Lateral Loads vs. Midspan Lateral Deflection During the Damage Cycle of Test SP2.1

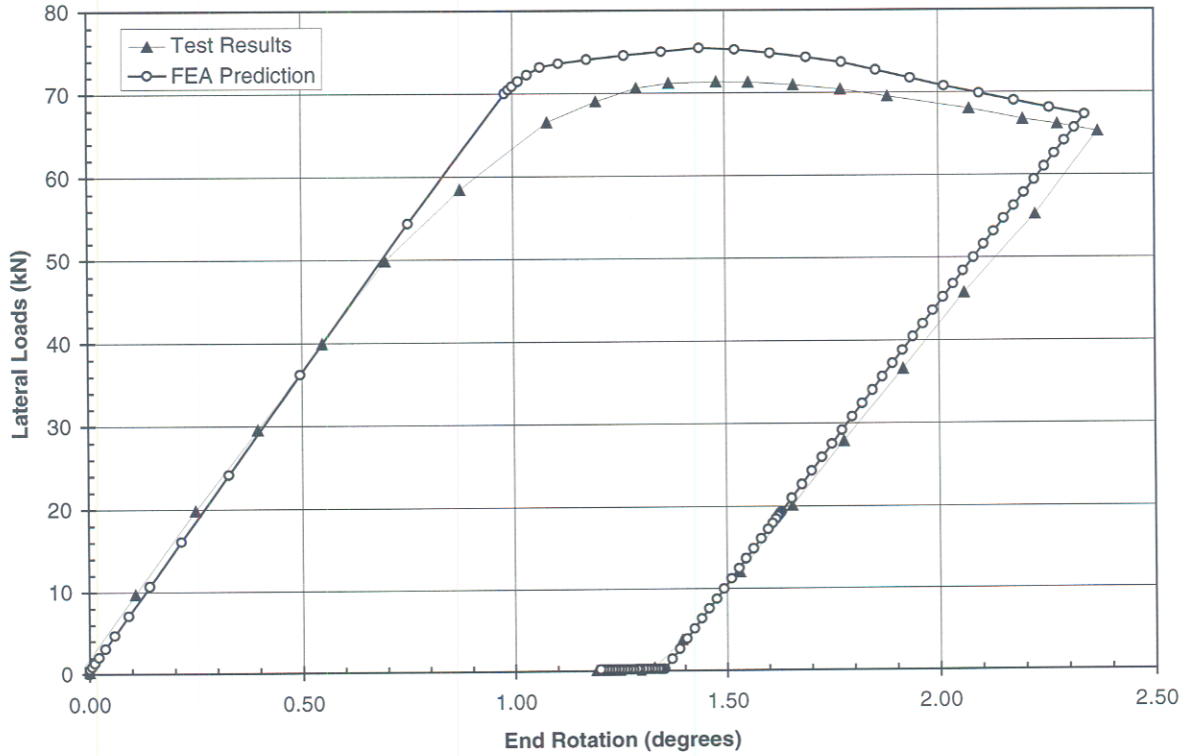


Figure A-29. Lateral Load vs. End Rotation During the Damage Cycle of Test SP2.1

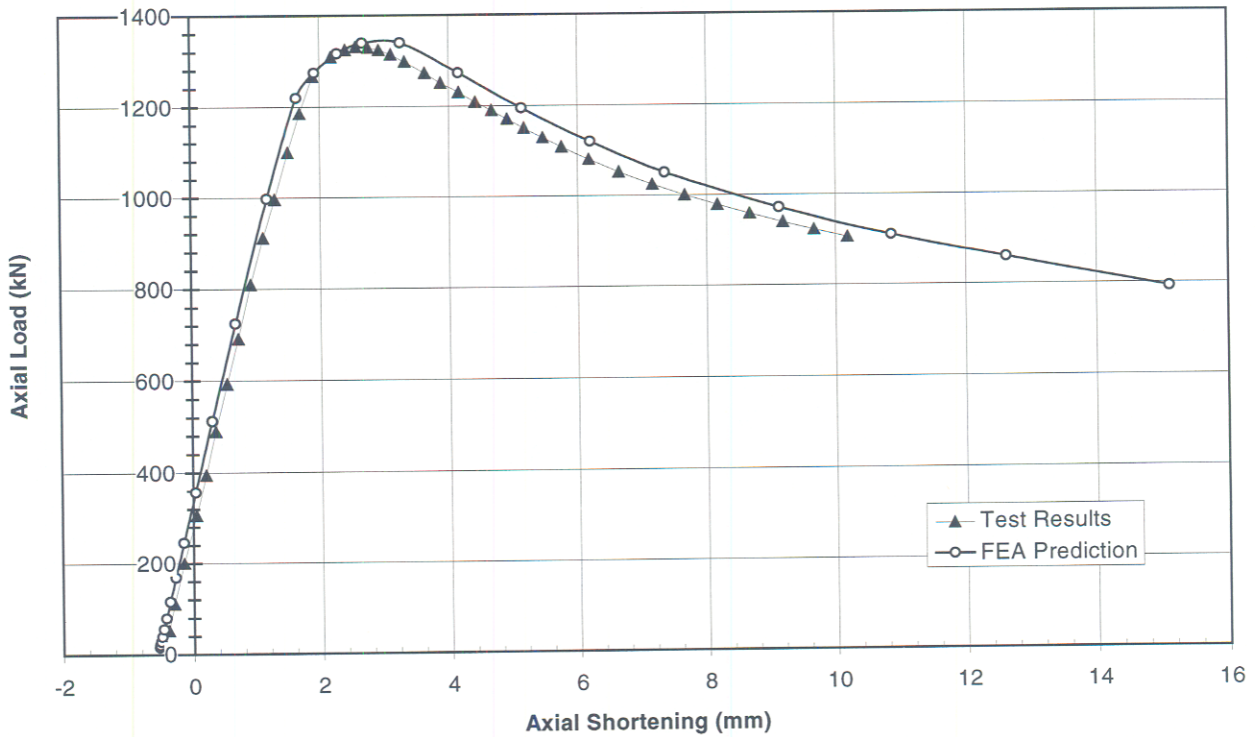


Figure A-30. Axial Load vs. Axial Shortening During the Test Cycle of Test SP2.1

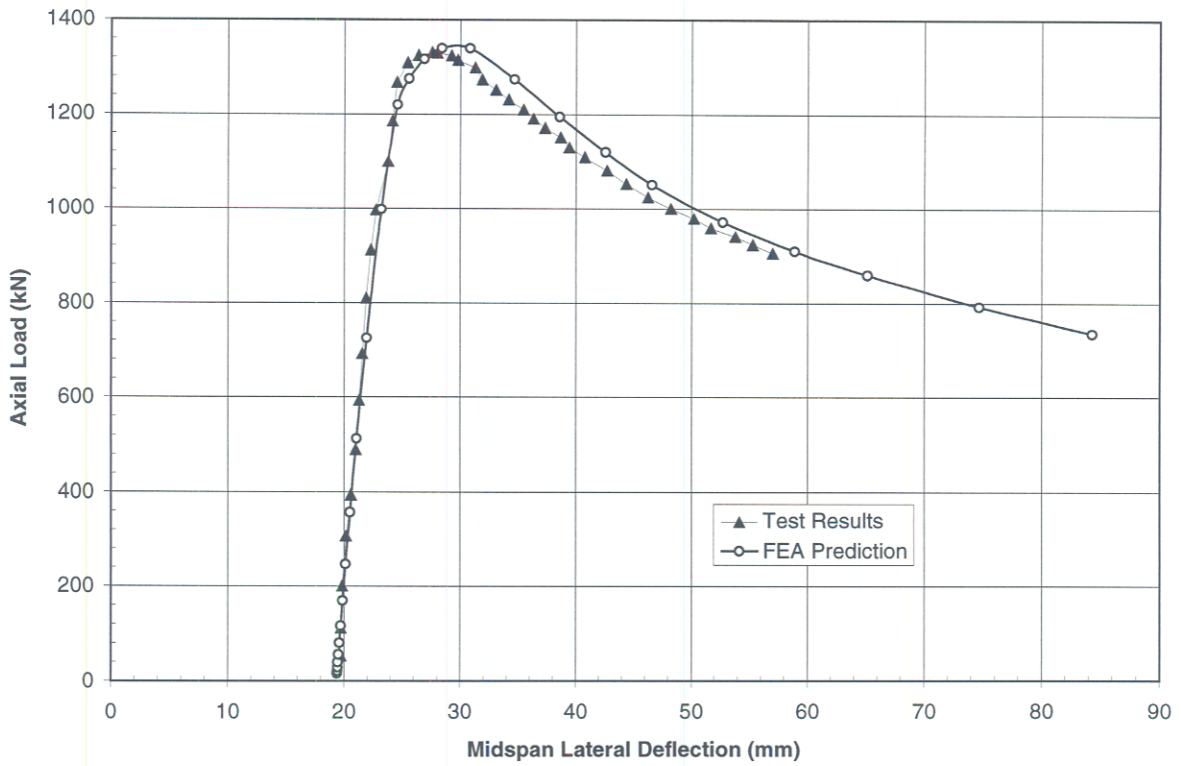


Figure A-31. Axial Load vs. Midspan Lateral Deflection During the Test Cycle of Test SP2.1

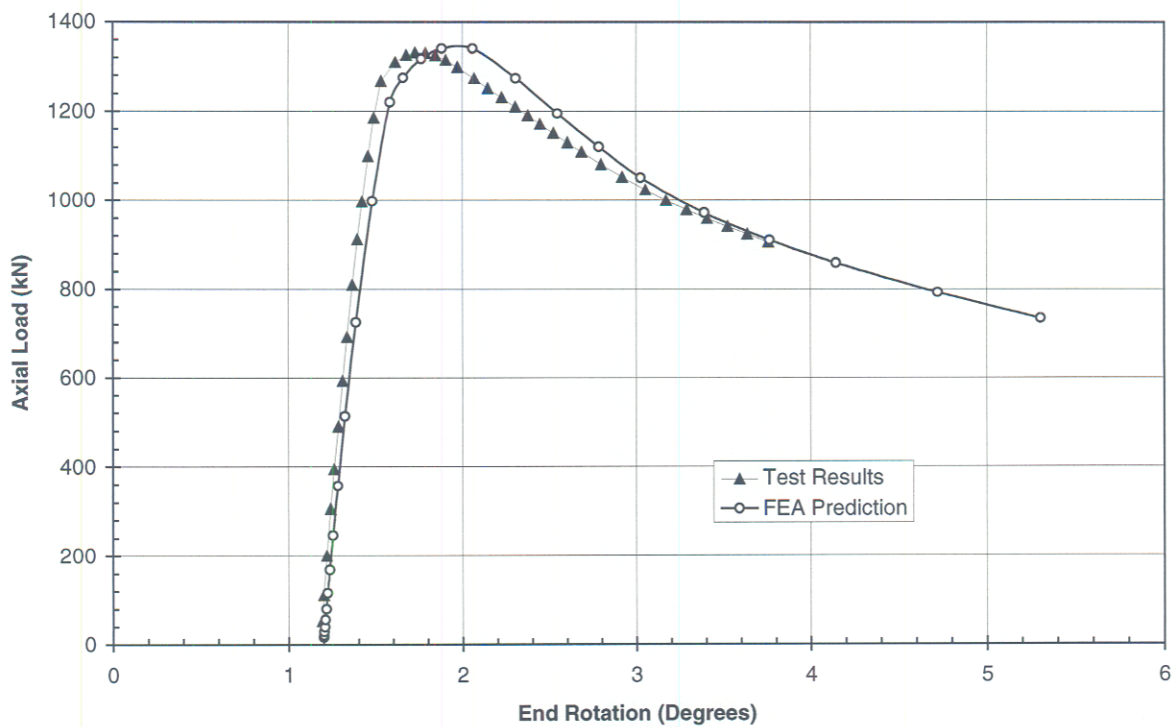
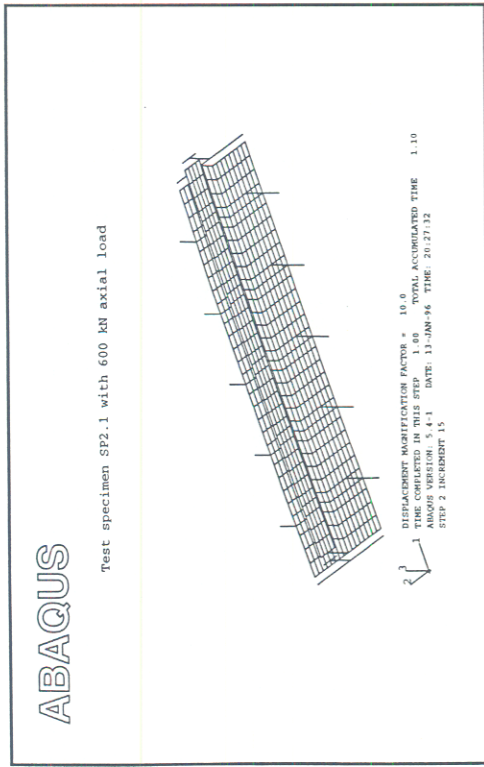
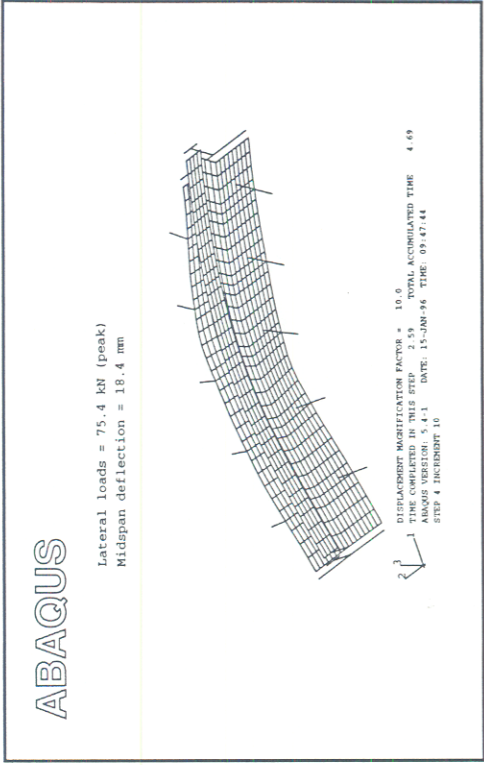


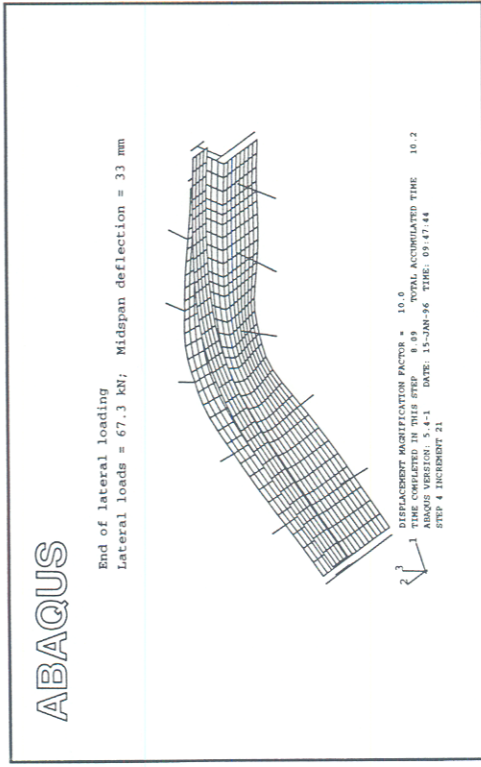
Figure A-32. Axial Load vs. End Rotation During the Test Cycle of Test SP2.1



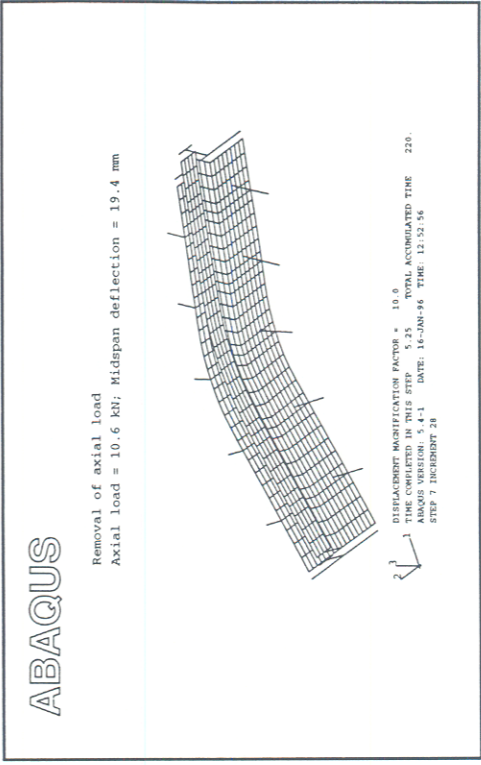
(a) Plate with 600 kN axial load before damage (displacements magnified by 10)



(b) Lateral loads of 75.4 kN (peak) during the damage cycle (displacements magnified by 10)

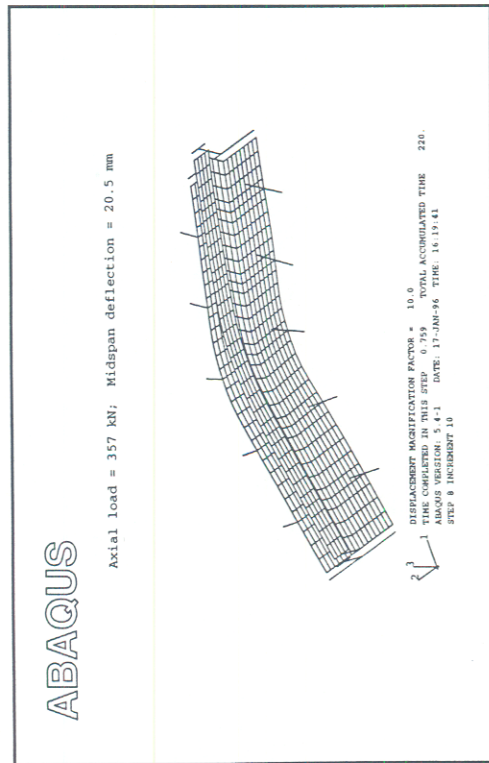


(c) End of lateral loading in the damage cycle (displacements magnified by 10)

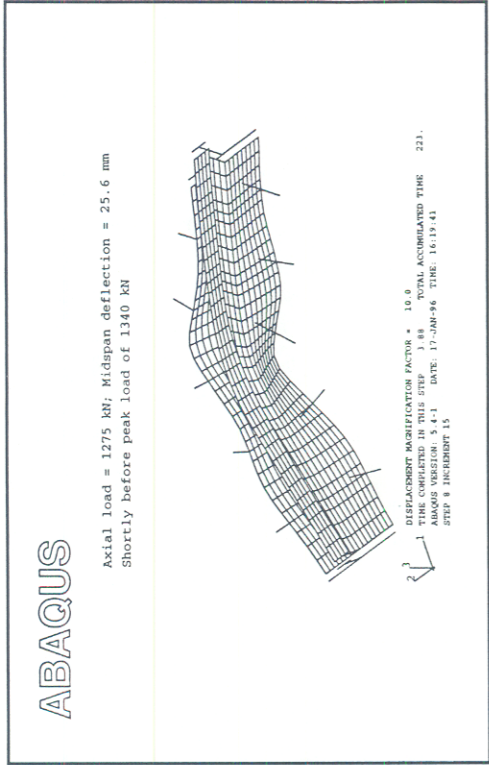


(d) Plate at the end of the damage cycle (displacements magnified by 10)

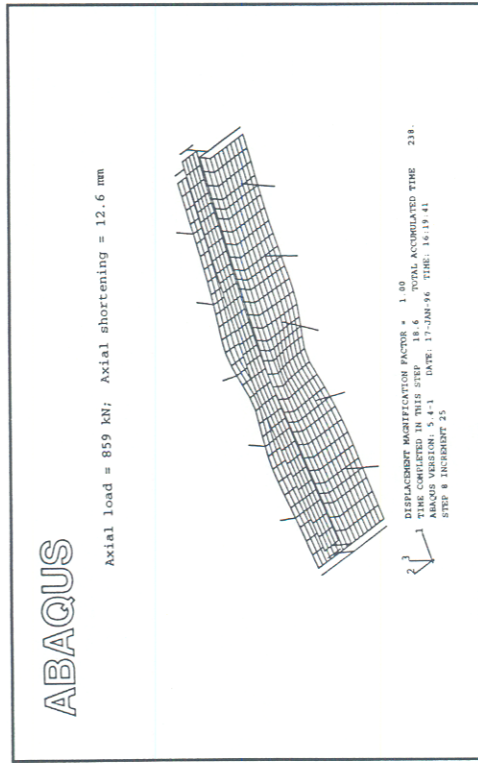
Figure A-33. Deformed Shape of SP2.1 at Various Stages of the Damage Cycle



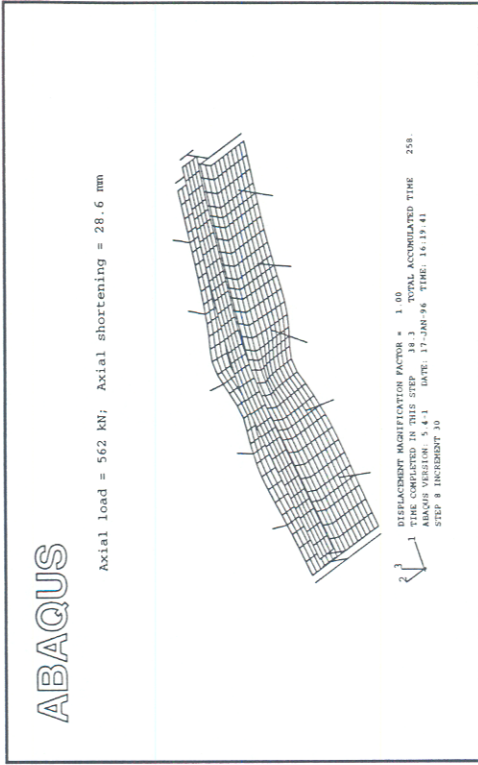
(a) Plate at 27 percent of the peak axial load (displacements magnified by 10)



(b) Plate at 95 percent of the peak axial load (displacements magnified by 10)



(c) Plate at an average axial strain of 0.6 percent



(d) Plate at an average axial strain of 1.4 percent

Figure A-34. Deformed Shape of SP2.1 at Various Stages of the Testing Cycle

APPENDIX B

Residual Stresses and Material Properties

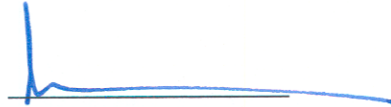
Centre for Frontier Engineering Research

Material Testing and Residual Stress Measurements in a Stiffened Steel Plate

Final Report — Project 95026.008

Prepared by :


J.J.R. Cheng, P. Eng.


A. E. Elwi, P.Eng.


G. Y. Grondin, P. Eng.


G. L. Kulak, P.Eng.

Acting as a Sub-Contractor

to

Centre for Frontier Engineering Research

February 16, 1996

Executive Summary

The measurement of residual stresses for one complete cross section and for three partial cross-section was taken at three locations along a 6 m long stiffened plate panel has been completed. Material characterization for two sections of tee stiffener and a section of steel plate used for the fabrication of stiffened panels have also been completed.

The method of sectioning was used to measure residual stresses in 75 strips from the cross-section. The residual stress distribution and magnitude of residual stresses were as expected. High tensile residual stresses in the order of the yield strength of the material were measured near the weld between the plate and the stiffener. Tensile residual stresses of less than 20% of the yield strength were measured near the free edges of the plate and at the flange to web junction of the stiffener itself. Compressive residual stresses of less than 30% of the yield strength were measured in the remainder of the cross-section.

Residual stress measurements around the stiffener to plate junction at four locations along the length of a stiffened plate have indicated that residual stresses are constant along the length of stiffened plate used for the measurements.

The results of tension coupon tests from two separate stiffeners and a plate specimen indicated that both the plate and stiffener are of the same grade of steel. The static yield strength level is approximately 405 MPa for the stiffeners and 425 MPa for the plate. These levels are typical of CAN/CSA-G40.20-M Grade 350W, or equivalent, steel.

Measurement of Residual Stresses

Introduction

Residual stresses are locked-in self-equilibrating stresses that can exist in materials under uniform temperature conditions without external loading. Consequently, the resultant force and the resultant moment produced by residual stresses must be zero. Residual stresses are produced if regions of a member are inhomogeneously deformed in such a manner that strain incompatibilities occur. The area over which inhomogeneous residual stresses are present can vary from submicroscopic (residual stresses created by the presence of a dislocation in a crystal) to macroscopic, or over several grains (residual stresses created by differential cooling). The later are usually of greater interest since they affect the more general behaviour of structural members such as yielding and stability.

Several techniques of residual stress measurements have been developed over the years. Since different techniques are based on different principles (e.g., X-ray diffraction is based on the measurement of the change in crystal lattice spacing whereas the sectioning technique is based on the release of macroscopic strains released when material is removed) it cannot necessarily be expected that they will yield identical results. In selecting a technique for residual stress measurements one must carefully consider the type of residual stresses that are important (microscopic or macroscopic), the direction in which the gradients of residual stresses are to be measured (through the thickness or over the surface), and whether non-destructive or destructive methods are acceptable.

When considering the problem of buckling of a stiffened plate, it is apparent that macroscopic residual stresses are the most influential type of residual stresses. Microscopic residual stresses that are self equilibrated over a very small surface, such as over a few grains, are not likely to have a significant effect on stability of a structural member containing a very large number of grains. Furthermore, the variation of residual stresses through the thickness of the plate elements of a stiffened plate is not considered to have an important effect on the overall behaviour of the member. The magnitude and variation of residual stresses (average through the thickness) in the cross-section are the two parameters considered to be important on the behaviour of a structural member under monotonic loading.

On the basis of these considerations, it was decided to use the method of sectioning to determine the residual stress distribution in one cross-section of a stiffened plate panel. The method of sectioning is based on the principle that macroscopic residual stresses in a material are relieved when a specimen is cut into strips of small cross-sectional area. The residual stress distribution in a cross-section is determined by measuring the length of each strip before and after sectioning and applying Hooke's law. Two basic assumptions are made when this method is used, namely that the transverse stresses are negligible and that the method of cutting the strips produces no appreciable strain. Both improper sectioning and the existence of strong residual stress gradients beneath the surface can lead to uncertainties in the results.

Procedure

In order to avoid the influence of end effects on the magnitude and distribution of residual stresses, the location used for the residual stress measurements was taken at about 2 m from the end of a 6 m long panel. During the preparation of the specimen for measurement, the long stiffened plate panel was first supported so as to minimize the effect of bending under self weight. Strips to be cut were first laid out in the pattern shown in Figure B-1. This figure indicates that strips of either 6 or 12 mm width were created. The 6 mm strips were used in regions where the gradient of residual stresses was expected to be more significant, such as near the welds and near the free edges. The 12 mm strips were used throughout the rest of the cross-section. A total of 75 strips were laid out at a given cross-section.

The longitudinal residual stresses distribution along the length of a stiffened plate was assessed by measuring the residual stresses at four sections along the length of a 6 m long panel. The location of the sections used for these measurements are shown in Figure B-2. Location F.S. is the section described above for which the residual stresses were measured over the entire cross-section. At locations A, B, and C, taken at 400 mm intervals, the residual stresses were measured only in strips 21 to 27 and strips 58, 59, and 60.

Gauge points were created by embedding 1.6 mm dia. steel balls onto the surface of the strips and at a gauge length of 100 mm. These gauge lengths were laid out on both faces of each strip. The distance between the gauge points was measured with a mechanical extensometer positioned on the steel balls. The extensometer used for the measurement has a precision of 1/1000 mm. To decrease experimental errors attributed to mechanical and human factors, three sets of readings were taken from each strip before sectioning of the specimen. The number of readings required to obtain a maximum error in measured change in length corresponding to about 10 MPa was calculated based on the assumption that the sample is normally distributed. Because the population standard deviation is not known, a t-distribution was used to obtain the required number of data points as follows:

$$n = \left(\frac{t_{\alpha/2} s}{\text{error}} \right)^2$$

where, n = required number of readings
 $t_{\alpha/2}$ = t value for a level of confidence of $(1 - \alpha)$
 s = standard deviation of the sample

For a given set of three readings the calculated value of n was compared to the actual number of readings taken and, if the calculated value was larger than the actual sample size of three, additional readings were taken. The process was repeated until a valid set of readings was obtained.

After the initial readings were obtained, a specimen 350 mm long and containing the gauge points was cut from the 6 m long specimen. The portion containing the residual stress strips

was then sectioned along the lines shown in Figure B-1 using a band saw. Cutting fluid was used in order to minimize heat generation during cutting. Following this, the distance between the gauge points was again measured using the same procedure outlined above.

Residual stresses released by sectioning were calculated using the measured gauge length before and after sectioning. An elongation of a strip after sectioning indicates that a compressive residual stress has been released by sectioning, whereas shortening of a strip results from the release of tensile residual stresses. Stresses are calculated from the relationship:

$$\sigma_r = \frac{L_b - L_a}{L_b} E$$

where, σ_r = the residual stress magnitude. (A positive value corresponds to tension.)
 L_b = average gauge length before sectioning.
 L_a = average gauge length after sectioning.
 E = modulus of elasticity. (An average of the measured values was used).

Results of Residual Stress Measurements

The distribution of residual stresses measured at one cross-section of a stiffened plate panel is summarized in Figure B-3. Figures B-4 to B-6 show the distribution for each plate component of the cross-section individually. Both the distribution and magnitude of residual stresses in the cross-section are as expected, namely, high tensile residual stresses near the weld between the tee stiffener and the plate, and tensile residual stresses of lower magnitude at the junction of the flange and stem of the tee. Tensile residual stresses are measured within a distance of 30 to 40 mm from the welds. Relatively small tensile residual stresses were also measured near the edges of the plate, which had been cut to size initially by a water jet. The residual stresses close to the weld are at the yield strength level of the material. The compressive residual stresses in the cross-section are approximately 100 MPa over most of the cross-section.

In order to verify the accuracy of the measured residual stresses, equilibrium of forces and moments on the cross-section was checked. An imbalance of axial forces of 0.70 kN (compression) was calculated. The imbalance in moments was calculated to be 0.6 kN·m about an axis parallel to the web and 3.0 kN·m about an axis parallel to the plate. All these values are considered to be well within the accuracy that can be expected from this technique.

The residual stresses measured in strips 21 to 27 and in strips 58, 59, and 60 at three different sections along the length of a stiffened panel are summarized in Table 1. No correlation between the magnitude of the residual stresses and the distance along the stiffened plate is noted.

Tension Coupon Tests

Tension coupons were taken from one 300 mm long tee section received from C-FER on July 19, 1995, and from a 10 mm steel plate section and a 300 mm tee section received on July 21, 1995. Six 50 mm gauge length coupons were prepared from each tee section and three coupons were obtained from the 10 mm plate specimen.

Tension tests on the coupons were conducted in accordance with ASTM Standard A370-88a at a controlled strain rate of 1500 $\mu\epsilon/\text{min}$. in the elastic range and about 3000 $\mu\epsilon/\text{min}$. in the plastic and strain-hardening ranges. Stress vs. strain curves were obtained for each coupon. Both the static and dynamic properties were obtained. A summary of the static and dynamic material properties is presented in Table 2. A comparison of the tension coupon test results for the two sections of tees indicates that both sections are of the same grade of steel. An average static yield strength of 403 MPa and dynamic yield strength of 421 MPa was obtained. The static and dynamic yield strength for the steel plate was measured to be 425 MPa and 439 MPa, respectively. Static and dynamic values of the ultimate tensile strength listed in Table 1 also indicate little difference between the material used for the steel plate and the material in the tee stiffeners. The engineering stress vs. strain curves for the tee sections are presented in figures B-7 to B-10 and the engineering stress vs. strain curves for the plate material are presented in Figure B-11.

The measured values of yield and tensile strength indicate that the steel grade for the stiffeners and the plate meet the requirements for CAN/CSA grade G40.21M 350W or 350WT steel.

Table B-1

Residual Stresses At Various Sections Along the Length of a Stiffened Plate (MPa)

Strip	Location			
	A	B	C	F.S.
21	39	76	90	87
22	107	153	151	144
23	208	180	311	190
24	423	426	426	430
25	96	234	209	270
26	128	205	207	240
27	207	239	210	195
58	257	210	212	170
59	228	211	217	249
60	358	330	341	310

Table B-2

Tension Coupon Test Results

Coupon	Static Yield (MPa)	Dynamic Yield (MPa)	Static Ultimate (MPa)	Dynamic Ultimate (MPa)	Rupture Strain	Reduction in Area (%)	
Tee received July 19							
Flange	Coupon 1	390	420	529	561	0.308	64.2
	Coupon 2	410	430	531	564	0.322	62.0
	Coupon 3	403	420	534	564	0.298	65.7
Average for flange		401	423	531	563	0.309	64.0
Stem	Coupon 1	407	423	532	562	0.293	68.0
	Coupon 2	415	430	528	559	0.275	68.9
	Coupon 3	414	432	534	564	0.303	66.7
Average for stem		412	428	531	562	0.290	67.9
Average for section		407	426	531	562	0.300	66.0
Tee received July 21							
Flange	Coupon 1	393	411	537	551	0.340	71.1
	Coupon 2	386	405	520	550	0.327	75.0
	Coupon 3	390	403	520	552	0.312	75.0
Average for flange		390	406	526	551	0.326	73.7
Stem	Coupon 1	404	420	529	557	0.305	63.8
	Coupon 2	409	424	535	560	0.295	71.4
	Coupon 3	418	432	534	560	0.277	69.0
Average for stem		410	425	533	559	0.292	68.1
Average for section		400	416	530	555	0.309	70.9
Plate received July 21							
	Coupon 1	422	436	510	532	0.369	70.9
	Coupon 2	427	440	509	532	0.380	67.6
	Coupon 3	426	440	509	533	0.365	67.8
Average for Plate		425	439	509	532	0.371	68.8

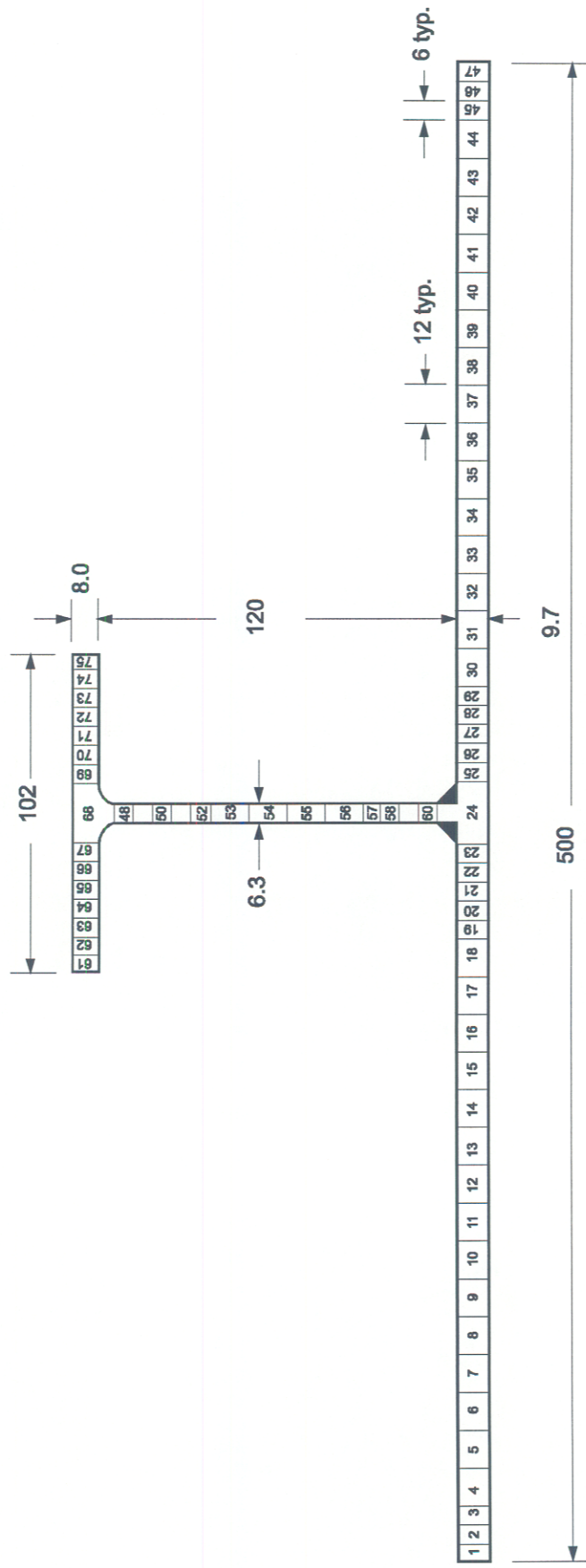


Figure B-1. Sectioning Pattern for Residual Stress Measurements in Stiffened Plate

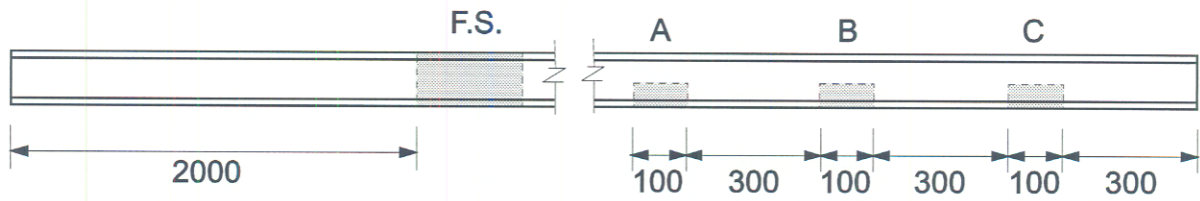


Figure B-2. Sections for Residual Stress Measurements

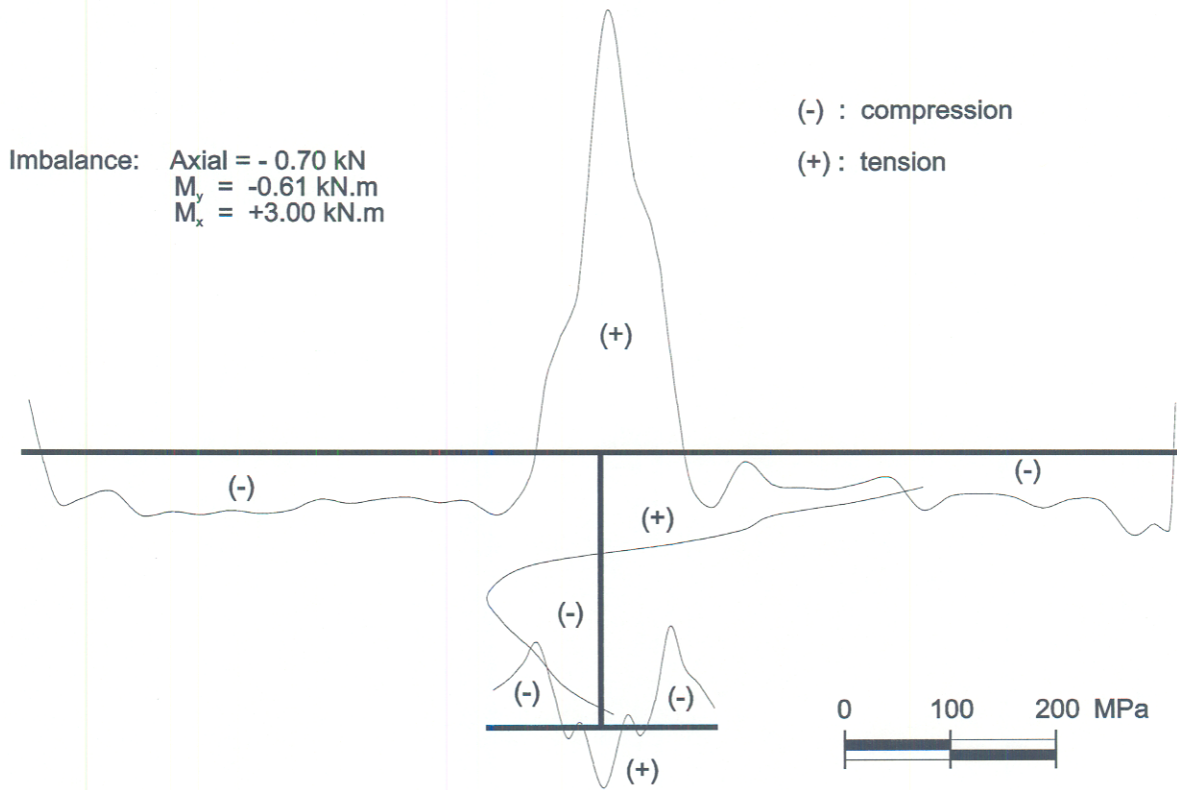


Figure B-3. Measured Longitudinal Residual Stresses in Stiffened Steel Plate at Section F.S.

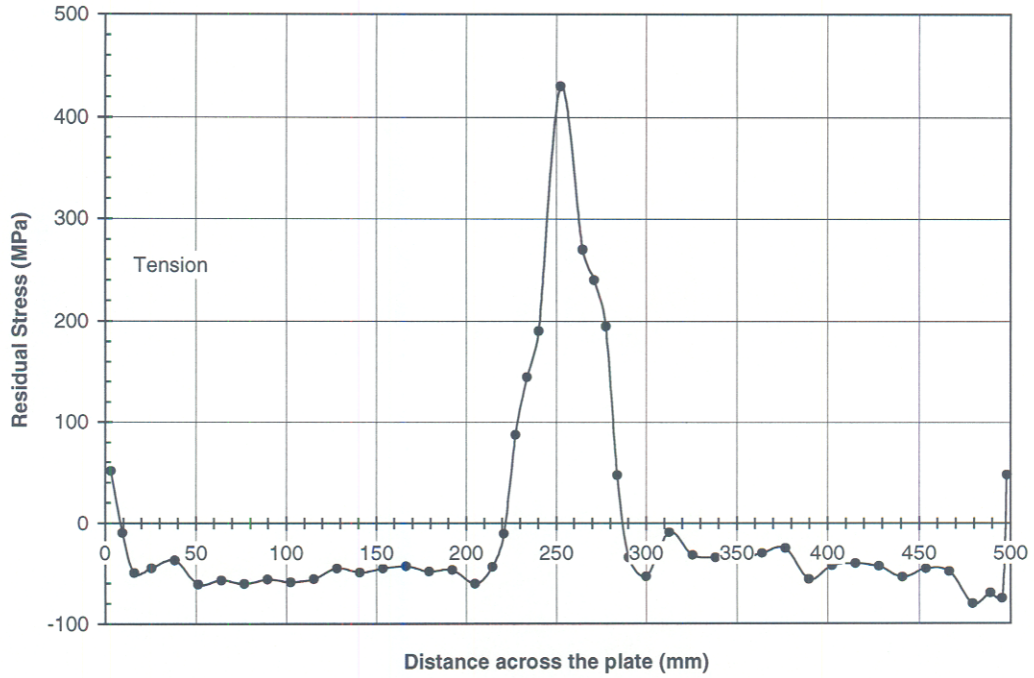


Figure B-4. Residual Stress Distribution in the Plate

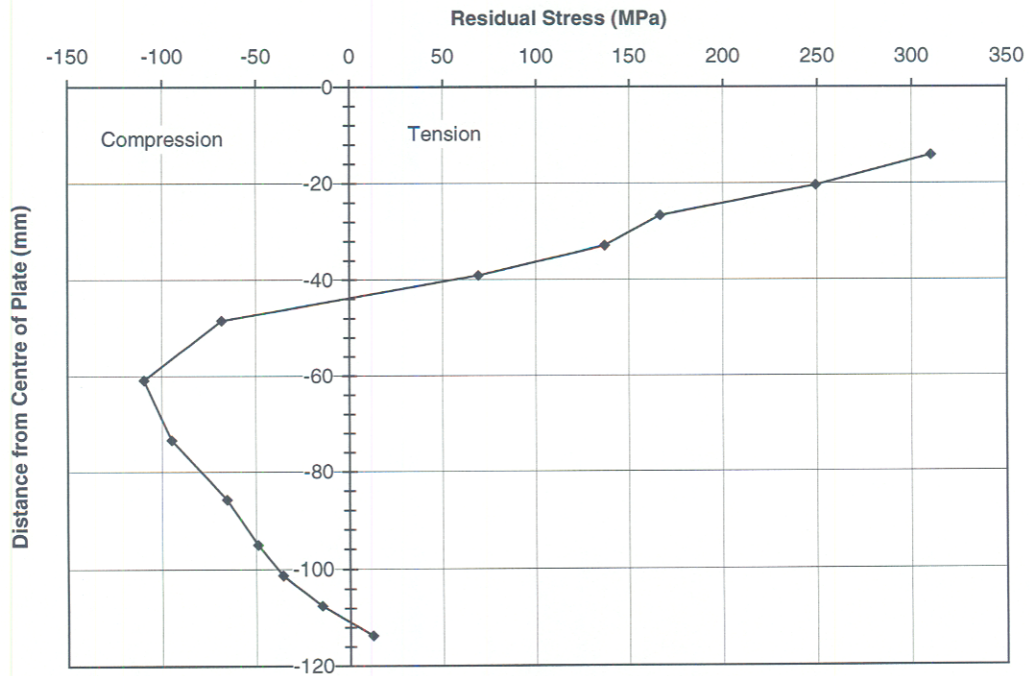


Figure B-5. Residual Stress Distribution in Stem of Tee

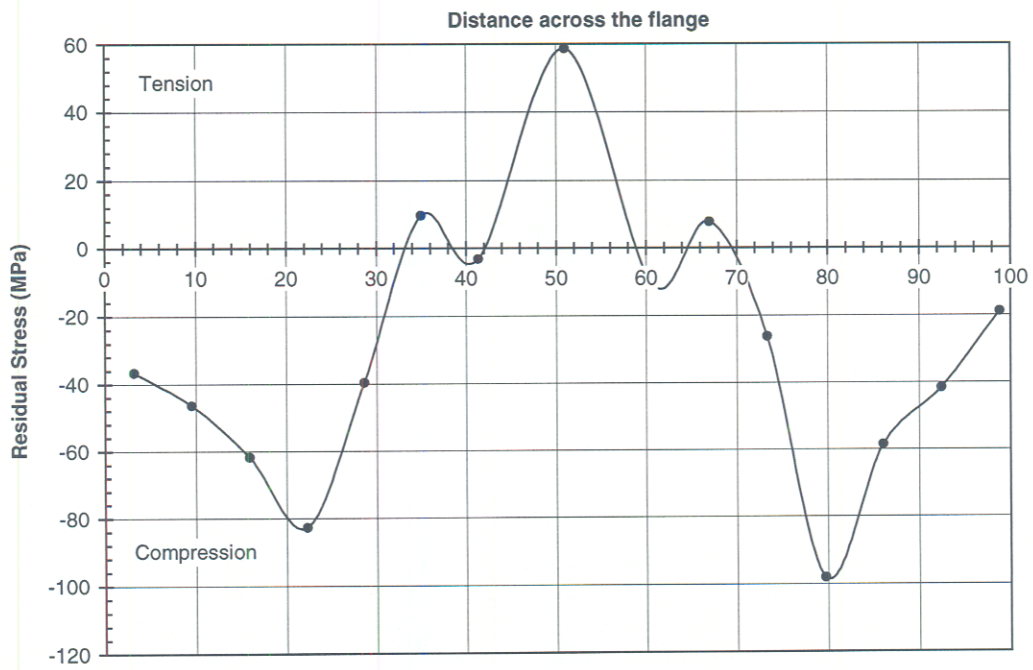


Figure B-6. Residual Stress Distribution in Flange of Tee

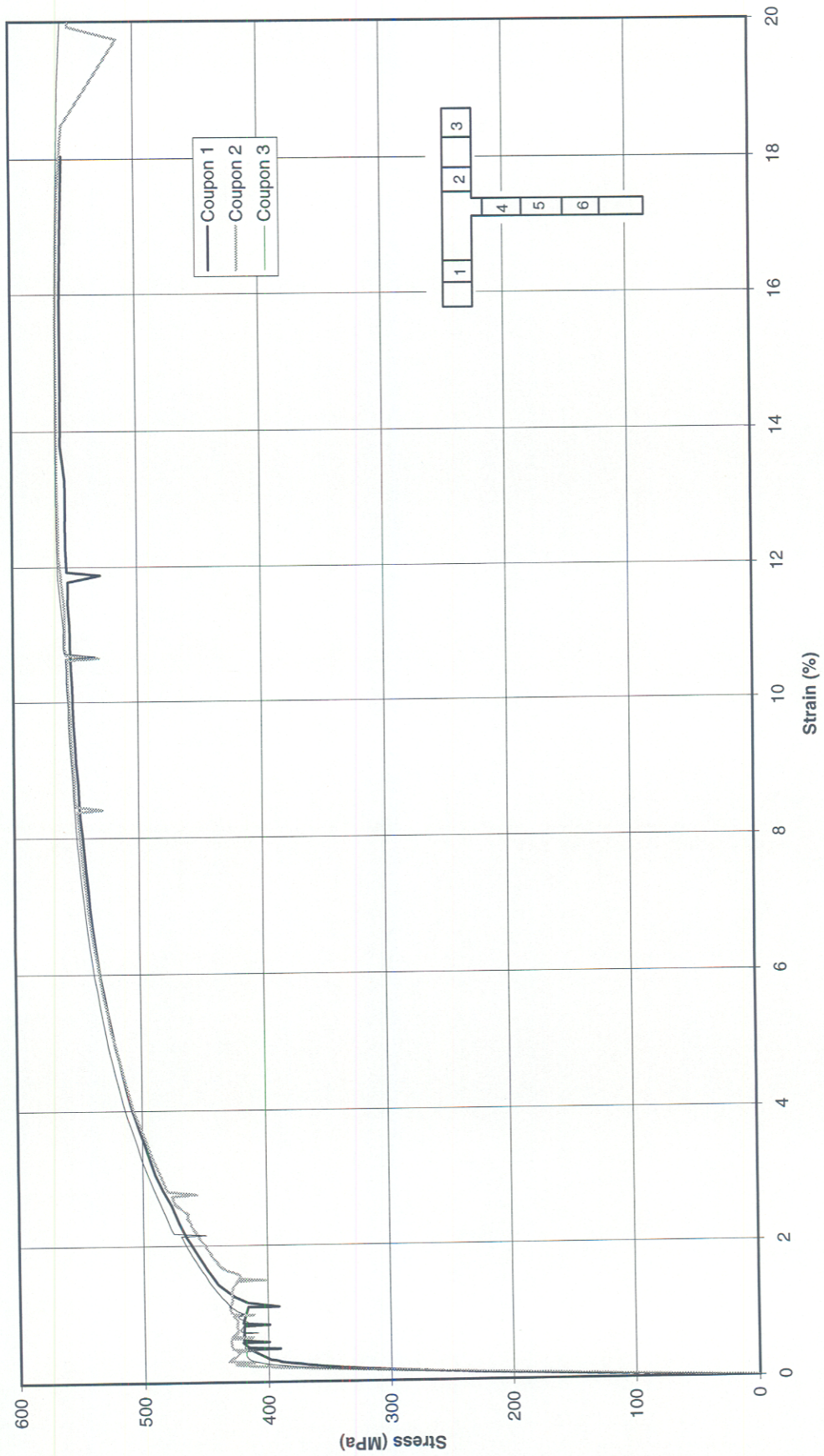


Figure B-7 Stress vs. Strain Curves for Flange of Tee Section Received July 9, 1995

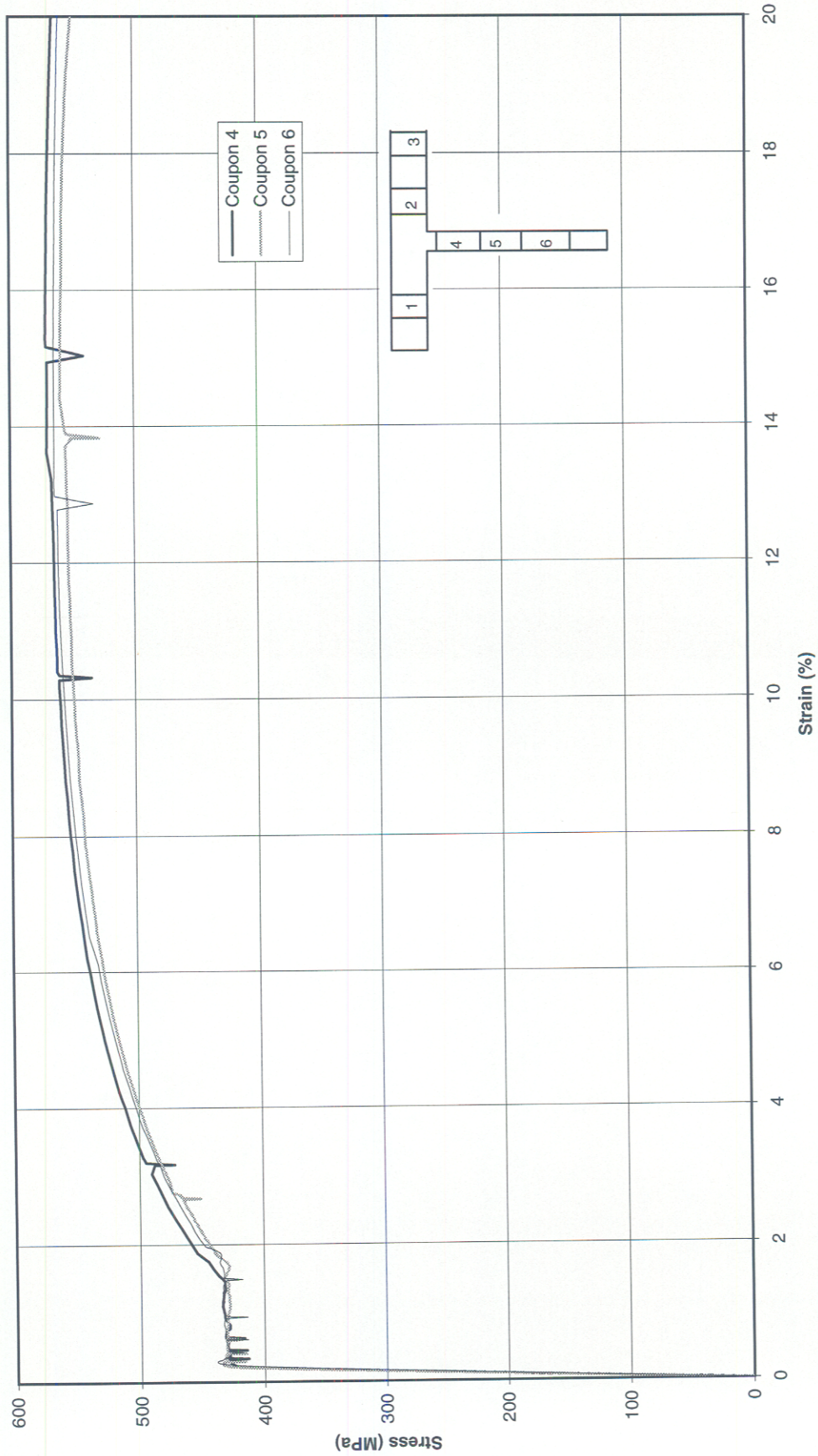


Figure B-8. Stress vs. Strain Curves for Stem of Tee Section Received July 9, 1995

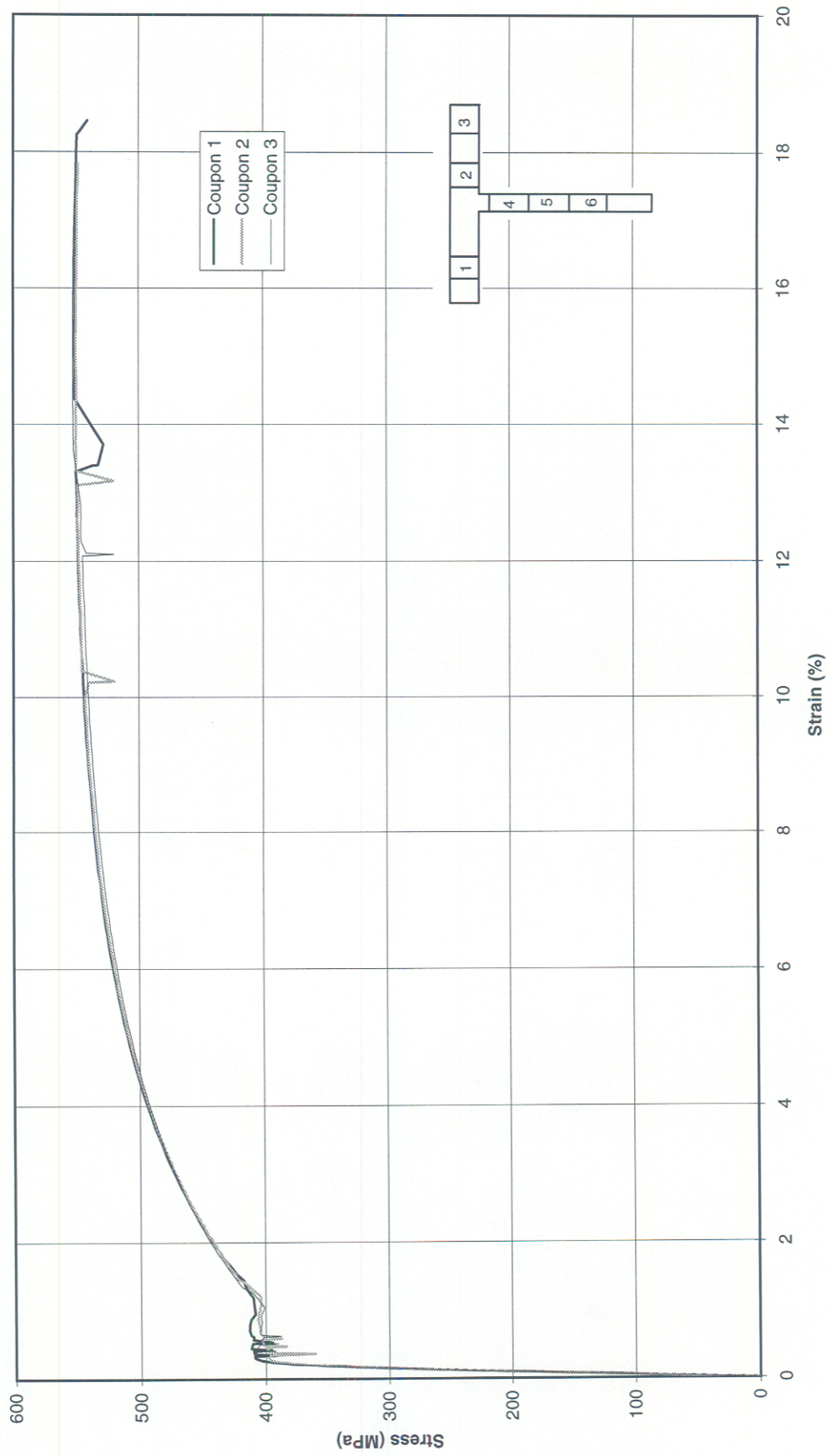


Figure B-9. Stress vs. Strain Curves for Flange of Tee Section Received July 21, 1995

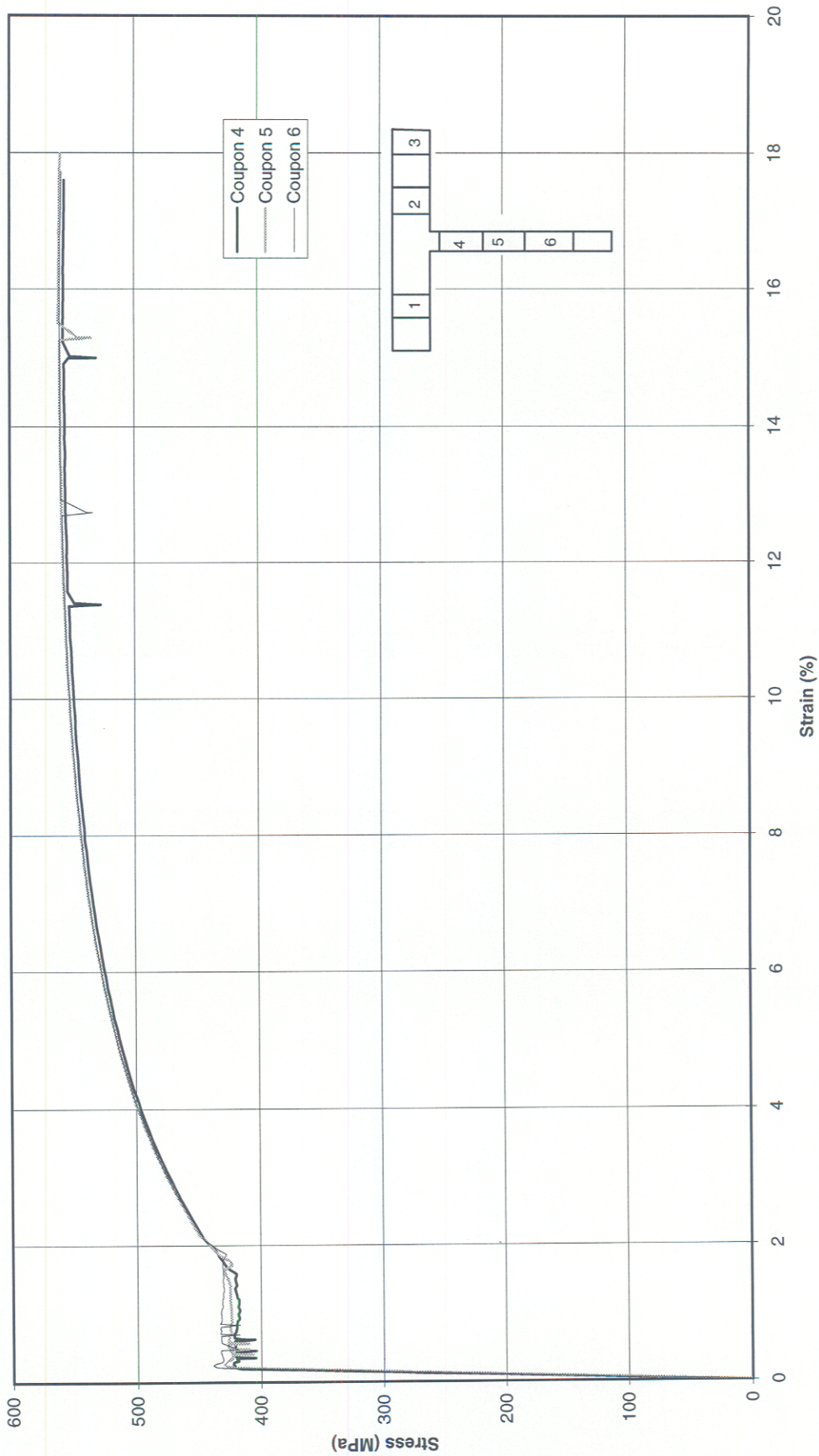


Figure B-10. Stress vs. Strain Curves for Stem of Tee Section Received July 21, 1995

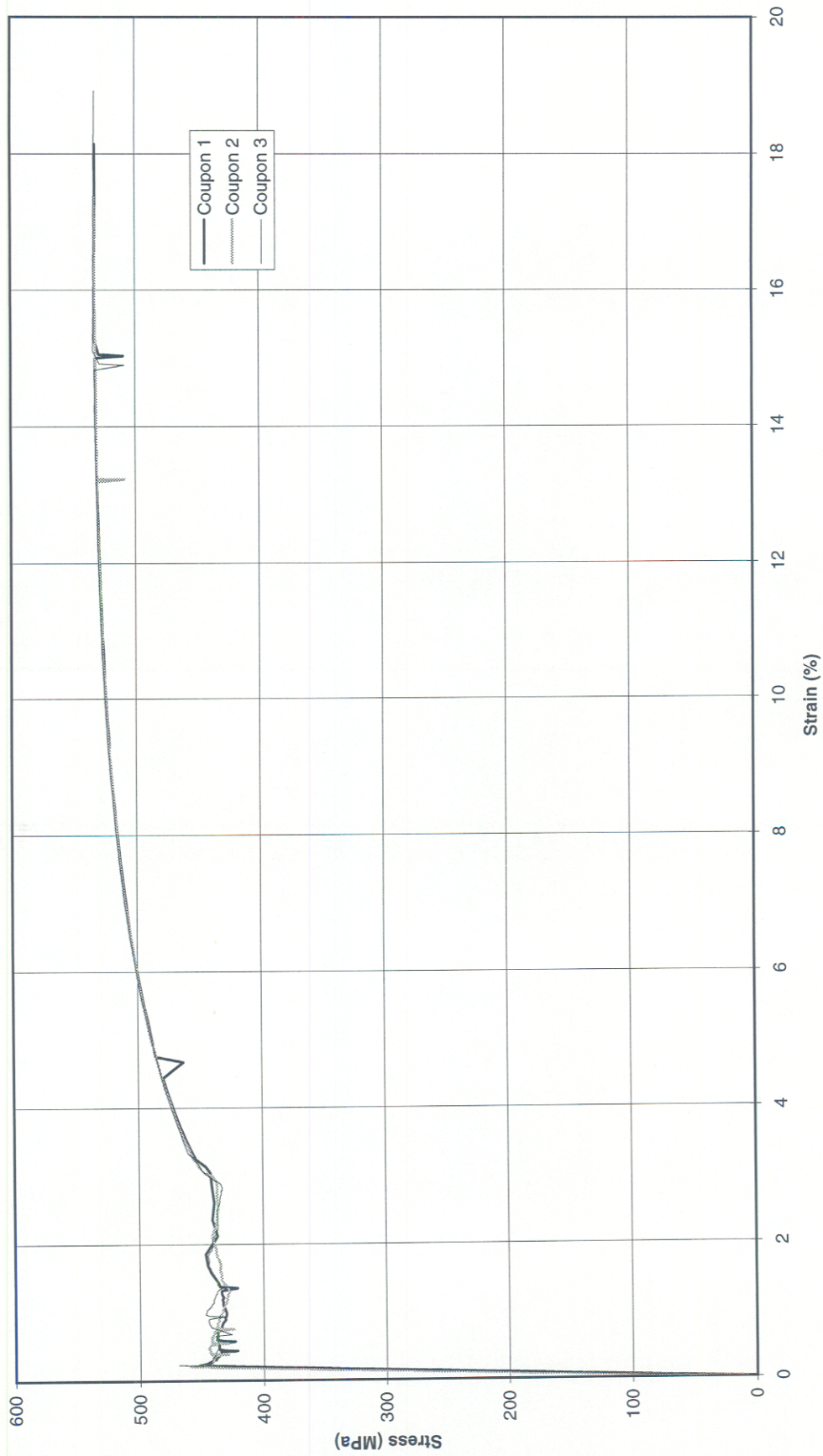


Figure B-11. Stress vs. Strain Curves for Plate Material

COMMITTEE ON MARINE STRUCTURES

Commission on Engineering and Technical Systems

National Academy of Sciences - National Research Council

The **COMMITTEE ON MARINE STRUCTURES** has technical cognizance over the interagency Ship Structure Committee's research program.

Dr. John Landes, *Chairman*, University of Tennessee, Knoxville, TN
Mr. Howard M. Bunch, University of Michigan, Ann Arbor, MI
Dr. Dale G. Karr, University of Michigan, Ann Arbor, MI
Mr. Andrew Kendrick, NKF Services, Montreal, Quebec
Dr. John Niedzwecki, Texas A & M University, College Station, TX
Dr. Alan Pense, NAE, Lehigh University, Bethlehem, PA
Dr. Barbara A. Shaw, Pennsylvania State University, University Park, PA
Dr. Robert Sielski, National Research Council, Washington, DC
CDR Stephen E. Sharpe, Ship Structure Committee, Washington, DC
LT Thomas Miller, Ship Structure Committee, Washington, DC

DESIGN WORK GROUP

Dr. John Niedzwecki, *Chairman*, Texas A&M University, College Station, TX
Dr. Bilal Ayyub, University of Maryland, College Park, MD
Mr. Ovide J. Davis, Pascagoula, MS
Mr. Andy Davidson, NASSCO, San Diego, CA
Dr. Maria Celia Ximenes, Chevron Shipping Co., San Francisco, CA
Mr. Jeffrey Geiger, Bath Iron Works, Bath, ME
Mr. Hugh Rynn, Sea-Land Services, Elizabeth, NJ

MATERIALS WORK GROUP

Dr. Barbara A. Shaw, *Chairman*, Pennsylvania State University, University Park, PA
Dr. David P. Edmonds, Edison Welding Institute, Columbus, OH
Dr. John F. McIntyre, Advanced Polymer Sciences, Avon, OH
Dr. Harold S. Reemsnyder, Bethlehem Steel Corp., Bethlehem, PA
Dr. Bruce R. Somers, Lehigh University, Bethlehem, PA

RECENT SHIP STRUCTURE COMMITTEE PUBLICATIONS

Ship Structure Committee Publications on the Web - All reports from SSC 392 and forward are available to be downloaded from the Ship Structure Committee Web Site at URL:

<http://www.shipstructure.org>

SSC 391 and below are available on the SSC CD-ROM Library. Visit the National Technical Information Service (NTIS) Web Site for ordering information at URL:

<http://www.ntis.gov/fcpc/cpn7833.htm>

SSC Report Number	Report Bibliography
SSC 398	<u>Assessment of Reliability of Ship Structures</u> A. Mansour, P. Whirshing, et al 1997
SSC 397	<u>Commercial Ship Design and Fabrication for Corrosion Control</u> J. Parente, J. Daidola, N. Basar, R. Rodi 1997
SSC 396	<u>Optimized Design Parameters for Welded TMCP Steels</u> L. Malik, R. Yee, B. Graville, A. Dinovitzer 1997
SSC 395	<u>Ship's Maintenance Project, Pt. II and III</u> R. Bea, T.Xu, K. Ma, R. Shulte-Strathaus 1997
SSC 394	<u>Strength Assessment of Pitted Plate Panels</u> J. Daidola, J. Parente, I. Orisamolu, K-t. Ma 1997
SSC 393	<u>Evaluation of Ductile Fracture Models</u> R. Dexter, M. Gentilcore 1997
SSC 392	<u>Probability Based Ship Design: Implementation of Design Guidelines</u> A. Mansour, P. Wirsching, G. White, B. Ayyub 1996
SSC-391	<u>Evaluation of Marine Structures Education in North America</u> R. Yagle 1996
SSC 390	<u>Corrosion Control of Inter-hull Structures</u> M. Kikuta, M. Shimko, D.Ciscom 1996
SSC 389	<u>Inspection of Marine Structures</u> L. Demsetz, R. Cario, R. Schulte-Strathaus, R. Bea 1996
SSC 388	<u>Ship Structural Integrity Information System-Phase II</u> M. Dry, R. Schulte-Strathaus, R.Bea 1996
SSC 387	<u>Guideline for Evaluation of Finite Elements and Results</u> R.I. Basu, K. J. Kirkhope, J. Srinivasan 1996
SSC 386	<u>Ship's Maintenance Project</u> R. Bea, E. Cramer, R. Schulte-Strauthaus, R. Mayoss, K. Gallion, K. Ma, R. Holzman, L. Demsetz 1995